ADVANCED ENERGY MATERIALS
www.advenergymat.de

2D Layered Nanomaterials as Fillers in Polymer Composite Electrolytes for Lithium Batteries

Vidyanand Vijayakumar, Meena Ghosh, Kiran Asokan, Santhosh Babu Sukumaran, Sreekumar Kurungot, Jonas Mindemark, Daniel Brandell, Martin Winter, and Jijeesh Ravi Nair**

Polymer composite electrolytes (PCEs), i.e., materials combining the disciplines of polymer chemistry, inorganic chemistry, and electrochemistry, have received tremendous attention within academia and industry for lithium-based battery applications. While PCEs often comprise 3D micro- or nanoparticles, this review thoroughly summarizes the prospects of 2D layered inorganic, organic, and hybrid nanomaterials as active (ion conductive) or passive (nonion conductive) fillers in PCEs. The synthetic inorganic nanofillers covered here include graphene oxide, boron nitride, transition metal chalcogenides, phosphorene, and MXenes. Furthermore, the use of naturally occurring 2D layered clay minerals, such as layered double hydroxides and silicates, in PCEs is also thoroughly detailed considering their impact on battery cell performance. Despite the dominance of 2D layered inorganic materials, their organic and hybrid counterparts, such as 2D covalent organic frameworks and 2D metal–organic frameworks are also identified as tuneable nanofillers for use in PCE. Hence, this review gives an overview of the plethora of options available for the selective development of both the 2D layered nanofillers and resulting PCEs, which can revolutionize the field of polymer-based solid-state electrolytes and their implementation in lithium and post-lithium batteries.

1. Introduction

Since the inception of lithium-ion batteries (LIBs) in the early 1980s and their subsequent commercialization by Sony in 1991, there have been tremendous efforts to improve their performance, safety, cost-effectiveness, and sustainability.[1] In the last four decades, dedicated research in material science toward developing electrodes, separators, electrolytes, current collectors, packaging materials, etc., have significantly contributed to the advancement of LIB technology.[2] Indeed, the progress in cell engineering and processing conditions has aided the evolution of high energy density LIBs (energy density >250 Wh kg^{-1}), leading to their widespread application spanning from electronic devices to electric vehicles and stationary/grid energy storage.[1] Considering the contributions that led to the invention of LIB technology, John B. Goodenough, Stanley Whittingham, and Akira Yoshino received the Chemistry Nobel Prize in 2019.[3] Despite their huge success, research and development on LIBs and allied battery technologies are still a hot topic in both academia and industry offering opportunities for breakthrough innovations and discoveries.

Figure 1a presents a schematic illustration of the state-of-the-art LIB and its main components. Liquid electrolytes based on organic solvents and lithium salts are the primary choice as electrolytes in LIBs due to their high ionic conductivity and good

V. Vijayakumar, J. Mindemark, D. Brandell
Department of Chemistry–Ångström Laboratory
Uppsala University
Box 538, Uppsala SE-751 21, Sweden
M. Ghosh
Institute of Inorganic Chemistry 1
Ulm University
Albert-Einstein-Allee 11, 89081 Ulm, Germany

The ORCID identification number(s) for the author(s) of this article can be found under https://doi.org/10.1002/aenm.202203326.

DOI: 10.1002/aenm.202203326

K. Asokan, S. B. Sukumaran, S. Kurungot
National Chemical Laboratory (CSIR-NCL)
Dr. Homi Bhabha Road, Pune 411008, India
M. Winter, J. R. Nair
Helmholtz-Institute Münster
IEK-12
Forschungszentrum Jülich
Corrensstr. 46, 48149 Münster, Germany
E-mail: m.winter@fz-juelich.de; j.nair@fz-juelich.de
M. Winter
MEET Battery Research Centre
Institute of Physical Chemistry
University of Münster
Corrensstr. 46, 48149 Münster, Germany
M. Winter
Institute of Physical Chemistry
Westfälische Wilhems-Universitat Muenster
Correnstrasse 28/30, 48149 Münster, Germany

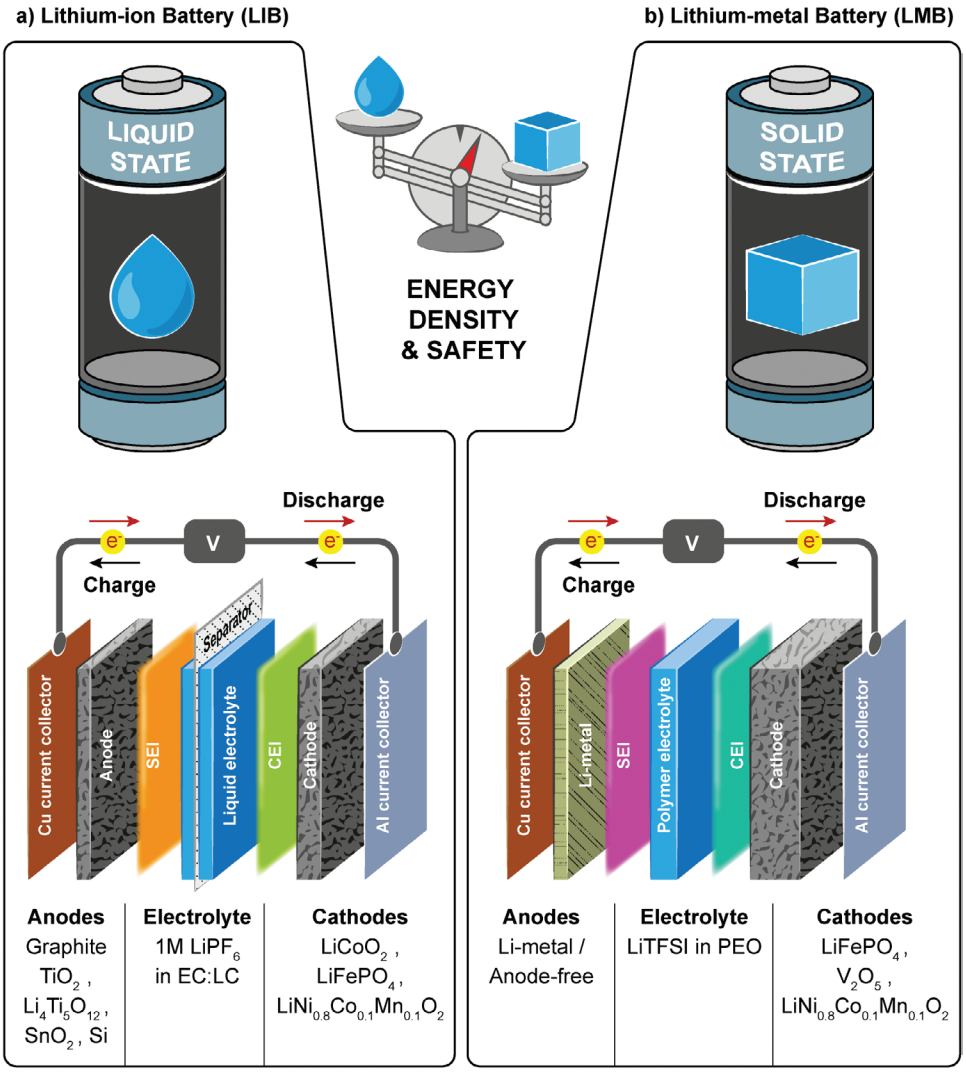

Figure 1. Schematic representation of state-of-the-art a) LIB and b) LMB configurations using liquid electrolyte and polymer electrolyte (PE), respectively. Image courtesy Andre Bar.

wettability of the porous electrodes.[4] However, flammability, a narrow operating temperature range, the chance of leakage, continuous decomposition leading to battery aging, and harmfulness of organic solvents often make the reliance on liquid electrolytes unsafe and less sustainable.[5] The quest for packing more energy per unit metric (high energy density) led to the resurgence of once discarded lithium–metal batteries (LMBs, Figure 1b).[6] The use of organic liquid electrolytes in LMBs often fail to prevent the growth of dendrites and formation of high surface area lithium (HSAL) over the Li metal anode surface during repeated charge–discharge cycles, resulting in cell failure and potential fire hazards.[7] There is a comprehensive agreement that a (partial) transition from liquid electrolytes to solid-state electrolytes (SSEs) would significantly increase the safety of batteries, in particular, LMBs due to the presence of metallic Li anode. In this context, polymer electrolytes (PEs) are strong contenders for producing solid-state LMBs (polymer electrolyte-based LMB, Figure 1b) due to their ease of processability, better mechanical properties (toughness and flexibility), lower cost of production, and the use of lower concentration of lithium compared to inorganic solid-state electrolytes (ISEs).[5,8,9]

The dawn of research interest in PEs started with the discovery of ionic conductivity in semicrystalline poly(ethylene oxide) (PEO) doped with various alkali-metal (Li, Na, K) ions by Wright et al. in the early 1970s.[10] In these classical (solvent-free) dry polymer electrolytes (DPEs), salt dissolution occurs due to the Lewis acid–base interactions between the ions and the coordinating (hetero) atoms in the polymer, e.g., oxygen atoms of ethylene oxide (-EO-) in PEO. Armand et al., in the early 1980s, discovered that the amorphous phase within a polymer matrix significantly facilitates ion conduction in DPEs, thereby highlighting the connection between polymer segmental motion and ionic transport.[11] In this regard, a lower glass transition temperature (T_g) of the polymer host indicates a high segmental motion of the polymer chains often favoring ionic transfer between coordination sites, thus enhancing ion mobility in the DPE.[12] **Figure 2**a illustrates the segmental motion of the PEO chains that assists in ion transport and

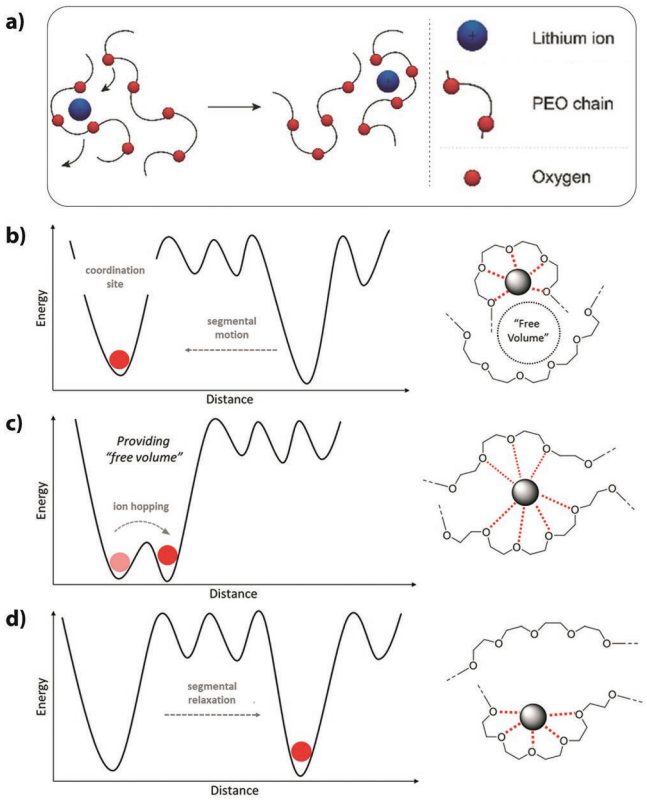

Figure 2. a) Illustration of Li^+-ion conduction in DPEs through the segmental motion of PEO chains assisted by cation coordinating oxygen atoms (top). b–d) Free-volume model: the detailed energy profile diagram associated with the significant stages of Li^+-ion transport in DPEs. Reproduced under the terms of the CC BY-NC 3.0 license.[13] Copyright 2019, The authors, published by Royal Society of Chemistry.

related energetics using a free volume model (Figure 2b–d).[13] Modifications made in the polymer host chemistry or its architecture (e.g., cross-links, branches, etc.) can influence the percentage of crystalline and amorphous regions in the PE, polymer chain segmental motion, mobility, and flexibility.[14] However, bringing the ionic conductivity of DPEs close to liquid electrolytes is challenging. Therefore, gel polymer electrolytes (GPEs), having polymeric and liquid components, have gained significant attention from the battery community.[1a,2a] While compromising safety, considerable benefits in terms of improved ionic mobility can be achieved by using GPEs. The polymers used in GPEs can be either intrinsically ionic conductors or inert polymers, however, they should be capable of retaining the liquid components. Typical GPEs have three essential constituents: salt, liquid solvent/plasticizer, and a polymer host. Most often, the primary role of a polymer host in such GPEs is to retain the liquid solvent/plasticizer to avoid the intricacies of leakage, hence, provide solid-like operability and performance. Indeed, in such systems, the ion conduction majorly occurs through the liquid phase (solvent/plasticizer) rather than the polymer chain segmental motion.

Apart from high ionic conductivity, PEs in general must possess features such as i) high Li^+ transference number (t_{Li}^+), ii) good interfacial and interphasial stability/compatibility with the electrode materials, iii) high thermal, chemical, and electrochemical stability, and iv) low cost and facile fabrication.[1a,15] Pre-addition of task-specific soluble organic and inorganic additives (e.g., $LiBF_4$ LiBOB, LiFSI, etc.) is one of the approaches to tailor the electrochemical and thermal properties of PEs For instance, PEs containing artificial SEI and cathode electrolyte interphase[16] forming organic additives, such as vinylene carbonate, can provide improved interphasial stability in both LIBs and LMBs.[17] Similarly, PEs with multisalt chemistry (main salt and co-salts) in which the replace all cosalt with co-salt is at a relatively lower concentration compared to the main salt, intended to modify the SEI and several other electrochemical properties, has also received significant attention in the recent years.[18] Besides, for improving the t_{Li}^+ value of PEs, incorporation of anion-trapping agents such as boron-based Lewis acids have also been successfully employed.[19] Additionally, to increase the nonflammable nature of GPEs and DPEs, organophosphorus compounds as flame-retardants and thermal stability boosters have also been widely applied.[20] Thus, it is important to highlight that there have been attempts to enhance properties of PEs by the so called "soluble additive chemistry" approach for the overall enhancement of physical, chemical, and electrochemical properties. However, a comprehensive study of evaluating the impact of soluble additives in PEs has not been investigated consistently unlike the liquid electrolytes. Hence, a knowledge gap still exists in this direction summarizing which type of additive suits for what type of PE, demanding further research.

Although soluble and low-molecular-weight (M_w), the use of molecular additives constitute one essential route for the realization of improved PEs. The alternative strategy of incorporating electronically insulating, insoluble, and nanosized solid-state organic, inorganic, and organic–inorganic hybrid materials (also known as nanofillers) as additives have been well explored for several decades.[21] Recent years have seen much of a renewed interest in this electrolyte category, generally referred as polymer composite electrolytes (PCEs).[22] The term polymer nanocomposite electrolytes (PNCEs) is also often used in the literature instead of PCEs to emphasize the use of nanosized fillers. According to IUPAC recommendation,[47] *a multicomponent material comprising multiple different (nongaseous) phase domains in which at least one type of phase domain is a continuous phase* is called a composite. Similarly, IUPAC also defines a polymer composite as a *composite in which at least one component is a polymer*.[47] Hence, polymer composites capable of exhibiting ionic conductivity (inherent ion conduction or ion conduction achieved by postprocessing such as activation by a liquid electrolyte), functional as separators/electrolytes in electrochemical devices are often called PCEs.

The most intriguing property of a PCE is the possible synergetic contribution of the individual components, resulting in properties that are not achievable with either component alone. The research interest in PCEs started parallel to the PE research in the early 1980s, where the first report from Weston and Steele explained the effect of α-alumina (α-Al_2O_3) in PEO-based DPE (PEO-$LiClO_4$) in enhancing the high-temperature performance.[23] Further research interest took off in the 1990s with pioneering efforts by the groups of Scrosati and Wieczorek.[22b,24] Unlike task-specific soluble additives that are

primarily capable of tuning the chemical and electrochemical properties of PEs, solid-state nanofillers can also modify their microscopic and macroscopic physical properties. For example, the presence of solid-state nanofillers reinforces GPEs and helps to improve their mechanical stability. Besides, nanofillers in optimum amounts can enhance ionic conductivity, t_{Li^+} value, thermal stability and amorphous character of PEs, and often alter the main ionic transport mechanisms. Moreover, the reports show that nanofillers can lower the T_g value of DPEs, indicating their plasticizing effect.[25] Thereby, it is important to note that solid-state nanofillers can act as a form of solid-state plasticizers, hence altering the physical characteristics of a polymer matrix and the resulting PCE.

Solid-state nanofillers that do not exhibit any inherent Li^+-ion conduction properties are called passive or inert fillers. In such PCEs where inert nanofillers are used the ionic transport is strictly dependent on the dissolved salt (the ion source).[29] Inorganic metal oxide nanoparticles (e.g., Al_2O_3, ZnO, TiO_2, MgO, CeO_2, etc.) and several organic materials (e.g., cellulose nanoparticles) are standard passive (= not ion conductive) filler components in PCEs.[30] Inherent Li^+-ion conducting solid-state nanofillers, called "active fillers," are common nowadays in PCEs.[31] These active fillers are based on ISE materials, such as Li^+-ion-containing garnets, sulfides, nitrides, and so forth.[32] PCEs with active fillers (generally with Li-salt and low to medium ISE loading) are often called hybrid polymer electrolytes (HPEs). In such HPEs, ionic conduction occurs through both the polymer and inorganic matrices. There is another variation of HPE system in which the polymer is mixed with low to very high loading of ISE particles (without any Li-salt) where the polymer functions as a binder holding the particles together. In such HPEs with ISEs (rather a PCE), the polymer imparts easy processability, flexibility, thin fabrication possibilities, etc. In these HPE/PCE systems, the polymer acts either passive or active for ion conduction but in any case, the Li^+-ion transport by the active ISE filler dominates. Therefore, the term hybrid electrolyte is usually used covering all these types of PCEs. Consequently, the classification of hybrid electrolytes is still not well-defined in the PE community.

In most cases, noncovalent bonding interactions (e.g., hydrogen bonding, electrostatic, dipole–dipole, and ion–dipole interactions, etc.) or Lewis acid–base type interactions between the nanofiller, polymer, lithium salt, and liquid solvent or plasticizer (if any) dictate the global ion transport properties and local transport mechanisms in PCEs (**Figure 3**a,c).[9,22b,26,27,33] An enhancement in ionic conductivity at the polymer–nanofiller interface regions is frequently suggested as an explanation for the improved ion transport properties in PCEs.[26,34] These polymer regions in contact with the nanofiller often cannot crystallize, which promotes higher amorphous character resulting in faster Li^+-ion transport. The local conformation of polymer segments at these polymer–nanofiller interfaces can also change, leading to various Li^+ conducting substructures.[34b] For instance, Figure 3b shows such an example where the crystalline PEO undergoes a transition to an amorphous phase due to chemical bonding interactions between PEO and SiO_2 nanofiller. Such bondings also proves the possible benefit of strong interactions (covalent/noncovalent interactions) between nanofillers and polymers affecting microstructure and global ion-transport mechanism in PCEs.[26] Apart from polymer–nanofiller interactions, the nanofiller–salt interactions (enhances salt solubility and dissociation) and, specifically, the nanofiller–anion interactions (increases Li^+-ion concentration close to the interface majorly

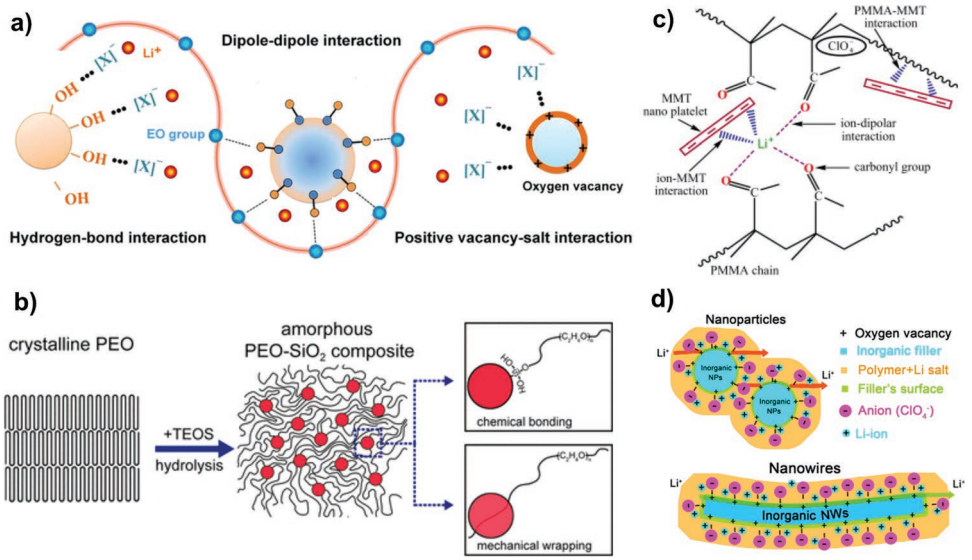

Figure 3. a) Illustration of various noncovalent bonding interactions between a nanofiller, polymer, and salt in PCEs. Reproduced with permission.[33c] Copyright 2019, Wiley-VCH. b) Illustration of chemical interaction (covalent bonding interaction) between PEO and SiO_2 nanofiller facilitating the transition of crystalline PEO to amorphous phase in a polymer composite/PCE. The physical interaction (mechanical wrapping of SiO_2 by amorphous PEO chains) is also shown. Reproduced with permission.[26] Copyright 2016, American Chemical Society. c) The Li^+–MMT, C=O–Li^+–MMT, and C=O—Li^+ complexes formed within a PCE of silicate clay mineral, $LiClO_4$ and, PMMA. Reproduced with permission.[27] Copyright 2014, Elsevier. d) Illustration of interactions between the surface groups of nanofiller and lithium salt anions as a function of change in the filler morphology. Reproduced with permission.[28] Copyright 2016, American Chemical Society.

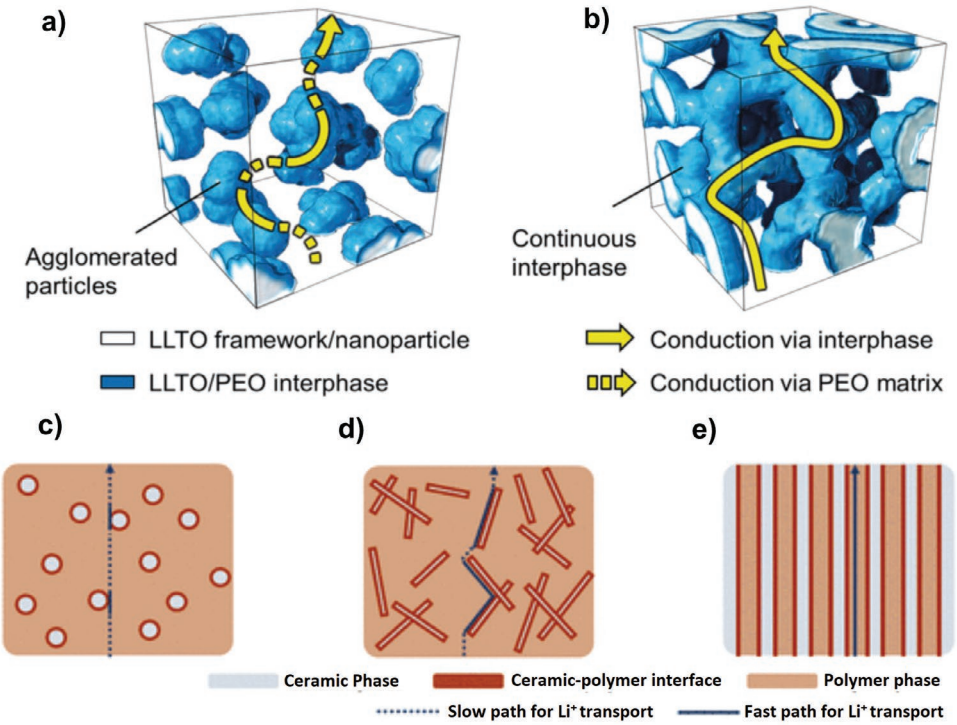

Figure 4. Schematic illustration of ion conduction pathways in PCEs with a) agglomerated LLTO nanofillers and b) 3D continuous LLTO nanofiller, c) low-aspect-ratio nanoparticle fillers, and d) high-aspect-ratio nanowire-shaped fillers. e) Polymer–filler interface and ion transport pathways in a PCE consisting of densely packed, vertically aligned, and continuous nanofiller–polymer interfaces. (a,b) Reproduced with permission.[35a] Copyright 2018, Wiley-VCH. (c–e) Reproduced with permission.[34b] Copyright 2018, American Chemical Society.

due to the immobilization of the anion molecules) are also essential. The nanofillers' size, shape, and morphology along with its compatibility with the polymer matrix will ultimately influence the physical properties and ion conduction mechanism of the resulting PCEs (**Figures** 3d and **4**a–e).[28,34b,35]

A high aspect ratio of the nanofiller is essential for forming an effective polymer–nanofiller interface and, thereby, creating plenty of fast ion transport pathways in PCEs. For instance, low-aspect-ratio nanofillers (e.g., nanospheres, nanocubes, etc.) result in short-ranged and isolated polymer–nanofiller interfaces limiting the ionic conductivity enhancement (Figure 4c–e).[34b] The high loading of such nanofillers in PCEs aiming at achieving a continuous polymer–nanofiller interface can also be a disadvantage due to the tortuosity of the conducting pathways and particle agglomeration. Therefore, high-aspect-ratio nanowires, nanorods, nanofibers, nanotubes, etc., are vital for developing PCEs, since they promote the formation of extended and continuous polymer–nanofiller interfaces leading to fast and well-connected ion transport pathways even at moderate loading. In this context, 2D layered nanomaterials constitute a class of high-aspect-ratio materials already widely explored for various interdisciplinary applications within physics, chemistry, biology, and engineering.[36] They are sheet-like materials with an average thickness of a few nanometers and a lateral size ranging from hundreds of nanometers to a few micrometers.[37] Due to their high aspect ratio and many atoms exposed at the surface, they can induce unique interactions with the polymer host, hence contribute to excellent polymer–nanofiller interfaces and improved physicochemical properties.

This review focuses on the application and impact of 2D layered nanomaterial fillers in PCEs for lithium batteries (LBs). In the context of PCEs, the 2D layered nanofillers covered in this review include i) inorganic (synthetic and naturally occurring), ii) organic–inorganic hybrid, and iii) organic materials (**Figure 5**). The synthetic inorganic 2D layered nanofillers discussed here include graphene oxide (GO), hexagonal boron nitride (h-BN), transition metal chalcogenides and oxides, MXenes, and phosphorene. The naturally occurring inorganic 2D layered clay minerals (2D silicates and layered double hydroxides (LDHs)) are discussed in a separate section. Besides, a general discussion on the scope of using 2D metal–organic frameworks (2D-MOFs) appears in the section dedicated to organic–inorganic hybrid nanofillers for PCEs. Recently, 2D layered organic materials have also started to emerge, where one of the leading contenders is 2D covalent organic frameworks (2D COFs). Considering the potential of COFs as active and passive components in PCEs, one of the sections of this review provides an overview of 2D COFs in the futuristic polymer organic composite electrolytes (POCEs). While discussing key literature reports, this review article also emphasizes the electrochemical properties of the PCEs and related LB cells. The final section of the review summarizes the landscape of PCEs based on 2D layered nanomaterials followed by a brief outlook on their prospects.

2. 2D Layered Nanomaterials: Synthesis, Exfoliation, and Intercalation

Layered materials possessing weakly stacked 2D platelets forming 3D structures with characteristic features like strong in-plane covalent and weak out-of-plane noncovalent bonds (e.g., van der Waals interaction) exhibit unique physical and chemical properties.[49] 2D layered nanomaterials are derived from bulk 3D layered materials by exfoliation (top-down) or precursors by restricting the growth in 2D (bottom-up) approaches. Although a single-layer (monolayer) of a 2D nanosheet is commonly ideal, the out-of-plane interactions between individual 2D nanosheets lead to stacked multiple layers (less than ten), often called few-layered 2D nanomaterials.[50] Both single- and few-layered 2D nanomaterials are suitable for PCE preparation.

The bottom-up synthesis of single- and few-layered 2D nanomaterials is possible using various types of chemical/physical vapor deposition (CVD/PVD) techniques, wet chemical routes, etc.[51] The basic concept behind the bottom-up approach is the construction of 2D layered nanomaterials from atomic or molecular precursors by chemical reactions or self-assembly processes. **Figure 6**a–c summarizes the primary methods for bottom-up synthesis of 2D layered nanomaterials.[51a–e,g] A detailed explanation of the bottom-up synthesis of 2D layered nanomaterials is beyond the scope of this review, and readers are referred to other dedicated review articles in this respect.[52]

As an alternative to bottom-up approaches, the top-down approach of the 2D layered nanomaterial synthesis is equally essential.[51c,53] The top-down approach involves exfoliating bulk layered structures to 2D counterparts by pure mechanical effects (shockwaves, shear and compression effects, tensile stress, etc.)[54] or assisted by intercalation from a liquid solution. **Figure 7** summarizes the common top-down approaches for 2D layered nanomaterial synthesis. Perhaps, the best example is the scotch-tape method for the mechanical exfoliation (micromechanical cleavage) of graphite (bulk material) to produce individual graphene layers.[50,55] Similar mechanical exfoliations of h-BN, MoS_2, etc., are also known.[56] Ball-milling (wet or dry), ultrasound-assisted exfoliation, etc., are the other top-down exfoliation methods governed by mechanical effects.[54]

In the case of intercalation-assisted exfoliation, the intercalating species (e.g., solvent molecules, ions, reactive species, polymers, surfactants, etc.) present in the solution access the interlayer galleries of the bulk layered material to facilitate the exfoliation.[49c,59] The intercalant disrupts the physical interactions between the interlayers, leading to the straightforward exfoliation of bulk layered materials into nanosheets aided by perturbations such as ultrasonic agitation or magnetic stirring. For example, solvent molecules that intercalate (swell) into the interlayer galleries of the bulk layered double hydroxide (LDH) help produce LDH nanosheets (**Figure 8**a).[44] Indeed, the co-intercalation of surfactant molecules and ions often improves the exfoliation quality.[49c,60,61,62] Alternatively, chemically reactive intercalants (e.g., oxidizing and reducing agents) in a solution can also facilitate the cleavage of bulk material to single- or few-layered 2D nanosheets, known as chemical exfoliation.[49a,b,51c,63] One of the most well-known examples of an oxidative chemical exfoliation process is the exfoliation of graphite to graphene oxide (Figure 8b).[57,64] Another example is converting a MAX phase into a MXene phase by hydrofluoric acid (HF)-based selective etching of aluminum (Al) from the interlayers (Figure 8c,d).[58,65] The exfoliation of layered MoS_2 bulk material by reaction with butyllithium is also frequently utilized.[51g,66] Secondary processes, such as mechanical agitation or solvent exchange/washing, can also improve the efficacy of chemical exfoliation.

A detailed overview of various exfoliation and other 2D layered nanomaterial fabrication methods is already available in the literature.[49b,51c,63a,67] In any case, 100% exfoliation of the bulk material into single layers is often not possible. In most

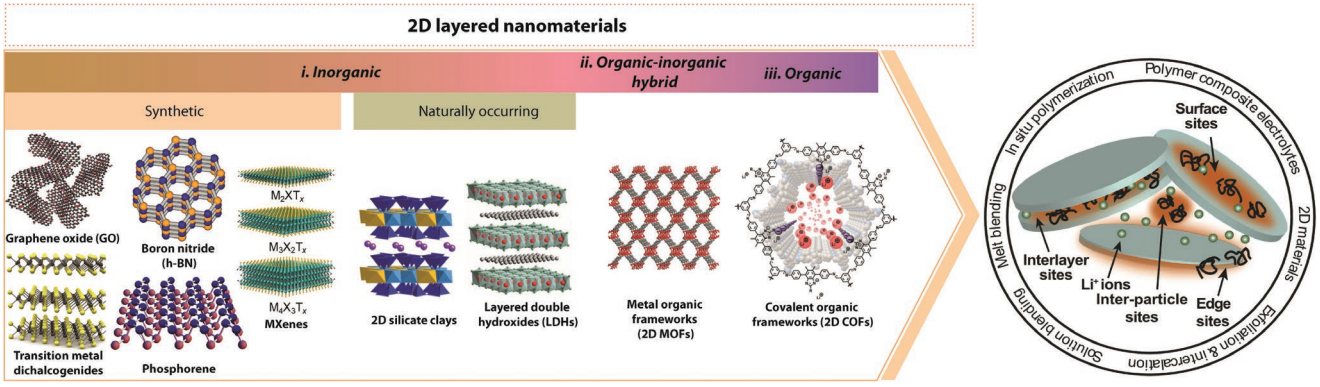

Figure 5. Representative structures of the 2D layered nanofillers covered in this review article along with the illustration of the possible interactions occurring in the resulting PCE. The illustration regarding the interactions within a PCE is partially inspired by Oreffo et al.[134c] Graphene oxide (GO): Reproduced under the terms of the CC BY 4.0 license.[38] Copyright 2018, The authors, published by Springer Nature. Boron nitride (h-BN): Reproduced with permission.[39] Copyright 2009, American Physical Society. Transition metal dichalcogenides: Reproduced with permission.[40] Copyright 2011, Springer Nature Customer Service Centre GmbH. MXenes: Reproduced with permission.[41] Copyright 2020, American Chemical Society. Phosphorene: Reproduced under the terms of the CC BY 3.0 license.[42] Copyright 2014, IOP Publishing Ltd and Deutsche Physikalische Gesellschaft. 2D silicate clays: Reproduced with permission.[43] Copyright 2018, Springer International Publishing Switzerland. Layered double hydroxides (LDHs): Reproduced with permission.[44] Copyright 2015, American Chemical Society. Metal organic frameworks (2D MOF): Reproduced with permission.[45] Copyright 2021, American Chemical Society. Covalent organic frameworks (2D COFs): Reproduced with permission.[46] Copyright 2019, American Chemical Society.

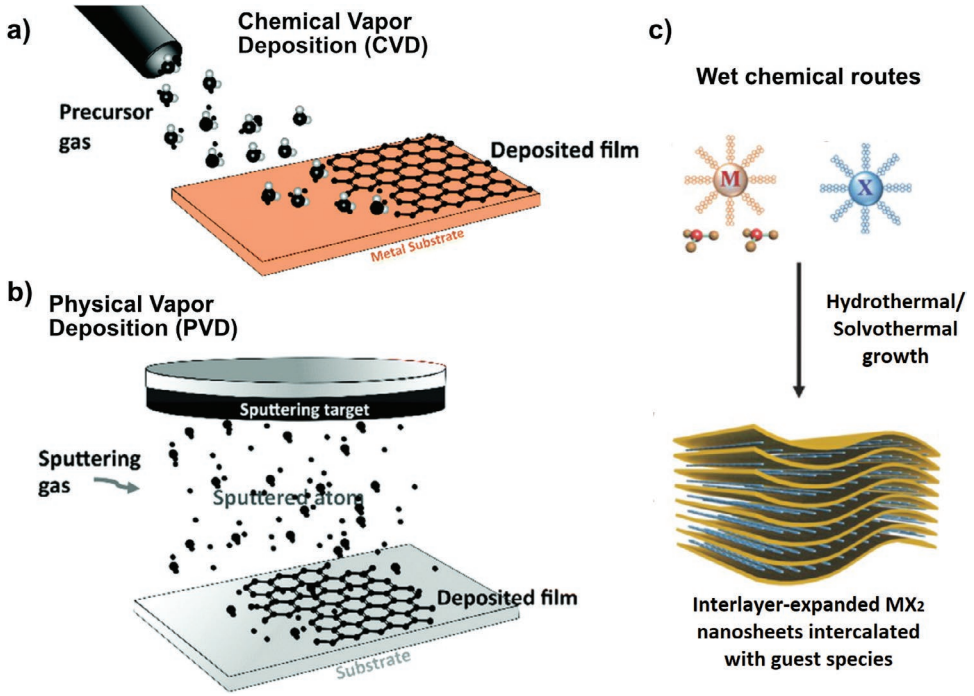

Figure 6. Schematic illustration of bottom-up approaches for the synthesis of 2D materials. a) CVD and b) PVD of 2D layered nanomaterials from gaseous precursors; Reproduced under the terms of the CC BY 3.0 license.[51e] Copyright 2020, The authors, published by Royal Society of Chemistry; permission conveyed through Copyright Clearance Center, Inc. c) Wet chemical synthesis of 2D layered nanomaterials. Reproduced with permission.[51g] Copyright 2017, Wiley-VCH.

cases, the 2D layered nanomaterials tend to restack and exist as few-layered nanosheets. Laboratory-synthesized and commercially available 2D layered nanomaterials are often a mixture of single and few-layered nanosheets, which are also suitable for composite preparation through mixing with polymers.

Secondary-intercalation of polymer molecules during polymer composite preparation is highly beneficial in polymer composites, which can further tweak interactions between individual layers of few-layered 2D nanomaterials, favoring further exfoliation. The extent of intercalation and exfoliation determines the microstructure of a polymer composite. Four different types of microstructures (**Figure 9**) viz., (a) unintercalated (phase-separated/conventional composites), (b) intercalated, (c) fully exfoliated, and (d) a mix of partially intercalated and exfoliated structures, are standard when using 2D layered nanomaterials for polymer composite preparation.[48b]

3. Processing of Polymer Composites and PCEs

Polymer composites capable of exhibiting ionic conductivity (inherent ion conduction or ion conduction achieved by post-processing such as activation by a liquid electrolyte), functional

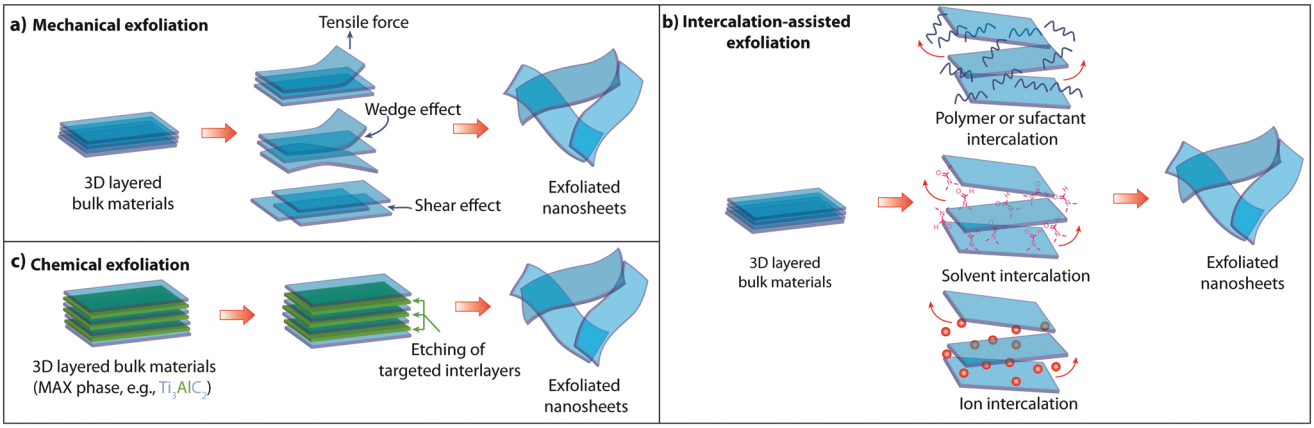

Figure 7. Schematic illustration of top-down approaches for 2D layered nanomaterials fabrication. a) Mechanical exfoliation, b) intercalation-assisted exfoliation, and c) chemical exfoliation. This illustration is inspired by Singh et al.[49d]

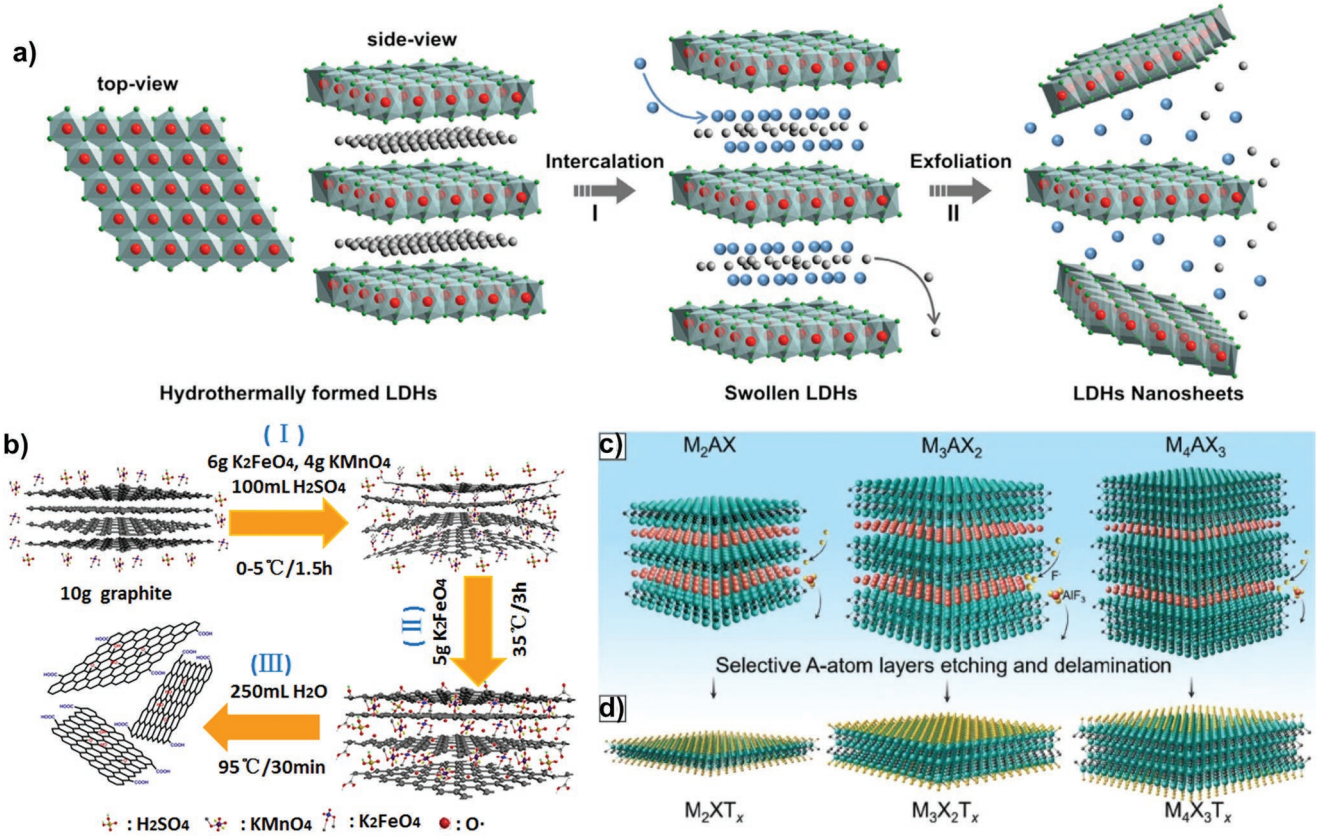

Figure 8. Examples of intercalation-assisted exfoliation of bulk layered materials into 2D layered nanomaterials. a) Solvent intercalation: LDH nanosheets produced from bulk LDH by solvent intercalation. Reproduced with permission.[44] Copyright 2015, American Chemical Society. Oxidative chemical exfoliation: b) chemical exfoliation of graphite into graphene oxide by a modified Hummers' method. Reproduced under the terms of the CC BY 4.0 license.[57] Copyright 2016, The authors, published by Springer Nature. c,d) Exfoliation of MAX into MXene layers by the selective etching of Al in the MAX phase by HF treatment. Reproduced with permission.[58] Copyright 2020, Springer Nature.

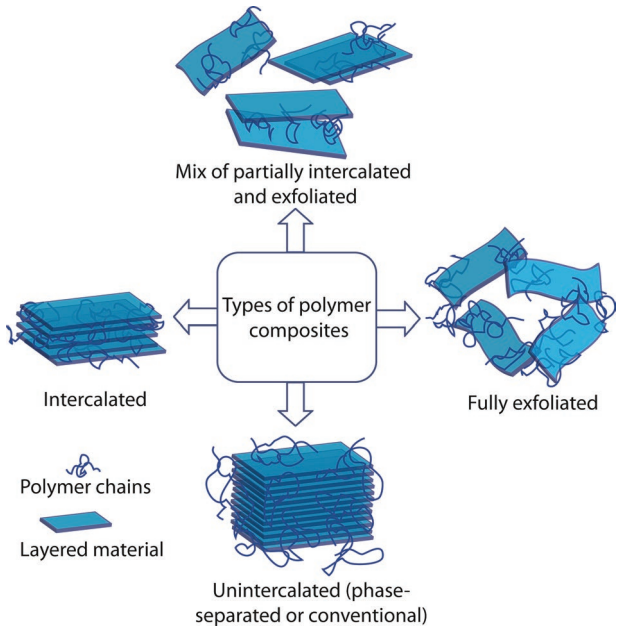

Figure 9. Microstructures of polymer composites based on 2D layered nanomaterials. The illustration is inspired by Chua et al.[48b]

as separators/electrolytes in electrochemical devices are called PCEs. Generally, three methods are widely popular in the processing of PCEs: 1) solution-blending, 2) melt-blending, and 3) in situ polymerization.[9,48] The following part of this section emphasizes the processing of PCEs based on 2D layered nanomaterials.

3.1. Solution-Blending

Solution-blending is a polymer composite preparation technique involving the mixing (blending) of polymer and (2D layered) nanofiller in a suitable solvent to form a polymer–nanofiller solution/dispersion.[68] Vigorous agitation is essential here to ensure proper dispersion of nanofillers in the polymer solution. Magnetic stirring, shear mixing, ultrasonication, etc., are a few examples of standard agitation techniques. The solution-blending process may be carried out at RT or by applying external heat depending on the chemical and physical properties of the used components. In most instances, the thermodynamic dissolution process of polymer accelerates at elevated temperatures.[69]

It is possible to adapt solution blending method to prepare different types of PCEs.[48a] This method involves a solvent system (or a mixture of solvents) that simultaneously dissolves

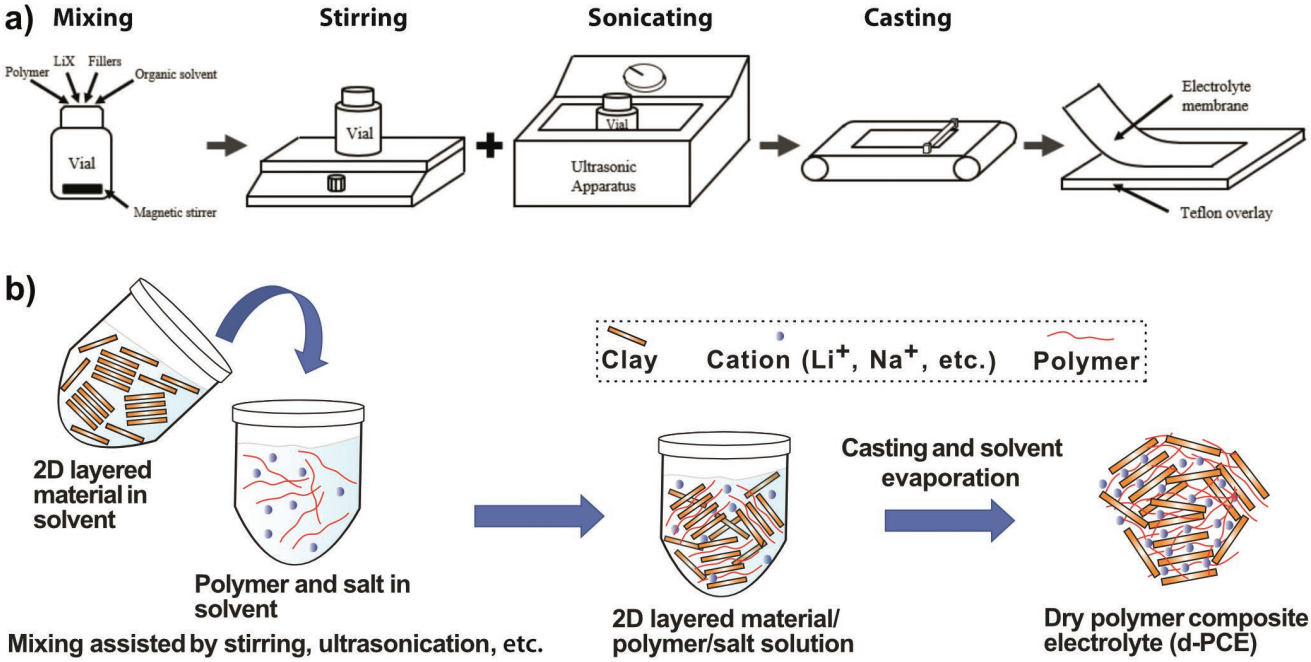

Figure 10. a) Illustration of a typical solution-blending method for d-PCE preparation. Reproduced under the terms of the CC BY 4.0 license.[31] Copyright 2021, The authors, published by Springer Nature. b) Solution-blending method for d-PCE preparation based on 2D layered nanomaterial. Reproduced with permission.[9] Copyright 2021, The authors, published by Royal Society of Chemistry.

the polymer and salt, and disperses the nanofiller (including 2D layered nanofillers). The polymer–nanofiller–salt slurry can be cast on a flat surface, followed by complete evaporation of the solvent to render a dry PCE (d-PCE) (the term d-PCE refers to PCEs that are free of any solvent or liquid plasticizer).[70] During the d-PCE preparation by solution-blending method, it is essential to confirm the complete evaporation of the solvent. Otherwise, the residual solvent may also contribute to the ionic conductivity or affect the electrochemical performance if the used solvent is incompatible with the battery components. It is also possible to intentionally add battery-compatible solvents or liquid plasticizers during the solution-bending process, which may aid the PCE processing, and, later, facilitates ionic conduction after the PCE film formation. Such PCEs with an intentionally added battery-compatible liquid plasticizer or a solvent can be called gel PCE (g-PCE). It is important to note that the terms d-PCE and g-PCE are not commonly used terminologies in the PCE literature. Still, we use these two terms throughout this review article to help the readers distinguish between PCEs with and without liquid components. Another method of g-PCE preparation involves the use of solution-blending approach for preparing a dry polymer composite film and activating the same in a liquid electrolyte. During this step, the otherwise insulating polymer composite film swells in the liquid electrolyte, leading to a semisolid g-PCE. **Figure 10**a shows a flowchart representing the general d-PCE processing (assume that the organic solvent evaporation is complete) steps by the solution-blending method,[31] and Figure 10b emphasizes the formation of d-PCE specifically using 2D layered nanomaterials.[9]

The solution-blending technique is simple but has the disadvantage of potential solvent wastage. An advantage is that the solution-blending allows an efficient nanofiller-dispersion irrespective of the polymer polarity.[68b] However, it is essential to consider the compatibility between the solvent and polymer/nanofiller to avoid undesirable chemical reactions, and in the case of g-PCE, the absorbed solvents/plasticizer should be retained.

3.2. Melt-Blending

Melt-blending is a solvent-free process used for polymer composite preparation, also called melt-processing.[48a,69] This technique is helpful in the industrial production of various types of polymer composites (**Figure 11**a).[31] It involves intermixing of nanofillers (including 2D layered) and polymers at a temperature above the softening point of the polymer, mostly under inert gas flux. Usually, the polymer is heated above its melting point (molten state), and then the nanofillers are introduced under mechanical mixing. In some cases, the dry polymer and nanofiller mixture is heated until the polymer is melted under a shear mixing force. The shear mixing allows the nanofiller to get effectively distributed in the molten polymer resulting in polymer composites with enhanced mechanical stability when cooled to RT. Industrial processes such as extrusion and injection molding, used in the commercial fabrication of thermoplastic and elastomer material, are compatible with melt-blending for incorporating nanofiller into the polymer melt. The hence-formed polymer–nanofiller melt can be subjected to secondary processes such as molding and casting to produce various shapes, including films. If the melting point of the polymer is too high, then low-M_w

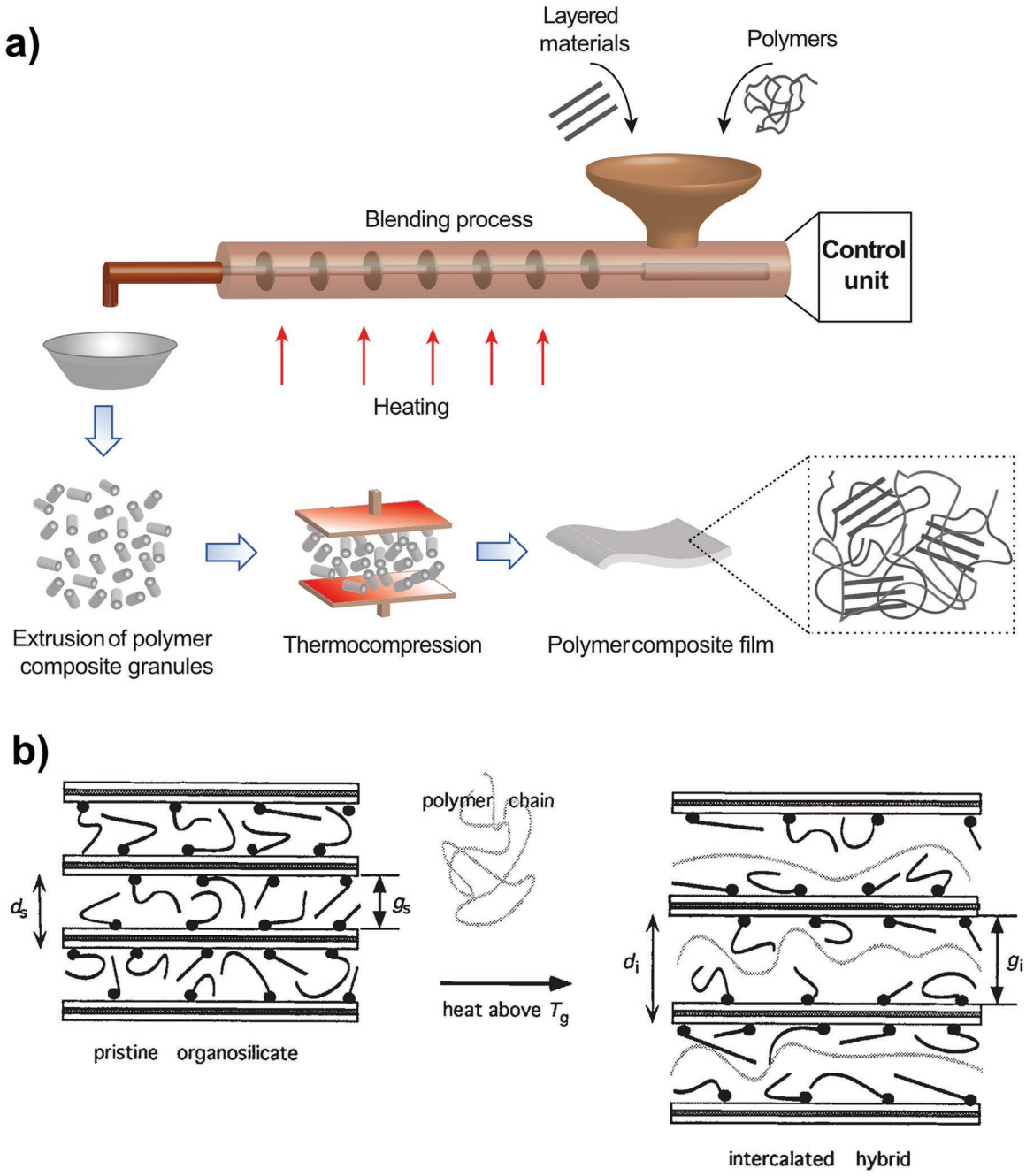

Figure 11. a) Scheme showing the industrial production of polymer composites by the melt-blending method. b) Illustration of intercalation of polymer chains into the interlayer galleries of layered silicates during melt-blending. Reproduced with permission.[71] Copyright 1996, Wiley-VCH.

polymer alternatives could be used to avoid unwanted thermal decomposition of nanofillers or other additives; however, such an effort may lead to poor mechanical stability of the resulting PCE.

Secondary polymer intercalation into 2D layered nanofillers is possible during the melt-blending process. This phenomenon is often called melt intercalation, which is a solvent-free intercalation process.[72] Figure 11b depicts the melt intercalation of polymers into layered silicates.[48a,71] The melt-blending process needs to be carefully designed since many lithium salts (e.g., $LiPF_6$, $LiBF_4$, etc.) decompose close to the melting temperature of the employed polymers melt. Besides, it is essential to ensure that the polymer melt dissolves the salt without precipitation, since the efficiency of solvent-assisted salt dissolution is absent in the melt-blending process unlike solution-blending. Therefore, the melt-blending process that involves pressing polymer–nanofiller–salt mixture under high temperature and pressure is often employed in preparing d-PCE films (**Figure 12**a). "Thermocompression" or "hot-pressing" is commonly used to address the above method of melt-blending.[31]

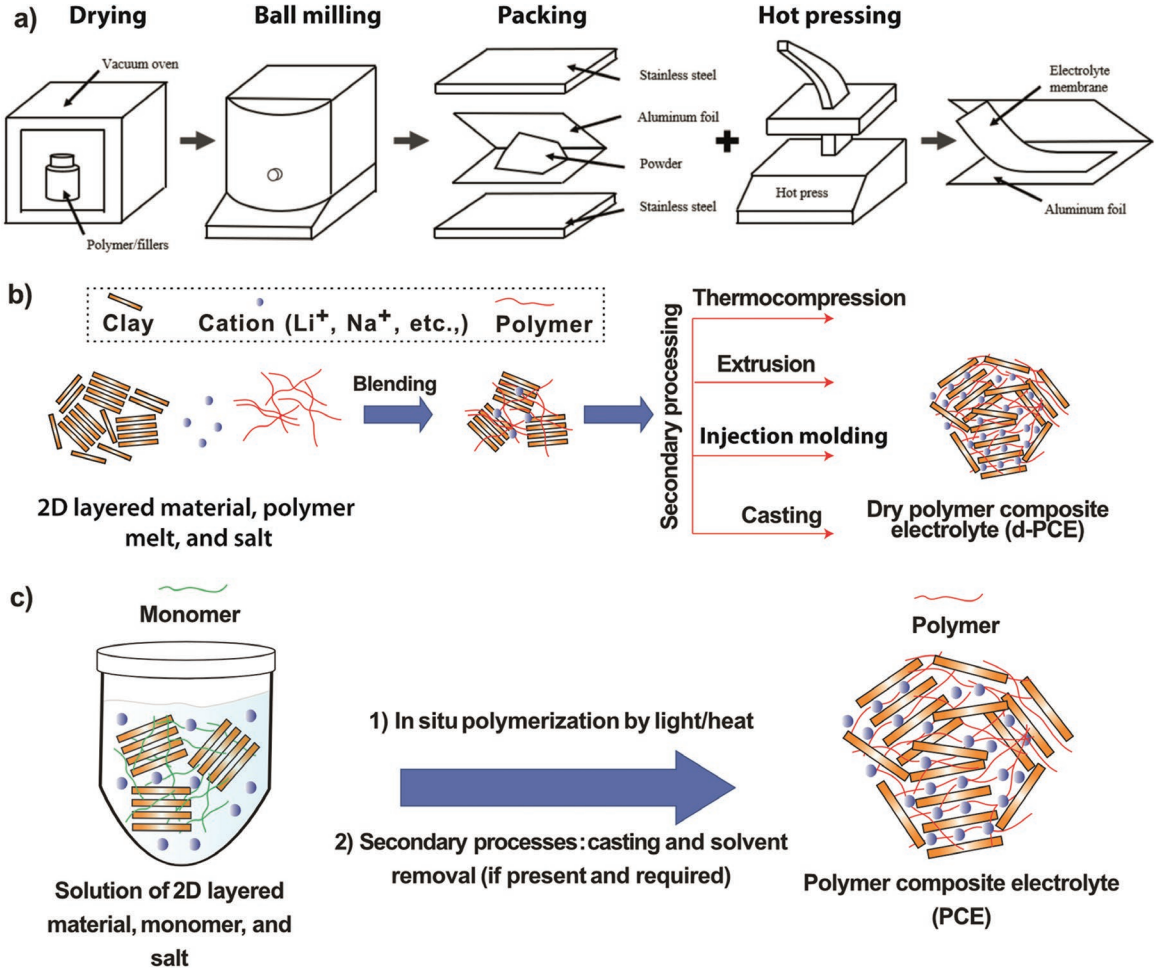

Figure 12. Schemes showing the preparation of PCEs using a) typical thermocompression/hot-press method. Reproduced under the terms of the CC BY 4.0 license.[31] Copyright 2021, Springer Nature. b) Melt-blending method (using 2D layered nanomaterials) and c) the in situ polymerization method. Reproduced with permission.[9] Copyright 2021, Royal Society of Chemistry.

In the thermocompression method, thorough dry mixing (at various temperatures) of the polymer, salt, and the nanofiller is ensured using a mortar and a piston or a ball mill. Later, the required amount of the mixture is placed between two stainless steel plates (sometimes, aluminum or polyethylene terephthalate foils are used in between to avoid the sticking of the polymer to the hot plate) and subjected to hot-press under high pressure, thereby providing peelable d-PCE films once cooled to RT. The pressure and temperature used in the hot press depend on the nature of the polymer. The advantage of the thermocompression is that a complete melting of the polymer is unnecessary. Compared to conventional melt-blending, the thermocompression technique is rapid and easy for shaping d-PCEs. However, the dry mixing step must be efficient to ensure the homogenous distribution of polymer, nanofiller, and salt in the d-PCE. Besides, the intercalation of polymer molecules and ions into 2D layered nanomaterials under thermocompression is relatively difficult to achieve compared to solution-blending and conventional melt-blending processes. Therefore, the PCEs from thermocompression will be mostly phase-separated unless the 2D layered nanofiller is pre-intercalated or pre-exfoliated. Figure 12b illustrates the general scheme of a conventional melt-blending process in the context of d-PCEs.

3.3. In Situ Polymerization

In situ polymerization is a method that has been getting attention as an alternative to solution-blending, melt-blending, and thermocompression for preparing PCEs. Figure 12c illustrates the typical steps involved in the in situ processing of PCEs using 2D layered nanofillers. Conventional methods of polymer composite processing employ fully-grown high-M_w polymer hosts to prepare nanofiller dispersions. By contrast, the in situ polymerization method follows an alternate approach involving the polymer host formed from a reactive polymerizable precursor solution.[1a] A precursor solution—a reactive mixture composed of the inorganic nanofiller, reactive monomer/oligomer/telechelic polymers, and often a polymerization initiator—is necessary for the in situ polymerization process.[73] The precursor solution polymerizes into polymer

chains or networks, often on light irradiation or heat. During the in situ polymerization process, the formed polymer chains intercalate between the interlayer galleries of the individual 2D layers, the surface, and the surroundings (wrapping) of the 2D layered nanosheets. Therefore, the in situ polymerization allows the fabrication of various PCE microstructures (Figure 9).

In situ polymerization should be considered a bottom-up approach since the final composite contains a polymer host derived from the reactive constituents present in the polymerizable precursor solution. The other methods of polymer composite preparation discussed earlier are instead top-down approaches, as they all involve mixing a fully grown polymer and nanofiller. While the in situ polymerization method is already known for preparing many types of polymer composites, it has not received much attention for the fabrication of PCEs, which is dominated by solution and melt-blending methods until now. However, the in situ polymerization method constitutes an attractive approach due to the processing advantages and design flexibility to realize both g-PCEs and d-PCEs.

In the following sections of this review article, a comprehensive overview of different types of 2D layered nanomaterials and their application as nanofillers in PCEs is presented.

4. PCEs for Lithium Batteries Using Synthetic Inorganic 2D Layered Nanomaterials as Fillers

4.1. Graphene Oxide as Nanofiller in PCEs

Graphene is a one-atom-thick electronically conducting 2D layered allotrope of carbon with sp^2 hybridized carbon atoms arranged in a hexagonal lattice.[55,74] The exfoliation of graphite is an example of a top-down synthesis of graphene, whereas bottom-up synthesis by chemical and physical deposition techniques is also well known.[75] Graphene is highly electrically conducting, hence it is often not used in PCEs in pristine form but it is useful as electrode materials and additives in LIBs.[76]

In this part, we explore the use of GO, a chemically modified and electronically insulating (often semiconducting depending on the degree of oxidation) form of graphene as a potential 2D layered nanofiller in PCEs. As mentioned in the previous sections, oxidative chemical exfoliation of graphite by Hummer's method results in GO.[57,77] The surface and basal planes of GO have various oxygen functional groups, e.g., C−OH, C−O−C, C=O, and O=C−OH, which disrupt the sp^2 hybridization of carbon and long-range π-stacking, resulting in a less electronically conducting form. Indeed, these oxygen-functional groups are suitable for PCEs as they act as anchoring sites for Li^+-ions and often interact with the polymer host.[9,78]

Yuan et al. used 2D GO nanosheets (1.0 wt%) for a d-PCE based on PEO host and lithium perchlorate ($LiClO_4$) salt (**Figure 13**a).[78a] The interaction between the GO and surrounding polymer host in the d-PCE accounts for 260% higher tensile strength than the pristine DPE. The GO nanofiller also disrupts the PEO crystallization and exhibits a maximum RT ionic conductivity of 0.02 mS cm^{-1}, nearly two orders higher than the DPE free of GO. However, for using this d-PCE in an LIB full cell ($LiCoO_2$ (LCO)||graphite), an additional step of surface wetting of electrodes by liquid electrolyte was required, which improved the contact between electrode and electrolyte. The cell displayed an areal capacity of 0.17 mAh cm^{-2} with stability over 70 cycles. In another report, Jia et al. developed a flexible PCE based on polyacrylonitrile (PAN)-based polymer matrix, $LiClO_4$ salt, and GO (1.0 wt%) 2D nanofillers.[78b] They proved that oxygen functionalities of GO could act as Lewis base sites to interact with the −C≡N functional groups in PAN aiding in an effective Li salt dissociation (Figure 13b). The resulting d-PCE demonstrated one order of increase in ionic conductivity (0.4 mS cm^{-1}, 30 °C) and doubled tensile modulus (80 MPa) than the GO-free counterpart. Finally, the d-PCE in an LFP||Li cell delivered a discharge capacity of 166 mAh g^{-1}, at least 25% higher than GO-free cells (136 mAh g^{-1}). As discussed earlier, here also surface wetting of the LMB electrodes by additional liquid electrolyte was unavoidable to ensure good electrode–electrolyte contact.

Grafting/functionalization of GO is also a valuable strategy for PCE preparation. The grafting process improves the dispersion of the nanofiller in the polymer host, resulting in homogenous PCEs. For example, Zhao et al. used PEO-grafted GO for PCEs composed of polyvinylidene difluoride (PVDF)-hexafluoropropylene (HFP) polymer host, a room temperature ionic liquid (RTIL) plasticizer, and Li-salt (lithium bis(trifluoromethylsulfonyl, LiTFSI).[79] The resulting g-PCE with PEO-grafted GO (2.4 wt%) was claimed to display better ionic conductivity (1.6 mS cm^{-1}, 30 °C) and interfacial compatibility with Li metal than its pristine-GO encompassed counterpart. In an LFP||Li cell, the g-PCE displayed a specific capacity of 40 mAh g^{-1} at a high C-rate of 5 C (RT). Another report also used a similar polymer-grafted GO for the preparation of d-PCE and V_2O_5||Li cells, which showed a discharge capacity of 287 mAh g^{-1} at 60 °C and 0.1 C.[80] It is worth mentioning that in several recent reports, RTILs and poly ionic liquids (PILs) are also used to postfunctionalize GO and use it as a nanofiller in PCE.[81]

Fouladvand et al. compared the effect of sulfonated GO (SGO) as a nanofiller in d-PCEs based on PVDF host.[83] The report claimed a high RT ionic conductivity (6.2 mS cm^{-1}) and t_{Li}^+ close to unity for a d-PCE loaded with a small quantity of SGO (0.004 wt%) over the GO counterpart. The high t_{Li}^+ value of the d-PCE could be due to the $-(SO_3)^-$ groups in SGO favoring selective Li^+-ion transport. The LMB cell ($LiMnO_2$||Li) based on the SGO-based d-PCE at RT delivered a specific capacity of 204 mAh g^{-1} at 0.1 C with 97% retention over 100 cycles. SGO is an exciting derivative of GO as its single-ion conducting feature can be applicable for preparing single-ion conducting PCEs. In such a work, Nicotera et al. loaded SGO in the lithiated Nafion host and activated it in liquid electrolyte (ethylene carbonate (EC)/propylene carbonate (PC), 1 M lithium trifluoromethane sulfonate, LiOTf), resulting in single-ion conducting g-PCEs (Figure 13c).[82] This g-PCE displayed an ionic conductivity close to 0.5 mS cm^{-1} at RT and t_{Li}^+ value close to unity. At 0.05 C, the LFP||Li cell with the SGO-based g-PCE

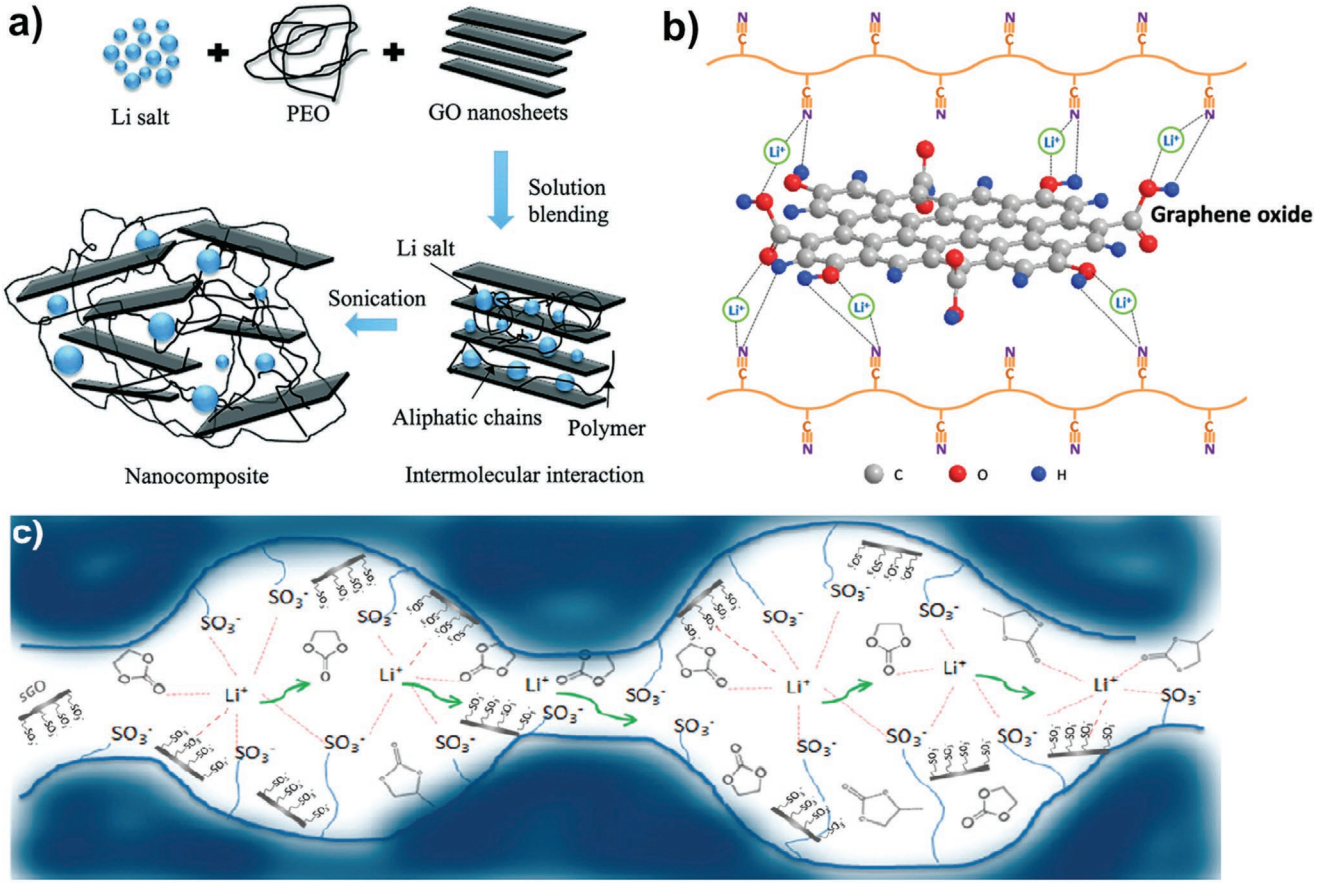

Figure 13. a) Solution blending of GO, PEO, and Li salt for the preparation of d-PCE and illustration of their intercalation and related intermolecular interactions. Reproduced with permission.[78a] Copyright 2014, Royal Society of Chemistry; permission conveyed through Copyright Clearance Center, Inc. b) Ion-transport mechanism in PCE made of GO, PAN, and Li salt assisted by Lewis acid–base interactions involving oxygen functionalities of GO. Reproduced with permission.[78b] Copyright 2018, Elsevier. c) Mechanism of single-ion conduction in g-PCE based on lithiated Nafion and sulfonated GO. Reproduced with permission.[82] Copyright 2019, American Chemical Society.

showed a specific capacity of 100 mAh g^{-1} (30 °C) with stability over 50 cycles.

All the above reports suggest that both GO and functionalized GO are equally suitable for d-PCEs and g-PCEs. GO provides opportunities for surface modification due to the availability of many oxygen functionalities. The general reason for using GO over graphene in PCE is its lower electronic conductivity. However, Liu et al. suggested that the electronic conductivity of graphene is not significant when used in tiny amounts for preparing g-PCEs. They used the graphene nanofiller in tiny amounts of 0.002 wt% in the PVDF host for the preparation of a polymer composite film, followed by its activation in liquid electrolyte.[84] Interestingly, the ionic conductivity was doubled to 3.61 mS cm^{-1} in the g-PCE with graphene than its graphene-free counterpart. The porosity of the polymer composite membrane was also improved by 50% in the presence of graphene, which influences the electrolyte uptake (160% increase). The researchers also demonstrated the cycling of g-PCEs at RT in an LCO||Li cell for more than 100 cycles without any issues related to short-circuit arising from the graphene nanofillers. Ultimately, all forms of graphene, e.g., pristine graphene, GO, functionalized GO, etc., or even the reduced GO (rGO), are suitable for PCEs, but in appropriate amounts according to its electronic properties. More investigations and validations are inevitable to bring maximum benefits out of various forms of graphene as 2D layered nanofillers for PCEs.

4.2. Boron Nitride as Nanofiller in PCEs

The chemical compound boron nitride (BN) has an equal number of B and N atoms in its structure. It is isoelectronic to sp^2 carbon lattice, and the structure is comparable to carbon allotropes. Therefore, BN is often called "white graphene/graphite."[39,85] The four different polymorphic forms of BN are i) hexagonal BN (h-BN), ii) rhombohedral-BN (r-BN), iii) cubic polymorph BN (c-BN), and iv) wurtzite BN (w-BN) (**Figure 14**a–d).[86] Among them, h-BN gained much attention due to its peculiar properties such as, low dielectric constant, high thermal/chemical stability, and intrinsic electrical insulation characteristics.[86c,87] The synthesis of h-BN employs mechanical separation, CVD, wet chemical routes, etc.[86c,88] In h-BN (honeycomb-like structure), B and

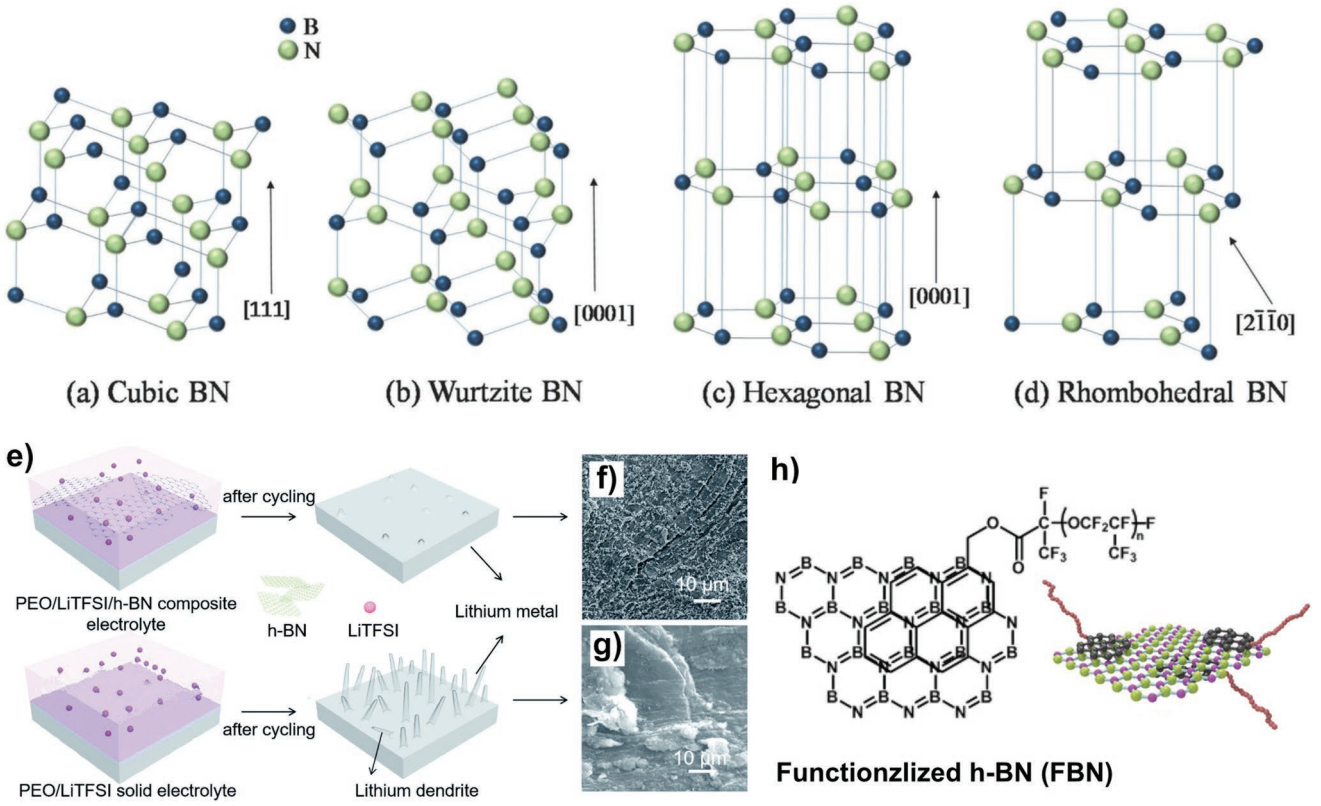

Figure 14. Various crystal structures of boron nitride: a) cubic, b) wurtzite, c) hexagonal, and d) rhombohedral. Reproduced with permission.[86c] Copyright 2018, Wiley-VCH. e) An illustration showing the role of h-BN in the PCE in suppressing the dendrite growth during cycling. f,g) The scanning electron microscopy (SEM) images of the Li metal surface after long-term Li plating/stripping cycling with respective PCEs. Reproduced with permission.[92] Copyright 2020, Royal Society of Chemistry. h) Structure of the functionalized h-BN (FBN). Reproduced with permission.[93a] Copyright 2017, Royal Society of Chemistry.

N atoms are arranged alternately where the B—N bond length is 1.45 Å. The interlayer spacing between two layers of h-BN is 0.333 nm (interlayer spacing in graphene is 0.335 nm).[89] Similar to graphene, the weak van der Waals forces hold the adjacent layers together, and the three sp^2 hybrids formed by each B and N atom in h-BN give a graphene-like layered structure.[89,90] h-BN finds application in batteries as an electrode additive, interfacial layers to resist dendrites related short-circuit, and 2D nanofillers in g-PCEs and d-PCEs. For example, h-BN has been studied as a nanofiller in LIB electrodes to produce binder-free anodes, which achieved enhanced cycling stability and specific capacity at higher C-rates.[91] However, in this review, we are discussing the role of h-BN as nanofiller in PCEs.

The porosity control and related electrolyte uptake as a function of h-BN nanofiller additive amount in a polymer host are shown by Aydin et al.[94] After the activation in 1 M $LiPF_6$ in EC:EMC (1:1) v/v solution, the g-PCE membrane exhibited a high ionic conductivity (>10^{-3} S cm^{-1} at RT) and higher oxidation stability (4.7 V vs Li|Li^+) than the h-BN-free sample. The g-PCE membrane in LCO||Li cells delivered a high specific capacity of 144 mAh g^{-1}. Indeed, it has been noted that the porosity of the polymer composite membrane and the uptake of liquid electrolyte are influenced by h-BN addition, which determines the overall performance of the resulting g-PCE. Therefore, it is worth highlighting that rather than acting as a true g-PCE, the polymer composite after activation functions as a separator to hold the liquid electrolyte components. An attempt to prepare a true d-PCE based on PVDF-HFP and h-BN nanofiller with improved electrochemical and physical properties was reported by Zhang et al.[95] The d-PCE composed of 1.0 wt% h-BN additive demonstrated enhanced ionic conductivity and mechanical characteristics compared to the h-BN-free counterpart. Although the PCE claims a high ionic conductivity of 1.82 mS cm^{-1} at RT, the contribution to the ionic conductivity from the residual solvent is evident. The presence of dimethylformamide (DMF) impurity could be one of the reasons for the considerable drop in capacity within the first 50 cycles of an LFP||Li cell. Therefore, more studies are necessary to decipher the exclusive influence of h-BN fillers in d-PCEs.

Recently, Li et al. reported for the first time a d-PCE based on h-BN nanofiller in PEO.[92] Interestingly, they observed a decrease in ionic conductivity by adding the h-BN nanofiller into the PE. Notably, the t_{Li^+} value and electrochemical stability window of the d-PCE containing h-BN were higher than the h-BN-free counterpart. The density functional theory (DFT) calculations and molecular dynamic (MD) simulations proved that h-BN has a peculiar feature of binding with TFSI anion; in other words, adding h-BN facilitates selective Li^+-ion

transport. The high t_{Li}^+ value of the d-PCE also reflected on its dendrite-suppression capabilities compared to a PCE free of h-BN (Figure 14e–g). In a recent report, Erikson et al. compared the effect of oxide nanofillers, e.g., Al_2O_3, TiO_2 and h-BN, in a d-PCEs made of poly(ε-caprolactone) (PCL) and lithium salt.[96] An apparent reduction in PCL crystallinity was evident in all the d-PCEs with nanofillers. However, they also observed no significant improvement in ionic conductivity in the case of h-BN compared to oxide nanofillers. Although this work did not consider the t_{Li}^+ values, it mentions that the difference in ion transport properties could be due to the varied nature of interactions of nitrides with PCL than oxides. All these recent reports indicate that more efforts are required to understand the behavior of h-BN against different polymer hosts and lithium salts while considering it as a potential nanofiller in PCEs.

Like GO, functionalized h-BN (FBN) also received attention as an additive in PCEs.[93] Shim et al. demonstrated the lithium dendrite suppression ability of PCEs based on functionalized few-layer h-BN-nanoflakes (BNNFs) in S||Li and Air||Li batteries.[93a] They functionalized the h-BN surface with perfluoropolyether (PFPE) (Figure 14h) and used it for PVDF-HFP-based g-PCEs. The functionalization increased the compatibility of the nanofiller particles with the polymer matrix. They observed that h-BN could interact with Li^+-ions enhancing the cation transport properties by trapping the anions. 1 M solution of LiTFSI in EC:DEC is used to produce g-PCEs. The hence produced g-PCE enhanced overall physicochemical and electrochemical characteristics even with 0.5 wt% of PFPE-functionalized BNNFs. Interestingly, unlike other reports, the presence of FBN in g-PCE improved the ionic conductivity (0.8 mS cm^{-1}), maintaining an appreciable t_{Li}^+ value (0.62). Overall, this report highlights that modifying h-BN could be a viable strategy to improve its compatibility with otherwise noncompatible polymer hosts, e.g., PCL. Similarly, h-BN functionalized by SiO_2 in the form of boron nitride nanosheets (BNNS) has been used as a nanofiller in d-PCEs to produce multicomponent systems such as PEO/LiTFSI/SiO_2@BNNS.[93b] Using this approach, thermal stability, electrochemical stability, dendrite resistance, t_{Li}^+ and long term cyclability of the d-PCEs are enhanced.

4.3. 2D Transition Metal Dichalcogenides (2D TMCs) and Oxides (2D TMOs) as Nanofillers in PCEs

Like graphite, layered TMCs, commonly represented as MX_2 (M and X represent the group 4–10 transition metals and group 16 chalcogen elements of the periodic table, respectively), consist of monolayers stacked to each other by van der Waals interaction along the crystallographic *c*-axis (**Figure 15**a).[40,97] The bulk TMCs can be downsized to obtain single- or few-layer forms, as in the case of other layered materials. The interest in exfoliating TMCs to their monolayer forms started in the mid-1970s, even before the discovery of graphene.[98] These earlier reports demonstrated the exfoliation of TaS_2 and NbS_2 by electrolysis

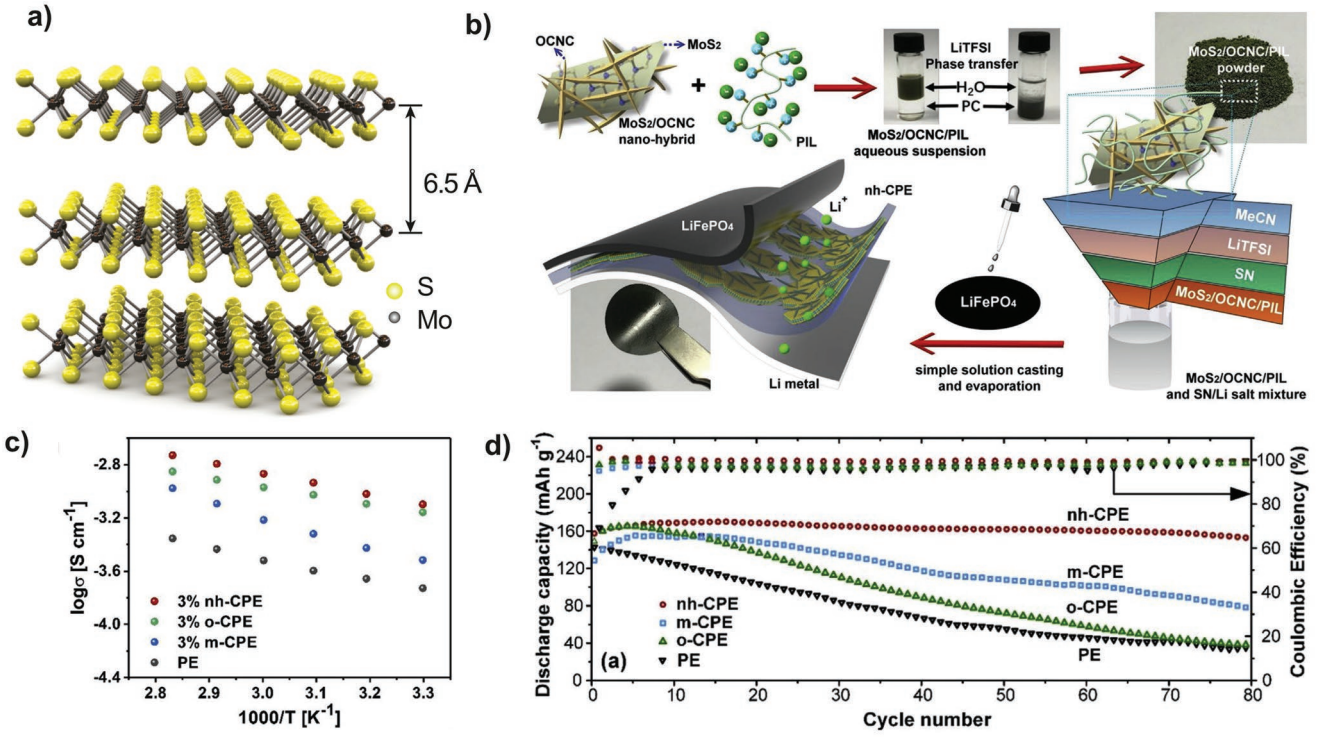

Figure 15. a) 3D structure of layered MoS_2. Reproduced with permission.[40] Copyright 2011, Springer Nature. b) Scheme showing the various stages of preparing a nanohybrid PCE with PDDA polymer (MoS_2/OCNC/PIL powder) and its coating onto LFP cathode. c) Temperature-dependent ionic conductivity data of DPE and nanohybrid PCE, and d) cycling stability performance of LFP-based LMB cells with respective electrolytes. Reproduced with permission.[101] Copyright 2018, Elsevier.

based on the insertion of hydrogen and water, which inspired further studies on monolayer TMCs.[99] Later, MoS_2 exfoliation using butyl lithium in hexane in 1986 by Joensen et al. opened up new avenues for semiconducting 2D layered nanomaterials fabrication.[66d] Interestingly, around the same time, 2D layered MoS_2 was also recognized as a potential electrode material for LIBs.[100] So far, the mainstream applications of 2D layered TMCs in the battery domain represent them as electrode materials for charge storage.

Although 2D layered TMCs are an appealing choice as nanofillers due to their high aspect ratio and the possibility of introducing desired surface functionalities,[102] their application in PCEs is rare. In 1990, Yang et al. reported TMC/polymer composites produced from water-soluble polymers such as PEO, poly(ethylene glycol) (PEG), and poly(vinylpyrrolidone) with monodispersed MoS_2 or WS_2 through a physical (solution) blending process.[103] The composite material showed random stacking and expanded interlayer spacing, indicating the ability of TMCs to encapsulate polymer chain in its interlayer space. Similarly, Ana et al. showed intercalation of PAN and Li^+-ions into MoS_2, leading to an expansion of interlayer spacing from 0.61 to 1.15 nm.[104] The interaction of Li^+-ions with the obtained organic–inorganic hybrid material led to a higher Li-diffusion coefficient (4.3×10^{-11} cm^2 s^{-1}, RT) and an ionic conductivity of 0.33 mS cm^{-1} (RT). After all, the composite material ($Li_{0.6}MoS_2(PAN)_{1.2}$) with mixed ionic and electronic conducting properties is oxidatively stable up to 2.85 V versus Li|Li^+. This value is higher than MoS_2 (pure), MoS_2 (restacked), $Li_xMoS_2(PEO)_1$, and $Li_xMoS_2(DEA)_{0.2}$ samples. Ultimately, this work gives insights into the improved electrochemical properties of polymer intercalated MoS_2 and the significance of the nature of intercalants in PCEs. Another report demonstrated that atomic layers of 2D MoS_2 can build surface protection on Li anode to prevent direct contact between the electrolyte and metallic Li in LMBs.[51d] During lithiation process, the transition of MoS_2 from the semiconducting 2H phase to a metallic 1T phase also plays a beneficial role in reducing the electrode|electrolyte interfacial resistance, hence controlling the smooth deposition of Li on the metallic anode.

Recently, Wu et al. pointed out a few exciting properties of MoS_2, which can rejuvenate the interest in developing TMC-based PCEs for LBs and other electrochemical devices.[101] As MoS_2 is a semiconductor, incorporating MoS_2 into the polymer electrolyte in a small quantity will not cause electrical contact between the electrodes. Earlier reports showed that layered MoS_2 can uptake many Li^+-ions during the exfoliation of the bulk phase in Li^+-containing solvents.[106] These intercalated ions can improve the ionic conductivity of the PCEs. Besides, the transition metal centers in TMCs will likely immobilize the electrolyte anions through Lewis acid–base interaction and offer free passages for Li^+-ion transport. Considering these possibilities, they developed a plastic crystal-based PCE by combining Li^+-intercalated exfoliated MoS_2, a cationic polymer (poly(diallyldimethylammonium chloride, PDDA), 1D-oxidized cellulose nanocrystal (OCNC), and a plastic crystal (succinonitrile, SN) (Figure 15b).[101] The improved ionic conductivity (0.8 mS cm^{-1} at 30 °C), t_{Li^+} value (0.65), and cycling stability (≈100% capacity retention over 80 cycles at RT and 60 °C) offered by the PCE compared to the MoS_2-free PDDA–LiTFSI counterpart indeed validated the advantages of MoS_2 nanofiller (Figure 15c,d).[101] The MoS_2 layers when used in PCEs often restack and agglomerate during the electrolyte processing, resulting in reduced polymer|nanofiller interfacial contact. These aggregates can block ion transport channels and hamper the mechanical properties of the electrolyte. However, the negatively charged OCNC in the reported PCE prevented the restacking of the exfoliated MoS_2 by inducing electrostatic interactions and steric hindrance within the PCE. After all, since the selected polymer (PDDA) carries a positive charge, the uniform coating of the polymer around the negatively charged MoS_2/OCNC hybrid is highly favorable.

The physicochemical properties of TMO and TMCs are often alike.[107] Like TMCs, 2D TMOs can host neutral or charged species, including polymers, metal ions, etc., through coordination, ion-exchange process, acid–base coupling, and other weak interactions.[107b] Due to the semiconducting nature and multiple oxidation states of transition metal centers, TMOs have been primarily considered as electrode materials for LBs. Although, a few earlier reports studied the effect of polymer on Li^+-ion diffusion in TMOs, the end application of these TMO/polymer composites was focused on electrode materials.[108] For example, studies by Nazar et al. suggested that the intercalation of PEO into layered MoO_3 facilitates Li^+ -ions diffusion through the inorganic lattice.[109] However, the recent reports on polymer electrolytes show that the ethylene oxide units in PEO strongly coordinate with the Li^+-ions causing restricted ionic mobility. In this case, introducing a lithiophilic material as an additive into the polymer could minimize the interaction between Li^+-ion and the polymer. This concept inspired Li et al. to develop a new TMO-based PCE by dispersing MnO_2 nanoflakes in the PEO matrix (**Figure 16**a–c).[105] A 5.0 wt% of MnO_2 nanofiller in PEO–LiTFSI (PEO/LiTFSI/5.0 wt% MnO_2) significantly improved the ionic conductivity and oxidative stability of PCE to 0.21 mS cm^{-1} at 60 °C and 4.5 V versus Li|Li^+, respectively compared to a MnO2-free PEO/LiTFSI system. The improved properties of the PCE are attributed to the lithiophilic nature of MnO_2 nanosheets, which increase the dissociation of lithium salt in the polymer and facilitate the diffusion of Li^+-ions among the PEO chains. The advantages of PCE are also evident in the low overpotential and stable cycling performance of corresponding Li||Li and LFP||Li cells (Figure 16d,e). Hence, in summary, the reports suggest that the use of 2D layered TMCs can enhance electrochemical stability, ionic conductivity, and Li^+-ion transport properties of PCEs. However, the material and its quantity should be appropriately selected and more practical validations in LB full cells must be conducted to improve the overall performance of TMC-based PCEs.

4.4. MXene as Nanofiller in PCEs

MXenes are the youngest member of the inorganic 2D layered nanomaterials family. They are few-atom-thick layers of transition metal carbides, nitrides, and carbonitrides (Figure 8c,d).[41,110] MXene's general chemical formula is $M_{n+1}X_nT_x$ (n = 1–3), where M, X, and T_x stand for transition metal, carbon/nitrogen, and

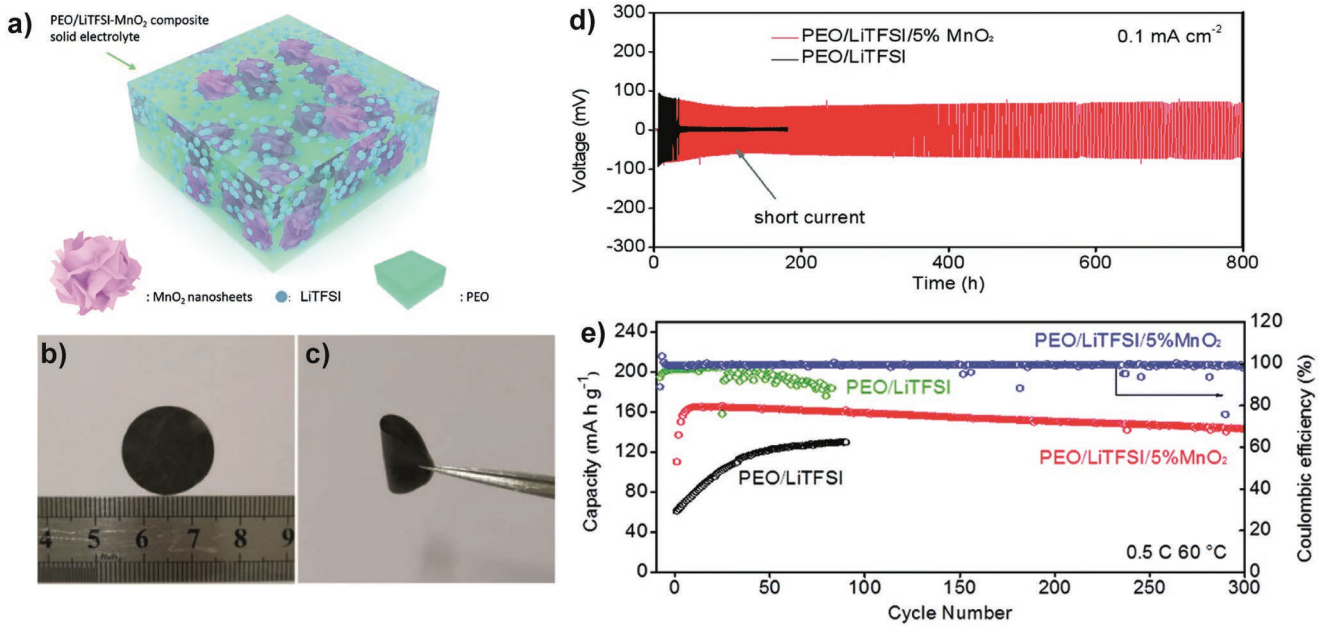

Figure 16. a) Scheme and b–c) digital images of a PEO/LiTFSI/MnO_2 based PCE. Cycling comparison of PEO/LiTFSI/MnO_2 PCE and PEO/MnO_2 electrolyte in d) Li||Li symmetric cell and e) LFP-based LMB cell. Reproduced with permission.[105] Copyright 2020, Royal Society of Chemistry.

surface termination groups (e.g., −OH (hydroxyl), −O (oxygen), −F (fluorine), etc.). MXenes are derivatives of the parent MAX ($M_{n+1}AX_n$) phase (bulk), a layered hexagonal material in which the alternating $M_{n+1}X_n$ layers and A atoms are connected through metallic M–A bonds (Figure 8c,d). Preparation of MXenes involves selective etching of the A layer from the MAX phase by chemical means (reaction with HF, fluoride salts, NaOH, etc.) without damaging the M–X bonds in the $M_{n+1}X_n$ layers.[111] Although most MXenes developed so far comprise one transition metal on the M sites (e.g., Ti_2CT_x, $Ti_3C_2T_x$, V_2CT_x, $Ta_4C_3T_x$, etc.), a few examples of double transition metal MXenes (e.g., $Ti_xTa_{4-x}C_3$) are also available.[112] The first MXene, developed by Gogotsi et al. in 2011, was titanium carbide ($Ti_3C_2T_x$, where T stands for −F or −OH terminations), which remains the most popular and widely used MXene.[65a,110a]

Following its discovery, extensive studies on MXenes have explored interesting properties from the material and application perspectives. MXenes, possessing a unique combination of high in-plane conductivity (contributed from the metal carbide/nitride layers) and hydrophilicity (originated from the oxygen-containing functional groups attached to the surface), play significant roles as electrode materials for charge storage.[112b] The functional groups are also responsible for creating a net negative surface charge (zeta potential below −30 mV)[113] that enables the intercalation of cationic species (TBA^+, Li^+, Al^{3+}, etc.) and polymers into the interlayer galleries of layered MXenes. Inspired by the intercalation property of MXene, Gogotsi and co-workers prepared $Ti_3C_2T_x$ MXene-clay (also called "conductive clay") that shows cation exchange and hydration behavior, as seen in some clay solids.[111a,114] Such ion-exchange capacity is attractive in the context of inducing ionic conduction properties into MXenes for developing PCEs. The interactions of the surface functionalities of MXene flakes with the functional groups in the polymers via hydrogen bonds, van der Waals force, electrostatic force, etc., enable uniform mixing of the organic and inorganic phases in the resulting PCE. Studies show that the intercalation of polymer chains between the MXene layers increases the interlayer distance and homogenization; hence, reinforcing the stability and mechanical properties of the resulting polymer composites. For example, work done by Sheng et al. demonstrated that by introducing 0.5 wt% of exfoliated $Ti_3C_2T_x$ Mxene one can significantly augment the tensile strength and storage modulus of polyurethane.[115] These MXene based polymer composite can be prepared using ex situ blending (through direct physical mixing or surface modification) or in situ polymerization routes.[116] Indeed, the stability of the composites obtained through physical mixing mainly relies on the weak interactions between the surface groups anchored on MXene and hydrophilic units present in the polymer. Whereas, hydrophobic polymers show poor compatibility to the oxygen rich surface functionalities of MXene, resulting in an inhomogeneous mixing. So, approaches of chemical modification of the MXene surface via nitrogen doping, diazotization reaction, etc., are helpful to realize better interaction between MXene and polymer.

Pan et al. first demonstrated d-PCE using MXene as a nanofiller in PEO (**Figure 17**a–c).[117] The d-PCE comprising exfoliated $Ti_3C_2T_x$ MXene flakes embedded in PEO matrix exhibited enhanced ionic conductivity (0.69 mS cm^{-1}) compared to the nanofiller-free electrolyte (0.36 mS cm^{-1}, Figure 17b). However, the ion transport properties (t_{Li^+}) achieved by adding MXene as filler in the d-PCE was negligible. In an LFP||Li cell, the optimized MXene-based d-PCE displayed cycling stability over 100 cycles (Figure 17c). Optimizing the concentration of MXene in PCE is also crucial to control the aggregation and crystallinity of the polymer matrix. For instance, a trace or excess amount of MXene can accelerate PEO crystallization by heterogeneous nucleation, while an optimum loading can hinder the

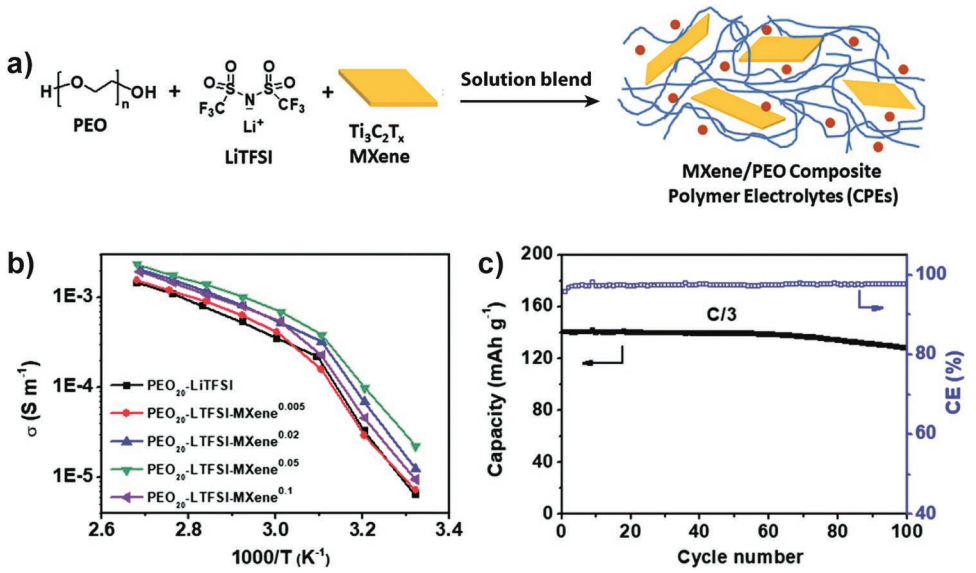

Figure 17. a) Scheme showing the components of MXene-based d-PCE prepared through solution blend method. b) Temperature-dependent ionic conductivity of various d-PCE membranes prepareds with different concentrations of MXene nanofiller. c) Capacity versus cycle number (at 60 °C) of LFP||Li cell assembled with PEO_{20}–LiTFSI–$MXene^{0.02}$ d-PCE. Reproduced under the terms of the CC BY-NC 3.0 license.[117] Copyright 2019, The authors, published by Royal Society of Chemistry.

growth of crystalline domains.[116a] Similarly, MXene-induced heterogeneous nucleation mechanisms for crystallizing other polymers are also available.[118] This property of MXene is different from the other 2D nanofillers favoring the amorphization of polymers and could result in interesting properties of MXene-based PCE.

Another interesting aspect of MXenes is their ability to direct the uniform nucleation of Li on Li metal anode to inhibit the growth of dendrites or HSAL. Both −O and −F containing functional groups on MXene can serve as nucleation sites for Li deposits, which eventually coalesce and agglomerate into large secondary particles to form a dense plating of Li.[119] Hence, many studies have utilized MXenes to develop artificial protection layers (artificial SEI), modification of separators, etc., for LMBs. In a recent report, Yang et al. demonstrated that MXene is beneficial as an additive in g-PCEs for lowering the interfacial resistance and smoothening the Li deposition on the surface of Li metal anode in a Li–O_2 battery.[120] The fluorine functionalities in $Ti_3C_2T_x$ MXene lead to the formation of a durable SEI layer; besides favoring good Li^+-ion transport, such SEI composition is equally desirable for dendrite-free Li plating on Li metal anode. Other than electrolyte additives, a few studies have considered MXenes for designing artificial SEI,[121] modifying the commercial polypropylene separator, etc., to improve the cycle life of LBs.[122] Similarly, the flame-retardant property of MXene could be also appealing in the context of developing fireproof PCEs for potentially safe nonaqueous batteries.[123]

Despite the merits mentioned above, the high electrical conductivity (≈10^3 S cm^{-1}) and aggregation of MXene nanosheets often downplay their prospect as nanofiller in PCEs. In this direction, Shi et al. developed a hybrid nanofiller (MXene-mSiO_2) consisting of $Ti_3C_2T_x$ MXene nanosheet sandwiched between mesoporous SiO_2 (mSiO_2) layers (**Figure 18**a).[124] The MXene-mSiO_2 was synthesized using the in situ hydrolysis of tetraethyl orthosilicate on the surface of cationic surfactant (CTAB)-coated MXene nanosheets, thanks to the negative surface charge of Ti_3C_2. The MXene-mSiO_2 hybrid nanofiller (0.023 mS cm^{-1}) displayed a seven-order magnitude less electronic conductivity than bare Ti_3C_2 (1400 mS cm^{-1}). Adding 2.0 wt% of this hybrid nanofiller in poly(propylene oxide)–LiTFSI (PPO–LiTFSI) g-PCE electrolyte (Figure 18b) increased the ionic conductivity to 0.46 mS cm^{-1}, which is higher than many of the then-reported PCEs. The better performance of MXene-mSiO_2-based g-PCE was attributed to the Lewis acid–base interaction of LiTFSI with the −F functionality on MXene and −OH in silica. Finally, the high oxidation stability (4.3 V vs Li|Li^+) and good compatibility with Li (plating/stripping cycling up to 2000 h) allowed the use of g-PCE as separator in LFP||Li full cell (Figure 18c). The influence of MXene nanofiller in the g-PCE for improving the specific capacity of the LFP||Li cell is apparent in Figure 18c. Hence, adopting a similar approach with MXenes to develop PCEs and investigate both their performance and their ability to regulate the surface morphology of the Li anode would be interesting.

4.5. Phosphorene as Nanofiller in PCEs

Phosphorene is the mono- or few-layered form of black phosphorous, the most stable allotrope of phosphorous.[126] Black phosphorous (BP), often viewed as the graphite analogy of phosphorous, is a layered material in which the individual atomic layers are stacked together by van der Waals interactions.[127] The number of layers can vary depending on the synthesis methods, resulting in 2D phosphorene nanosheets with thicknesses between 2 and 10 nm. Although graphene and phosphorene are conceptually similar, they are of distinct structural and chemical nature. In phosphorene, the sp^3

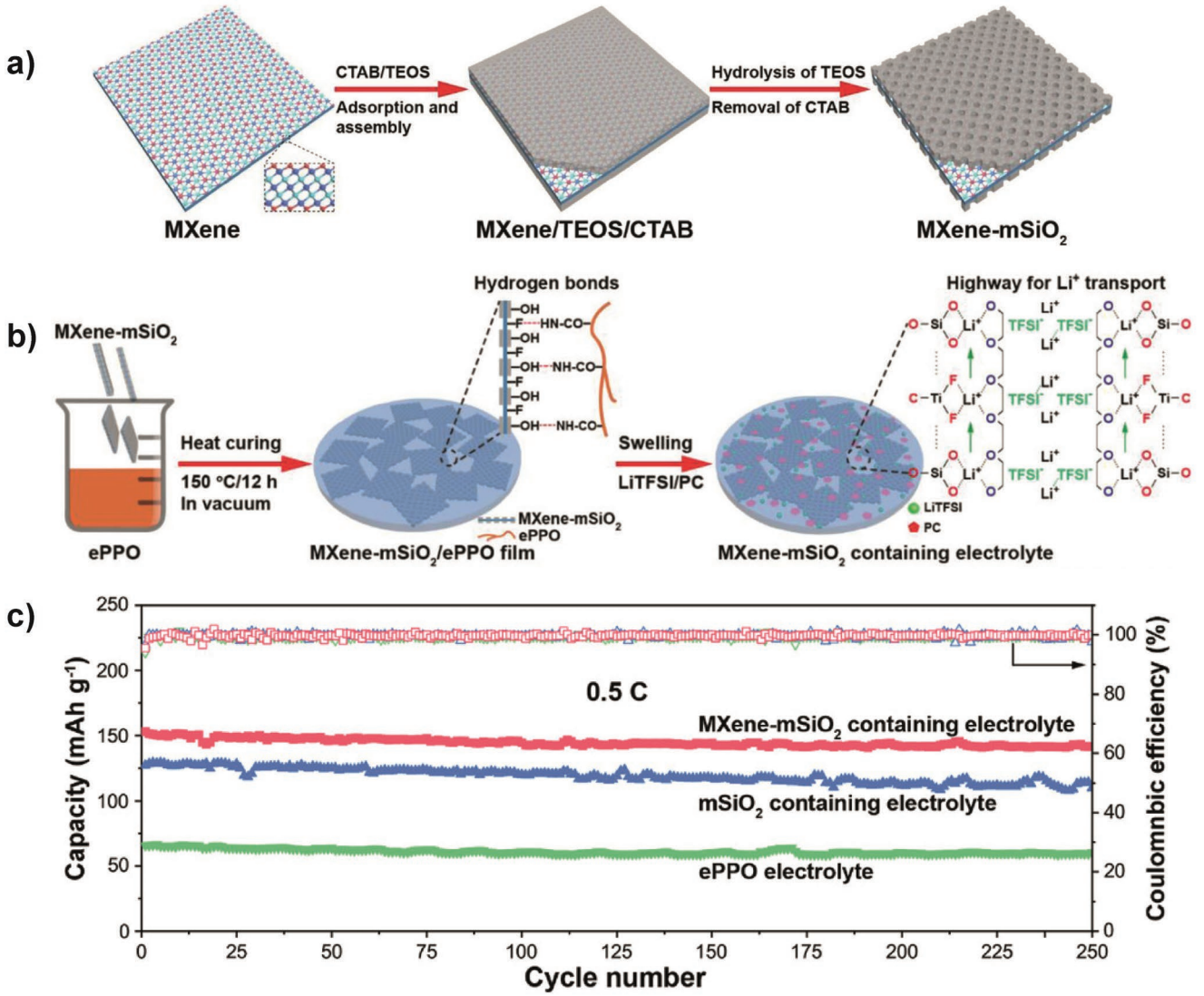

Figure 18. a) Steps involved in fabricating sandwich-like MXene and $mSiO_2$ composite. b) Preparation of g-PCE using MXene-$mSiO_2$ hybrid nanofiller and plausible Li^+-ion transport pathway. c) Cycling performance of LFP||Li cell with various electrolytes demonstrating the significance of MXene-$mSiO_2$ nanofiller compared to $mSiO_2$-based or nanofiller-free PEs. Reproduced with permission.[124] Copyright 2020 Wiley-VCH.

hybridized P_4 units (each phosphorous atom forms the covalent bonds with three adjacent phosphorous atoms) are connected to form a puckered honeycomb structure (**Figure 19**a–c), which differs from the planar structure of graphene.[42] Besides, unlike graphene, phosphorene is semiconducting and has a nonzero bandgap between 0.3 and 2 eV (bulk phase to monolayer).[126] These distinct properties of phosphorene, combined with graphene-like mechanical strength and flexibility, have driven its applications in electronics, energy storage, catalysis, etc. The monolayer of phosphorene was first isolated in 2014 (by Zhang and co-workers) from black phosphorous following a scotch-tape-based microcleavage method.[128] Isolation of 2D monolayer forms is also possible for other phosphorous allotropes, e.g., blue and red phosphorous.[129] These allotropes possess a similar layered structure as black phosphorous but exhibit distinct physical and chemical properties due to the difference in atomic configurations.[130]

Rojaee et al. reported a novel g-PCE by combining phosphorene with PEO/LiTFSI-based polymer electrolyte.[125] The addition of phosphorene in an optimum concentration of 0.5 wt% (PCE-0.5P) showed an enhanced Li^+-ion transport property and reduced interfacial resistance in electrochemical cells. The RT ionic conductivity and t_{Li^+} of PCE-0.5P reached 2.3 mS cm^{-1} and 0.32, respectively, much higher than the phosphorene-free (PCE-0P) electrolyte (0.59 mS cm^{-1} and 0.18). The improved ionic mobility mainly originated from the reduced ion-pair interaction of LiTFSI with BP nanosheets in the electrolyte, as revealed by the molecular dynamics simulation studies (Figure 19d). The results also showed that the degree of dissociated Li^+-ions increased from 71% (PCE-0P) to 94% (PCE-0.5P), which support low propensity toward ion-pair formation in the presence of BP nanosheets. The low plating/stripping overpotential and long cycling performance of Li|PCE-0.5|Li and LFP|PCE-0.5|Li (Figure 19e) cells compared to BP-free

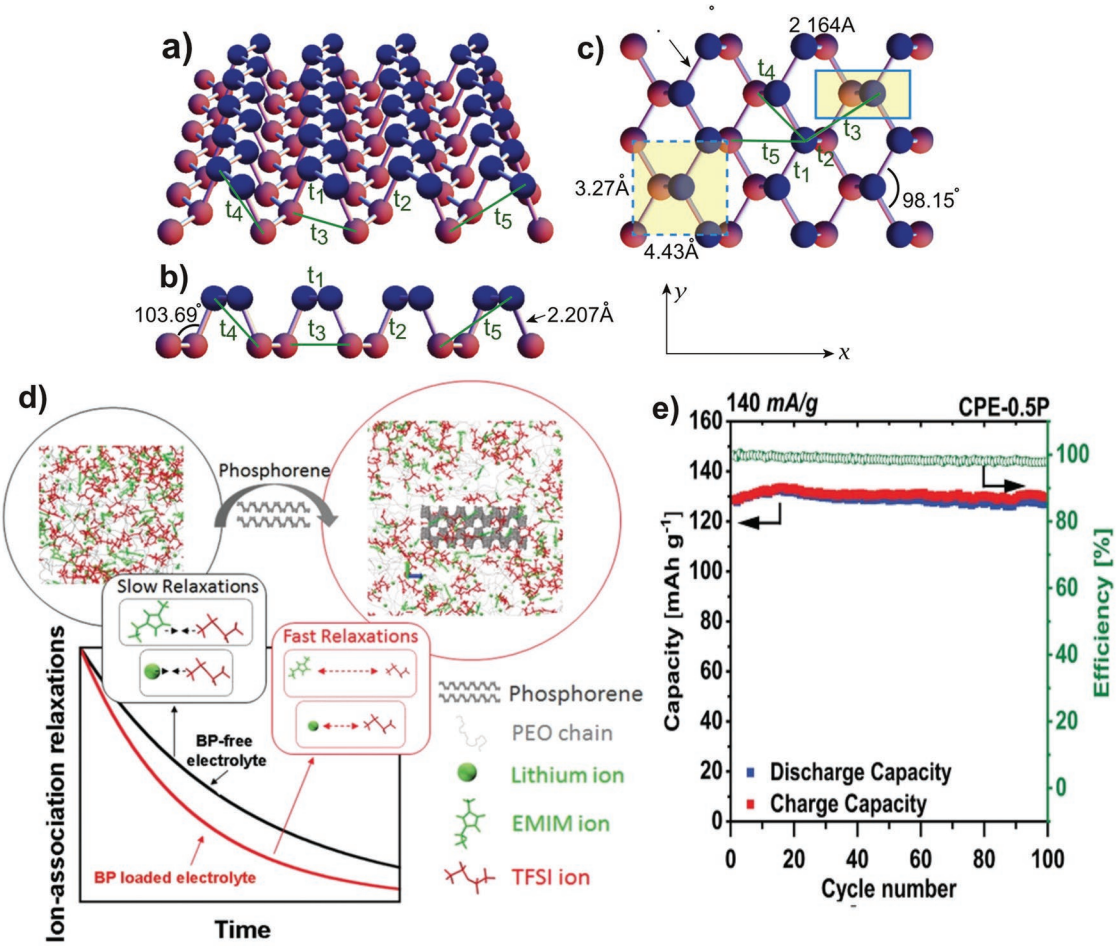

Figure 19. Illustration of the structure of phosphorene: a) bird's eye view, b) side view, and c) top view. Reproduced under the terms of the CC BY 3.0 license.[42] Copyright 2014, IOP Publishing Ltd and Deutsche Physikalische Gesellschaft. d) Ion transport mechanism in the bulk of the PCE demonstrating the role of phosphorene as a nanofiller. e) Cycling data of LFP||Li cell with PCE-0.5P as PCE. Reproduced with permission.[125] Copyright 2020, Wiley-VCH.

electrolyte combinations further evidenced the beneficial effects of BP nanosheet as an additive in PCEs.

Phosphorene with good Li^+-ion transport kinetics can also stabilize Li metal anode and tune the composition of the SEI layer in LMBs. Li-metal spontaneously reacts with phosphorous to form an electrochemically stable and Li^+-ion conducting Li_3P compound.[131] Wu et al. investigated the favorable effect of Li_3P formation on Li-metal surface, which is in contact with d-PCEs composed of BP, LiTFSI, and a cross-linked PEO-based polymer host derived from poly(ethylene glycol) methyl ether acrylate.[131c] The in situ formed Li_3P at the Li metal surface minimizes the interfacial resistance of the cell by offering intimate contact between the Li metal anode and the d-PCE. The improved electrode|electrolyte contact increases the LMB cells' rate capability. The report also claims that due to the presence of the in situ formed Li_3P interphase, the d-PCE displayed excellent HSAL and dendrite growth inhibition properties. Ultimately, the LFP||Li solid-state LMB cell cycled at 60 °C displayed a good capacity retention of 75% for over 200 cycles.

Despite the reports mentioned above, validating the superiority of phosphorene as electrolyte components requires further studies. Since phosphorene is one of the new entrants in the 2D materials landscape, there is still a lot of scope for investigation and improvements. **Table 1** represents the overall characteristics of the 2D TMCs, 2D TMOs, MXene, and phosphorene-based electrolytes reported for LB applications to summarize this section on synthetic inorganic 2D layered nanomaterials.

5. Naturally Occurring Layered Clay Minerals as Nanofiller in PCEs

Sections 4.1–4.5 considered several synthetically available inorganic 2D layered materials as nanofillers in PCEs. However, naturally occurring inorganic 2D layered materials can also act as passive and active nanofillers in PCEs.[132] In this direction, 2D layered silicates (often called phyllosilicates, sheet or layered silicates, or 2D silicates) and LDHs are popular nanofillers used

Table 1. Summary of electrochemical properties of PCEs based on 2D TMCs, 2D TMOs, MXene, and phosphorene nanofillers.

2D nanofiller	Polymer components	Conductivity [mS cm^{-1}]	t_{Li^+}	Voltage (V vs Li|Li$^+$)	Electrochemical performance in LB cell	Refs.
MoS_2-OCNC	PDDA	0.80 at 30 ° C 1.36 at 60 °C	0.65	2.5–4.2	≈120 mAh g^{-1} at 0.5 C and 60 °C and 90% capacity retention over 200 cycles (LFP cathode)	[101]
MnO_2 (5 wt%)	PEO	0.02 at 30 °C 0.21 at 60 °C	0.38	2.5–4.0	≈110 mAh g^{-1} at 0.5 C and 60 °C and 87% capacity retention over 300 cycles (LFP cathode)	[105]
$Ti_3C_2T_x$ MXene (1.5 wt%)	PEO	0.02 at 28 °C 0.69 at 60 °C (CPE with 3.6 wt% MXene)	0.18	2.5–4.0	≈140 mAh g^{-1} at 0.3 C and 60 °C and 91% capacity retention over 100 cycles (LFP cathode)	[117]
$Ti_3C_2T_x$ MXene-mSiO_2 (2 wt%)	PPO	0.46 at ≈20 °C	–	2.5–4.0	≈142 mAh g^{-1} after 250 cycles at 0.5 C and 25 °C (LFP cathode)	[124]
$Ti_3C_2T_x$ MXene	PVDF-HFP/PEO	0.55 at 25 °C	0.47	≈4.0 V	18 000 mAh g^{-1} (O_2 cathode)	[120]
Black phosphorous (5 wt%)	PMEA-TEGDA	0.20 at 60 °C	0.40	2.5–4.0	≈140 mAh g^{-1} at 0.1 mA cm^{-2} and 60 °C, and 76% capacity retention over 200 cycles (LFP cathode)	[131c]
Phosphorene (0.5 wt%)	PEO-TEGDME	2.4	0.32	2.5–4.2	≈130 mAh g^{-1} at 0.14 A g^{-1} and ≈100% capacity retention over 100 cycles (LFP cathode)	[125]

for PCEs. Both 2D layered silicates and LDHs are known as clay minerals, however, they are chemically distinct in terms of their net charge. For instance, 2D layered silicates are cationic clay minerals (CCMs) with a net negative charge and a high cation exchange capacity (CEC). On the contrary, LDHs are anionic clay minerals (ACMs) that possess a net positive charge, exhibiting anion exchange properties. Due to the charge characteristics, when CCMs and ACMs are used as nanofillers they can influence the ion transport properties (e.g., ionic conductivity, t_{Li^+}, etc.) of the resulting PCEs. The following subsections will highlight the importance of these two nanofillers in PCEs for LB applications.

5.1. 2D Layered Silicate Clay Minerals for PCEs

2D layered silicates (2D silicates) are CCMs finding immense attention as nanofillers in PCEs.[133] They comprise corner-sharing silicate tetrahedrons, covalently bonded to octahedrons of small cations (e.g., Al^{3+}, Mg^{2+}, etc.), resulting in a crystalline structure consisting of tetrahedral and octahedral layers (**Figure 20**a–c).[43,134] 2D silicates are attractive materials due to their high aspect ratio (≈1 nm layer thickness and lateral dimension ranges from dozens of nm to a few µm depending on the silicate origin and composition).[134b,135] Mainly, two types (1:1 and 2:1) of 2D silicates are available depending on the arrangement of tetrahedral and octahedral layers in them.[9,43,132,134a,136] The 1:1 type of 2D silicates contain each alternating octahedral and tetrahedral layers (Figure 20a). In contrary, in the 2:1 counterpart (Figure 20b,c), one octahedral layer is sandwiched between two tetrahedral layers.

Two major factors contribute to the net negative charge of 2D layered silicate CCMs: 1) permanent or structural charge and 2) variable charge. The former is due to the isomorphous substitution of the Si^{4+} in the silicate tetrahedral layers by trivalent ions (e.g., Al^{3+}, Fe^{3+}) and Al^{3+} in octahedral sheets by divalent ions (e.g., Fe^{2+}/Mg^{2+}/Mn^{2+}).[137] These negatively charged sites lie at the basal planes of the individual silicate layers and takes part in cation exchange reactions for charge neutralization (ion intercalation into 2D layered nanomaterials, explained in Section 2).[134b] This property of cation exchange reactions is unique to 2D silicates and is significant for PCEs for lithium and post-lithium battery applications. There is a possibility of introducing alkali-metal ions (e.g., Li^+, Na^+, etc.) and divalent cations (e.g., Ca^{2+}, Mg^{2+}, etc.) by replacing the naturally intercalated cations in their crystal structure, critical for post-lithium battery technologies. The net negative charge of 2D silicates is advantageous in a PCE since the anion migration between the clay layers will be minimal, resulting in high cation transference number values. In any case, 2D silicates possessing high CEC values are essential to facilitate structural modifications with exchangeable cations. **Table 2** summarizes the CEC values of various 2D silicate clay minerals.[138] The latter factor of variable charges in 2D silicates results from the nature of interactions between nonsaturated bonds of functional groups (e.g., hydroxyl groups) present at the amphoteric clay edges and the solution in contact with it.[137,139] It is worth highlighting that apart from the characteristic cation exchange properties, there are also special cases of 2D silicates exhibiting pH-dependent anion exchange reactions.[138a,140]

Many of the 2:1 silicate exhibits high CEC values, allowing facile incorporation of mobile cations (e.g., Li^+, Na^+, etc.), often making them active nanofillers in PCEs.[141,142] A high CEC value of 2D silicates is essential for delivering high ionic conductivity in PCEs. For the same reason, MMT, vermiculite, saponite, etc., are well-explored for PCEs. In such PCEs, the secondary intercalation of polymer chains between the interlayer galleries of phyllosilicate layers is also probable; hence all four types of polymer composite microstructures (Figure 9) may be achieved depending on the polymer/clay organization within the PCE. The interlayer galleries of 2D silicates act as nanochannels for cation transport, minimizing the effect of ion pairing in PCEs. Besides, intercalation into interlayer clay galleries can improve

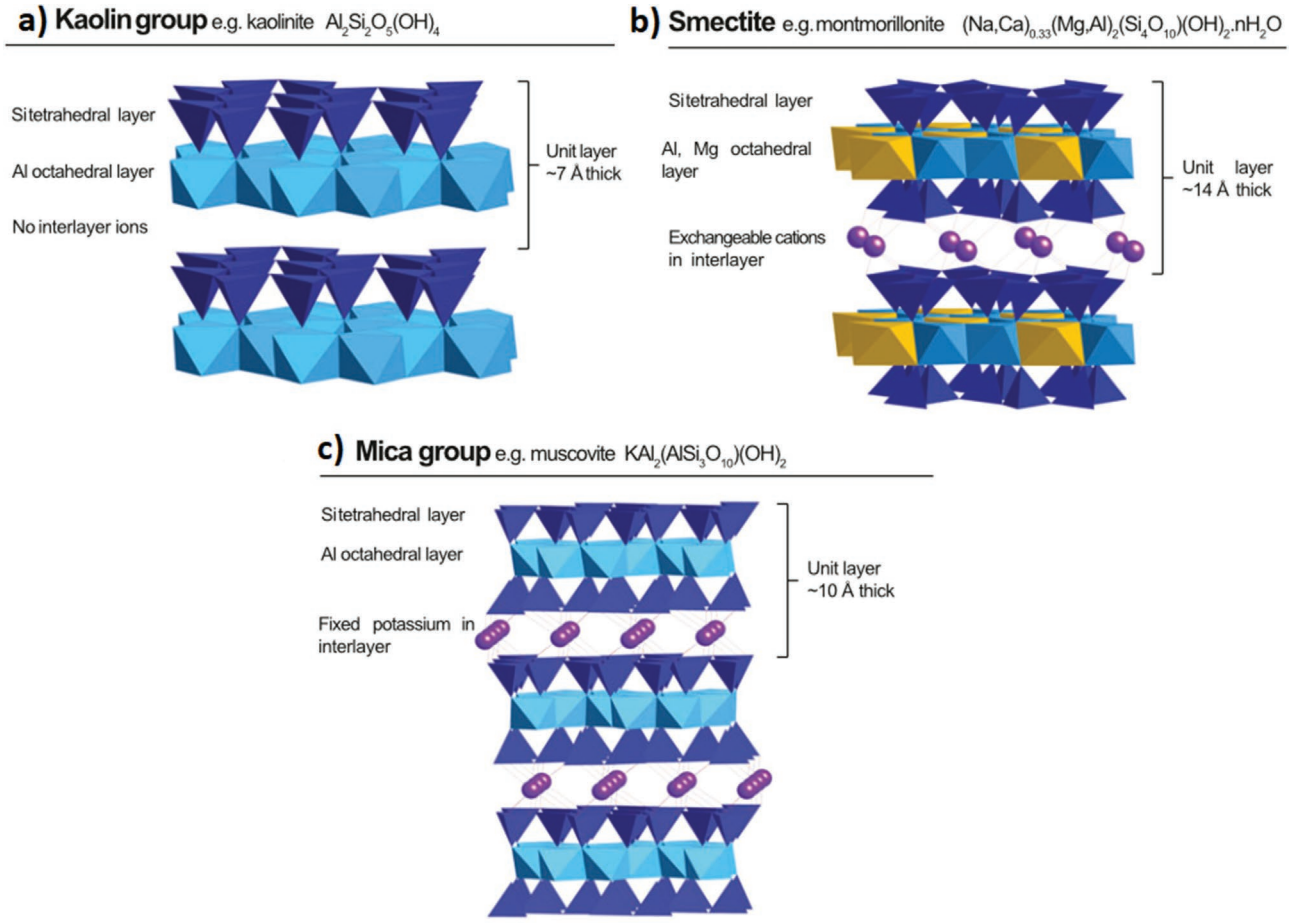

Figure 20. Representative crystal structure of 2D silicates in the a) kaolin (1:1 2D silicate), b) smectite (2:1 2D silicate), and c) mica (2:1 2D silicate) group. Reproduced with permission.[43] Copyright 2018, Springer International Publishing.

the polymer host's thermal, mechanical, and electrochemical behavior compared to the pristine polymer host in conventional DPEs. The drop in the crystalline character of the polymer host with the addition of 2D silicate nanofillers also benefits the ion transport properties of the related PCEs. Discussion on a few exciting results on PCEs of 2D silicates for LB applications appears in the following part of this section on CCMs.

Table 2. CEC values of commonly found 2D silicate clay minerals.

CCM type	Cation exchange capacity (centimole charge (+) per kg or cmol(+) kg^{-1})
Kaolinite	3–15
Halloysite·2 H_2O	5–10
Halloysite·4 H_2O	40–50
Montmorillonite	70–120
Vermiculite	130–210
Illite	10–40
Micas (biotite, muscovite)	Up to 5
Chlorite	10–40
Sepiolite, palygorskite	20–30

MMT is one of the most explored 2D silicates for PCE preparation and application in LBs (Figure 20b). Ion-exchange reactions may replace the intercalated Na^+ and Ca^{2+} ions with H^+, Li^+, Mg^{2+}, organic cations, etc., in MMT.[141,146] For instance, a multistep ion-exchange reaction involving proton intercalation followed by Li^+-ions for Li-MMT preparation is described in **Figure 21**a–c.[144,147] An advantage of MMTs is the weak interaction between the intercalated species and the layers due to the low ion substitution and appropriate interlayer charge (≈0.55 m.equiv./100 g). The weak interaction between the layers of MMT helps the secondary intercalation of polymer chains during the composite preparation, which exposes more interaction sites in the PCEs. Besides, it is reported that the energy barrier for the diffusion of Li^+-ions within the interlayer regions of the MMT framework is 0.155 eV, a lower value than the traditional functional polymers.[144,148]

Several polymer hosts, PEO, PMMA, PVDF, PVDF-HFP, etc., have been used to process MMT-based PCEs.[27,145] Zhao and Wang reported the preparation of a d-PCE comprising MMT, LiTFSI, and $Li_{6.4}La_3Zr_{1.4}$–$Ta_{0.6}O_{12}$ (LLZTO) in PEO for LMBs.[143] The d-PCE (indeed a HPE) preparation involved a solution-blending process. The report emphasizes that Li^+-MMT interactions in the HPE weaken the PEO-Li^+ coordination (Figure 21d), delivering improved Li^+ transport properties

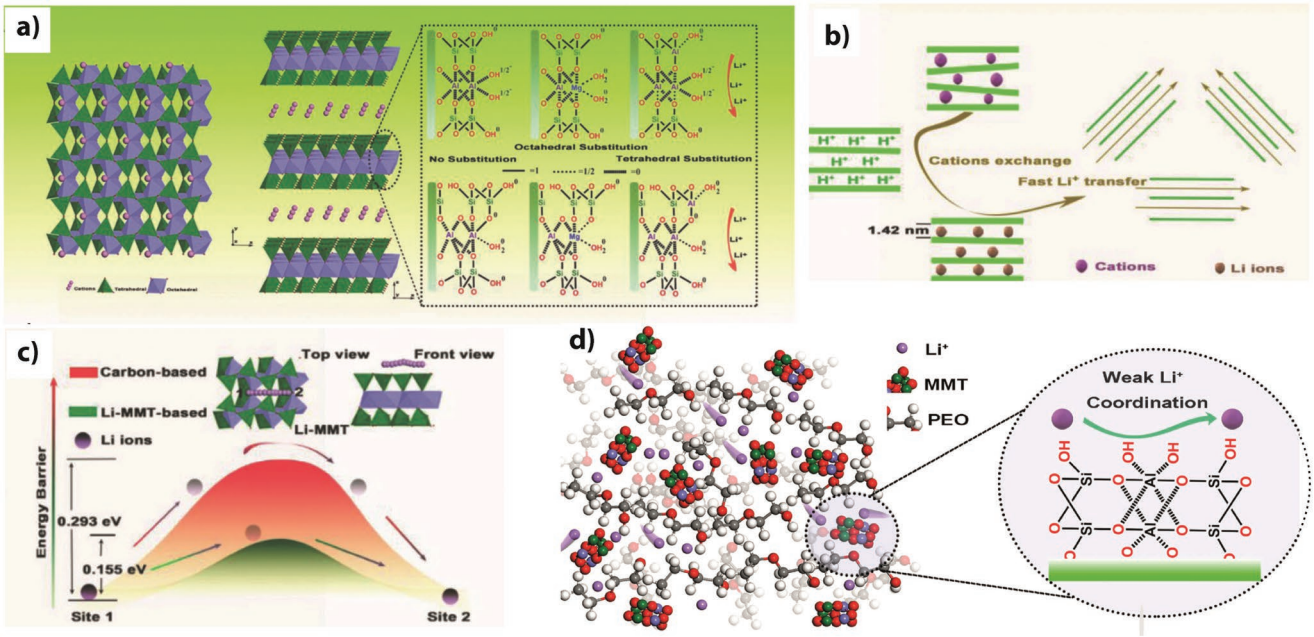

Figure 21. Illustration of a) framework of MMT and the cations present in the interlayer space. b) Multistep cation-exchange reaction of Na-MMT involving protons and Li^+-ions. c) Energy profile diagram depicting the favorable diffusion of Li^+-ions within the interlayer spacing of MMT framework compared to a carbon-based electrode. Reproduced with permission.[144] Copyright 2018, Wiley-VCH. d) Scheme showing the interactions in a d-PCE/HPE composed of PEO, MMT, and LiTFSI salt. Reproduced under the terms of the CC BY 4.0 license.[143] Copyright 2019, The authors, published by Springer Nature.

(ionic conductivity of 0.02 and 4.2 mS cm^{-1} at 30 and 70 °C, respectively). Besides, MMT claims to help remove trace water and impurities at the electrode|electrolyte interface, offering oxidation stability of 4.6 V versus Li|Li^+, higher than the MMT-free counterpart (3.9 V vs Li|Li^+). The advantage of MMT additives is apparent from the high specific capacity (140 mAh g^{-1}, 0.08 C, 70 °C) of the LFP||Li full cell, which is superior to the LMB cell without MMT filler (120 mAh g^{-1}). The sodium form of MMT (Na-MMT) is known as bentonite. In the work of Moreno et al., bentonite-Li^+ preintercalated with PEO (PEO@bentonite-Li^+) was used as nanofillers in PEO host for the preparation of d-PCE films by melt-blending process and hydraulic pressing.[149] The mechanical agitation (ultrasonication) and solvent swelling favored the preintercalation of neutral PEO chains into the interlayer galleries of bentonite-Li^+. The ionic conductivity of the resulting d-PCE with the PEO@bentonite-Li^+ nanofiller (PEO/PEO@bentonite-Li^+, 1.81×10^{-7} S cm^{-1}, 25 °C) was higher than the PEO-free bentonite nanofiller (PEO/bentonite-Li^+, 3.89×10^{-8} S cm^{-1}, 25 °C). Despite the low ionic conductivity values, this work demonstrated the advantage of polymer preintercalation in 2D silicates, which helps in achieving better blending of the nanofiller and the polymer host within PCEs.[149,150] Similar preintercalation strategies to make organophilic MMTs by organic cationic intercalants, such as dodecyl ammonium cations to improve the nanofiller–polymer host interaction are also known.[151]

The size of anions also influences the ionic conductivity of PCEs. For example, it has been reported that the ionic conductivity of melt-blended PEO-MMT (1.0–20 wt% MMT loading) PCEs with $LiClO_4$/$LiBF_4$ is higher than with $LiCF_3SO_3$.[152] In a report from Tominaga and co-workers, the directional orienting of MMT layers in a specific direction within the polymer host has been found to influence the ion transport properties of the PCE.[153] This involved utilizing an in situ polymerization technique for the PCE processing in three steps: 1) orientation of MMT in the monomer solution under a strong magnetic field, 2) solvent removal, and 3) in situ polymerization. Strong magnetic fields help align the MMT in parallel and perpendicular orientations toward the conductivity measurement direction (**Figure 22**a–c). Compared to the neat PEO-Li^+ DPE, the PCE with MMT layers parallel to the direction of conductivity measurement displayed six times higher conductivity (0.012 mS cm^{-1}, 30 °C, 5.0 wt% loading). This phenomenon is an example of anisotropy shown by the 2D silicates due to the intrinsic 2D structure.[9,136a]

MMT-based PCEs with polymer hosts other than PEO are also known for LB applications. Sengwa and Choudhary reported several d-PCEs and plasticized PCEs based on the PMMA-PEO blend and MMT in the presence and absence of PEG plasticizer.[155] Indeed, the dielectric properties and relaxation times of these PCEs varied as a function of the nanofiller and plasticizer amount. In the works of Srinivasan and co-workers, g-PCEs based on MMT in PVDF[156] or PVDF-HFP[154] hosts for LMB application are studied. The MMT/PVDF film (casting by phase inversion technique) or MMT/PVDF-HFP film (casting by electrospinning) composites have been prepared by the solution-blending method, and the obtained films follow activation in a carbonate-based liquid electrolyte (1 M $LiPF_6$ in EC:DEC). Figure 22d illustrates the effect of sonication time directing the microstructure of the resulting g-PCEs. An increase in sonication time helps achieve better exfoliation of MMT layers and improved Li^+-ion transport pathways within the g-PCE. These works also emphasize the benefit of converting hydrophilic-MMT to organophilic-MMT by preintercalating cationic

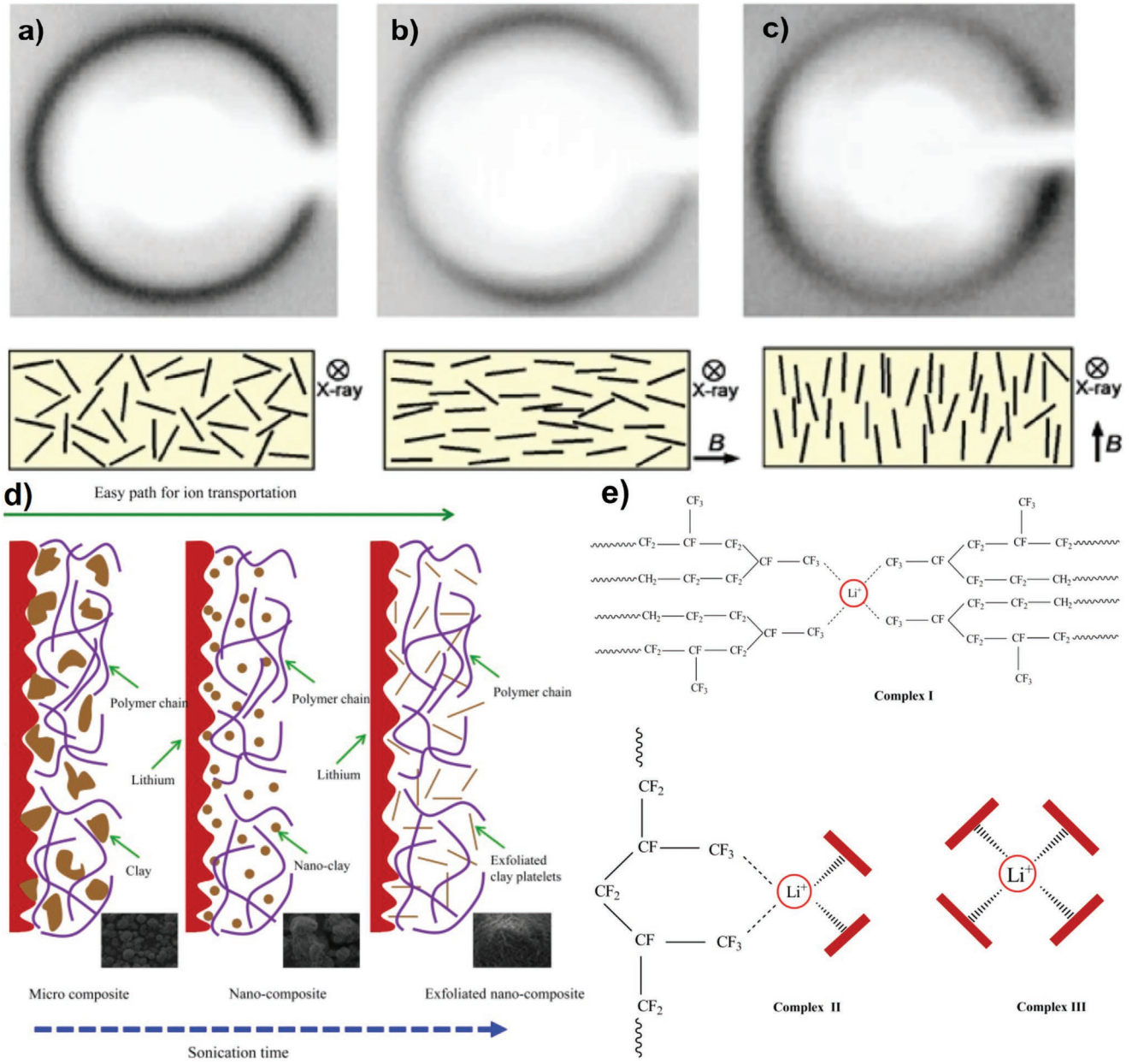

Figure 22. MMT orientation in PCE: a) random, b) parallel, and c) perpendicular directions to the direction of conductivity measurement and corresponding 2D wide-angle X-ray diffraction (WAXD) patterns. Reproduced with permission.[153] Copyright 2012, The Society of Polymer Science, Japan. d) Effect of sonication time in directing the microstructure of the PCE during the solution-blending process. e) Interactions between PVDF-HFP, exfoliated clay layers, and Li^+-ions in a PCE. Reproduced with permission.[154] Copyright 2013, Elsevier.

surfactants (e.g., quaternary alkyl amines) since the organophilic MMT exhibits superior interactions with the hydrophobic PVDF or PVDF-HFP. Adding 1.0–4.0 wt% of the MMT nanofiller into PVDF and PVDF-HFP widens/diminishes the XRD peaks of MMT (2θ = 2°–10°), indicating clay exfoliation and polymer intercalation. It is noteworthy that the PVDF and PVDF-HFP based g-PCEs exhibit 1.98 and 5.5 mS cm^{-1} (30 °C, 1.0 wt% MMT loading) ionic conductivities, respectively. The superior ion transport properties of the MMT/PVDF-HFP electrolyte are due to the additional Li^+ coordination interactions offered between the exfoliated clay layers and the $-CF_3$ groups of PVDF-HFP, which is absent in the PVDF counterpart (Figure 22e). The well-aligned nanofibers of electrospun PVDF-HFP must be another reason for the better ion transport properties of MMT/PVDF-HFP. The $LiMn_2O_4$|MMT-PVDF|Li and LFP|MMT-PVDF-HFP|Li cells differed in their specific capacity (120 and 160 mAh g^{-1}, respectively, at 25 °C).[154,156] Still, the performance was nevertheless superior to the individual MMT-free cells.

A recent report suggests incorporating Li-MMT into poly(ethylene)carbonate for PCE preparation.[157] In this work, the PCE processing involves solution casting followed by hot pressing. The PCE also contains LiFSI salt,

poly(tetrafluoroethylene), and fluoroethylene carbonate (FEC) to improve ionic conductivity, mechanical stability, and electrode|electrolyte interphase and interfacial properties, respectively. The presence of liquid additive (FEC) contributes to the resulting PCEs ionic conductivity (0.35 mS cm^{-1}, 25 °C). Therefore, the PCE reported in this work may fall into a g-PCE or plasticized PCE category. The report claims that the FSI anion of the lithium salt tends to approach the positively charged edges of the Li-MMT clay, facilitating Li^+ intercalation into the interlayer clay galleries. Besides Li^+-ions, the intercalation of FEC molecules is also feasible. The anion-trapping capability of the Li-MMT clay (**Figure 23**a) accounts for the high t_{Li}^+ value (0.83) observed for the optimized g-PCE. The g-PCE displays HSAL and dendrite growth inhibition capability with bare and 3D Li metal anodes (Figure 23b–d). Moreover, the high oxidation stability of the g-PCE (4.6 V vs Li|Li^+) is an additional advantage for allowing its applicability in high-voltage LMBs. For instance, the LMB full cell with NMC-111 cathode

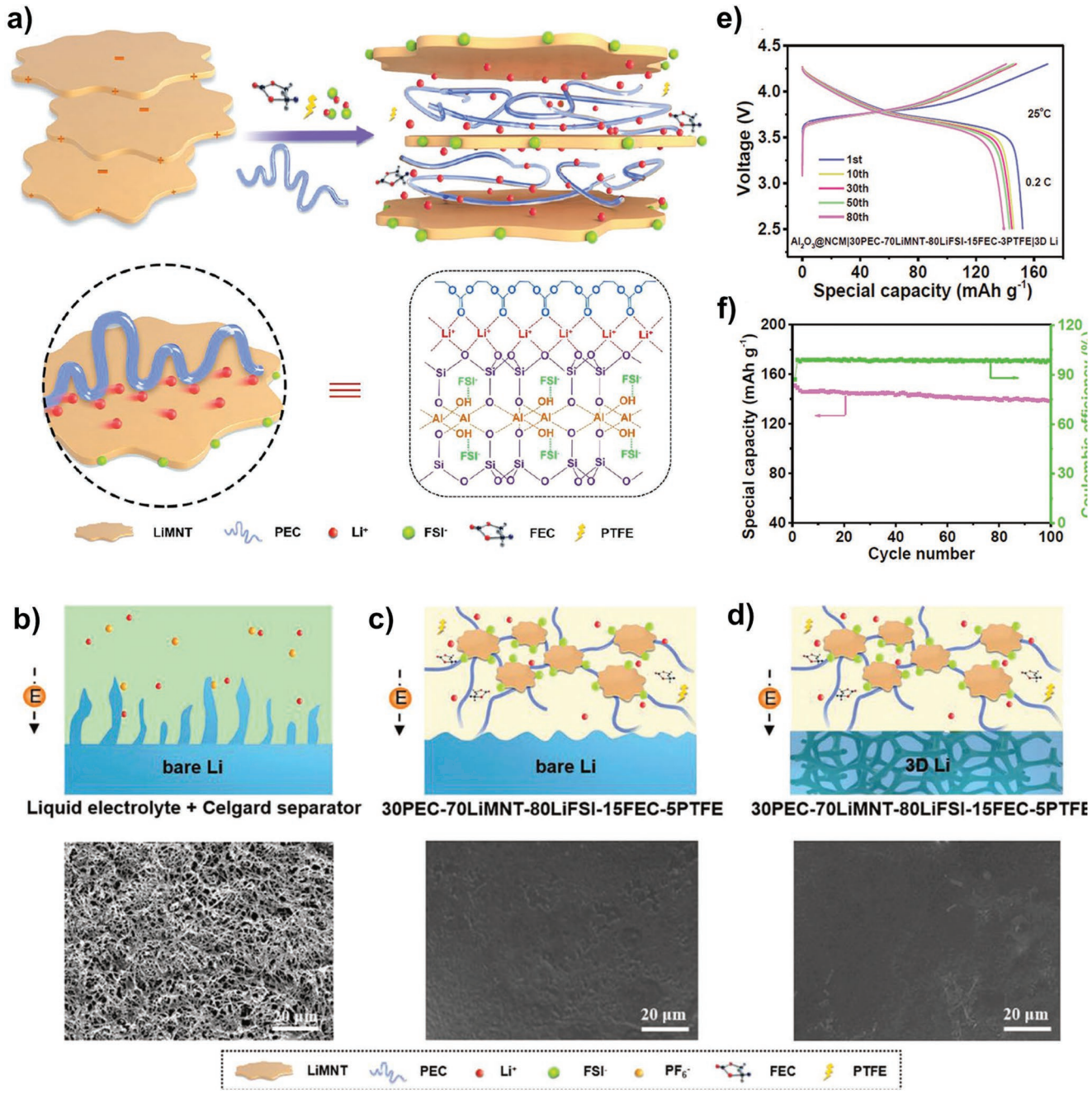

Figure 23. a) Illustration of anion trapping and ion transport mechanism in Li-MMT-based g-PCE. b–d) The HSAL inhibition property of Li-MMT-based g-PCE compared to a conventional liquid electrolyte-based LMB cell. The surface morphology of the bare and 3D Li metal anodes following cycling is also shown. The e) galvanostatic charge–discharge (GCD) and f) cycling stability profiles of NMC-111|g-PCE|Li cell. Reproduced with permission.[157] Copyright 2019, Wiley-VCH.

exhibits a specific capacity of 160 mAh g^{-1} (0.2 C, 25 °C) with a retention of 92% over 100 cycles (Figure 23e,f). The use of MMT to modify separators (polypropylene, polyethylene, etc.) to minimize polysulfide diffusion and dendrite-growth suppression is also known.[144,158] Although these MMT-separator systems cannot be directly called PCEs, the possibility of separator modification proves the compatibility of MMT, and the large pool of polymers used in separators other than the PE hosts.

Like MMT, vermiculites,[159] a magnesium aluminosilicate (2:1 2D silicate) with high CEC value, are also widely used for PCE preparation. Vermiculite's thermal expansion and solvent-swelling properties have recently gained immense attention for PCE processing.[160] The works of Tang et al.[161] discusses the prospect of tuning the ion transport and physicochemical properties of PEO using few-layered vermiculites. One of the works uses the property of thermally expanded vermiculite clay undergoing easy exfoliation on direct-ion exchange reactions in the alkali-metal salt solution.[161a] It is interesting to note the property of the exfoliated vermiculite (nano)sheet (VS) forming self-standing films (**Figure 24**a,b), even in the absence of any polymer host. Later, VS, PEO, and lithium salt (LiTFSI) undergo the solution-blending process in acetonitrile, resulting in d-PCE films (Figure 24c,d). The optimized d-PCE film (10 wt% VS) displayed high ionic conductivity (Figure 24e, 0.03 mS cm^{-1} at 25 °C and 1.2 mS cm^{-1} at 60 °C) and t_{Li^+} of 0.25 at 25 °C. The superior oxidation stability (4.5 V vs Li|Li^+) of the d-PCE over the nanofiller-free DPE is also a notable advantage (Figure 24f). The d-PCE is claimed to suppress the HSAL deposition and displays a specific capacity of 160 mAh g^{-1} (0.1 C, 60 °C) in LFP|d-PCE|Li cells.

The same group has also reported the advantage of infiltrating vertically aligned vermiculite (nano)sheets (VAVS, prepared by temperature gradient freezing) into a PEO host for improving the low-temperature performance (ionic

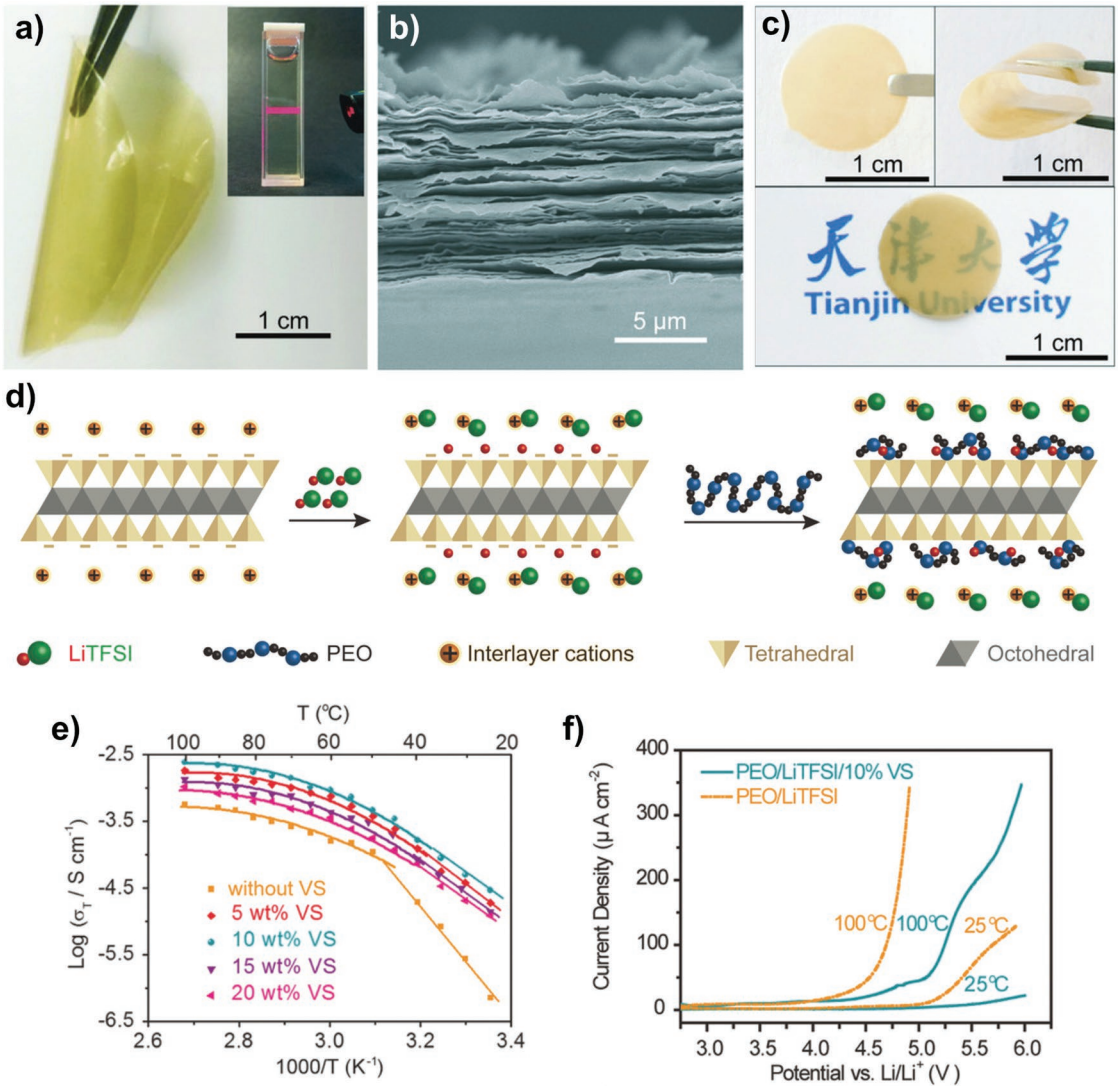

Figure 24. a) Photograph and b) SEM cross-sectional image of a vermiculite nanosheet (VS)-based self-standing film. c) Photographs of the VS-based d-PCE films. d) Illustration of the mechanism of ionic conductivity enhancement in VS-based d-PCE. e) Ionic conductivity of d-PCE loaded with varying amount of VS as a function of temperature. f) Linear sweep voltammetry analysis of d-PCEs with and without VS nanofiller at 25 and 100 °C for the determination of oxidation stability. Reproduced with permission.[161a] Copyright 2018, Wiley-VCH.

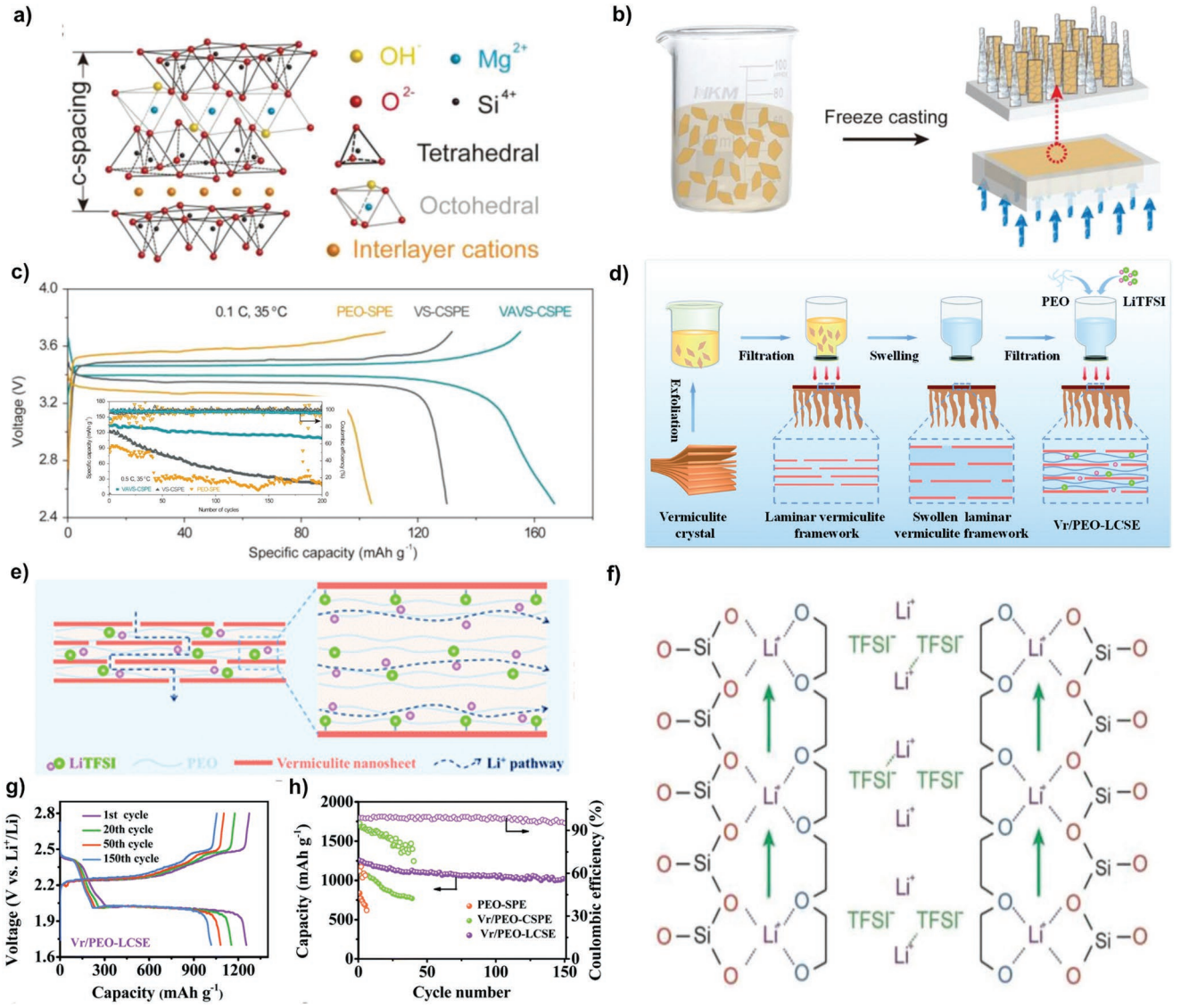

Figure 25. a) Illustration of the crystal structure of vermiculite clay. b) Temperature gradient freezing and casting of the d-PCE with vertically aligned vermiculite (nano)sheets (VAVS). c) GCD and cycling stability (inset) profiles of LFP|PCE|Li cell (35 °C). d) Illustration of the intercalation of PEO–LiTFSI into vermiculite interlayers by swelling and filtration process. e,f) Illustration of the ion transport channels and enhanced mobility of PEO chains within the laminar vermiculite framework. g) GCD and h) cycling stability profiles of S|PCE|Li cell (60 °C). (a–c,f) Reproduced with permission.[161b] Copyright 2019, Wiley-VCH. (d,e,g,h) Reproduced with permission.[162] Copyright 2020, Royal Society of Chemistry.

conductivity of 0.20 mS cm^{-1} (25 °C) and t_{Li}^+ of 0.5) of the d-PCE (**Figure 25**a,b).[161b] The performance improvement is apparent from the specific capacity (167 mAh g^{-1}, 0.1 C) and cyclic stability (82% retention, 200 cycles, 0.5 C) of the LiFP||Li cell at 35 °C (Figure 25c). Another interesting work from Zhai et al. put forward a novel approach for processing d-PCEs based on vermiculite and PEO for Li–S batteries.[162] The d-PCE preparation involves intercalating PEO–LiTFSI into the vermiculite layers by a swelling and filtration process (Figure 25d). The solid-state d-PCE displays high ionic conductivity of 0.01 mS cm^{-1} (25 °C), t_{Li}^+ of 0.42, and excellent mechanical properties. The improved ion transport is due to the enhanced mobility of PEO chains within the interlayers of the laminar vermiculite framework (Figure 25e,f). The d-PCE in the Li–S battery delivers an initial specific capacity of 1254 mAh g^{-1} (0.05 C, 60 °C), a value 50% higher than the vermiculite-free DPE (Figure 25g). The higher capacity retention (81% over 150 cycles) offered by d-PCE is also interesting, indicative of its capability to minimize polysulfide shuttling (Figure 25h).

Apart from using MMT and vermiculite, a few other silicates in the smectite family have also been investigated for PCEs. For example, saponite ($Na_x(Si_{4-x}, Al_x)(Mg_3)O_{10}(OH)_2$),[163] a trioctahedral clay, has been utilized for the preparation of d-PCEs with PEO.[164] For this purpose, Na-saponite is initially converted to Li-saponite by LiOH treatment in solution. The solution-blended d-PCE displayed a superior ionic conductivity (25 °C) of 4.1 mS cm^{-1} compared to the melt-blended counterpart (1.4 mS cm^{-1}), implying an improved PEO intercalation by the

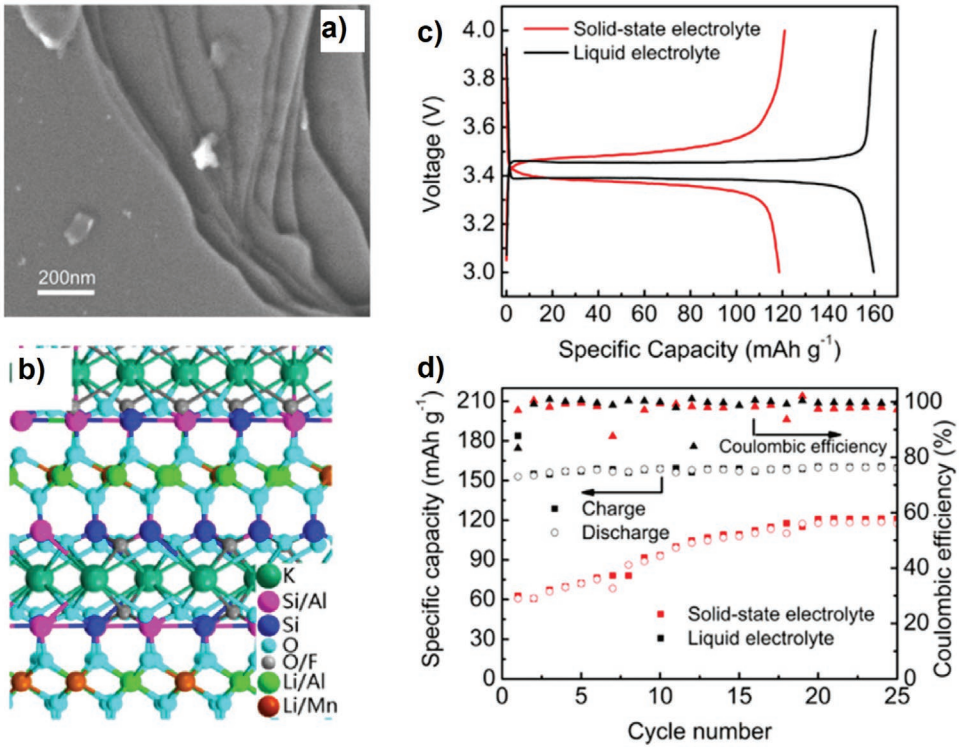

Figure 26. a) SEM image and b) crystal structure of lepidolite. c) GCD and d) cycling stability profiles of LFP|d-PCE|Li cells. Reproduced with permission.[142] Copyright 2019, American Chemical Society.

former processing method. The exceptionally high t_{Li}^+ value (0.99) and the high ionic conductivity of the saponite-based d-PCEs, in contrast to the classical PEO-Li DPE, are also worth mentioning.

Unlike the 2:1 silicate mineral in the smectite and vermiculite family, the CEC value of 2D silicates in the mica family is relatively low (Table 2). Besides, micas are generally known as non-expandable clays,[165] whereas smectites, vermiculates, etc., are examples of expandable clays.[166] Due to the low CEC value and non-expandable nature, the cations in muscovite mica ($KAl_2(AlSi_3O_{10})$ $(F, OH)_2$) are not exchangeable under ambient conditions,[133a] and have therefore received little attention for PCE preparation. However, a recent report by Wang et al. suggests that inherent solid-state Li^+-ion conductivity occurs in a modified muscovite called lepidolite, making it a suitable active nanofiller in PCEs (**Figure 26**a,b).[142,167] It is worth mentioning that the exchanged cations are not responsible for the observation of ionic conductivity in lepidolite. By contrast, the ionic conductivity is due to the doping of octahedral Al^{3+} by Li^+-ion in the crystal structure, creating ion transport pathways accompanied by defects. Hence prepared d-PCE (indeed an HPE) based on lepidolite and PEO displays an ionic conductivity of 0.015 mS cm^{-1} (100 °C). Indeed, it has been reported that incorporating additional $LiClO_4$ salt into the same d-PCE improves ionic conductivity (0.15 mS cm^{-1}, 35 °C). An optimum amount of 43 wt% of lepidolite in the d-PCE improves the t_{Li}^+ to 0.72. The LFP||Li cell fabricated using this optimized d-PCE delivers a specific capacity of 125 mAh g^{-1} (0.15 C, 60 °C, 25th cycle) (Figure 26c,d). Similarly, other reports have shown that integrating lepidolite (6 wt%) in PVDF in the presence of DMF (3.9 wt%) as plasticizer results in a g-PCE that shows an ionic conductivity of 0.125 mS cm^{-1} at RT.[168] Lepidolite clays have also recently attracted interest in the battery research community as a polypropylene separator modifier that prevent polysulfide shuttling and decrease Li^+-ion diffusion barrier (0.031 eV).[169] These new results suggest that, similar to other 2D silicates, lepidolites are also exciting candidates with great potential for futuristic PCEs for Li–S batteries.

5.2. Layered Double Hydroxides for PCEs

The well-known examples of 2D layered ACMs, characterized by their anion exchange capacity (AEC), are LDHs. The high AEC of LDHs could be functional for anion conducting (e.g., OH^-) PCEs for fuel cell applications.[170] Besides, the redox and electrocatalytic activity of several LDHs make them suitable as electrode materials for batteries, supercapacitors, fuel cells, etc.[171] The ideal structural formula of LDH minerals is $[M^{II}_{1-x}M^{III}_x(OH)_2]^{x+}{}_{intra}[A^{m-}{}_{x/m}\ .nH_2O]^{x-}{}_{inter}$, referred to as the subgroup of hydrotalcite natural mineral structure.[49c,172] M^{II} and M^{III} are divalent and trivalent metal cations, respectively, and A^{m-} is the anions. The layers of LDH compose of brucite-like ($(Mg(OH)_2)$ edge-sharing octahedrons ($M(OH)_6$) (**Figure 27**a).[173] Examples of M^{II} cations include Mg^{2+}, Mn^{2+}, Co^{2+}, Fe^{2+}, etc., whereas, Al^{3+}, Fe^{3+}, Ni^{3+}, etc., for M^{III}. Halide ions, CO_3^{2-}, SO_4^{2-}, etc., are a few of the anions (A^{m-}) found in

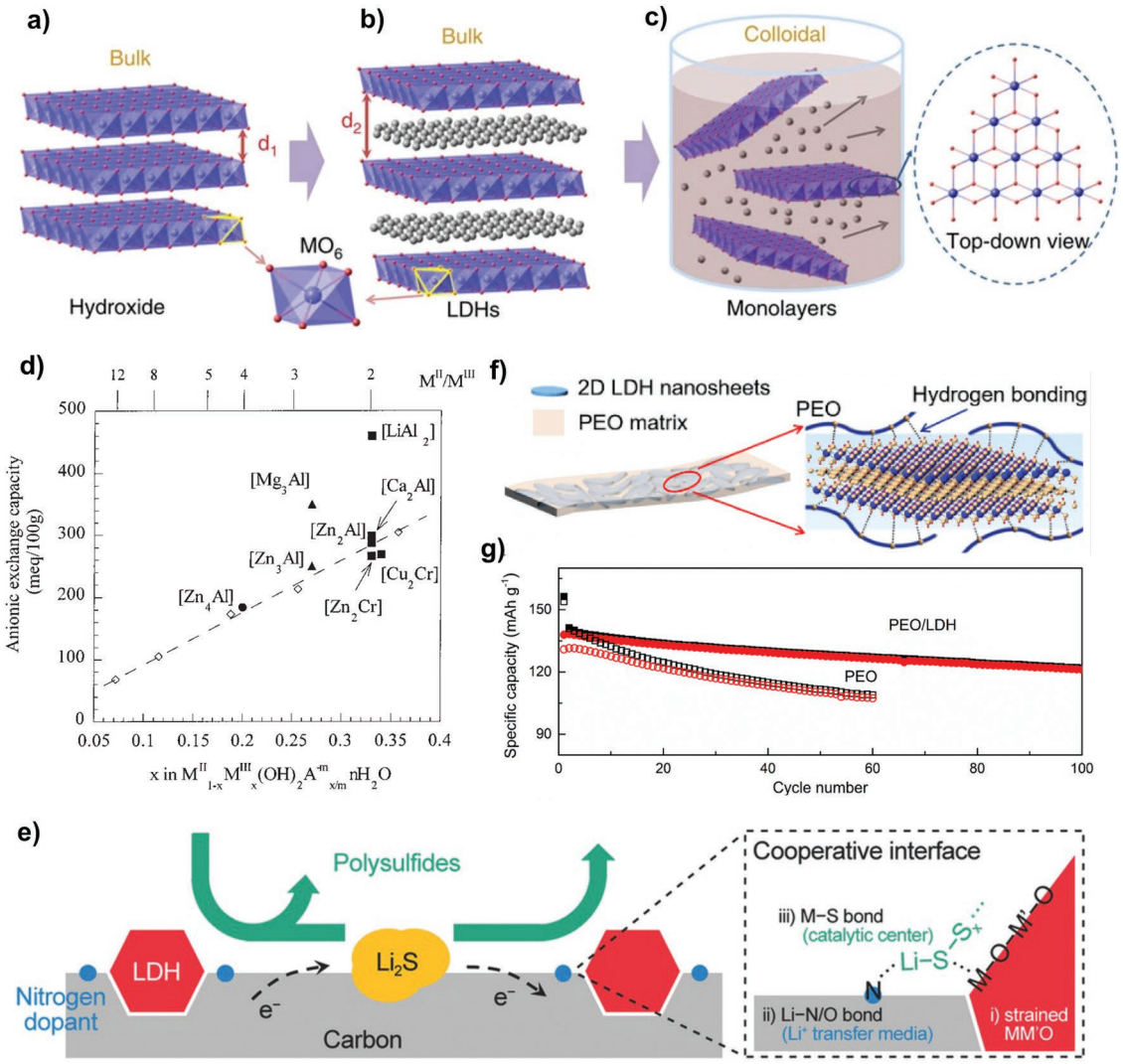

Figure 27. Crystal structure of a) brucite and b) LDH. c) Illustration of exfoliated LDH layers in a solvent.Reproduced with permission.[173] Copyright 2014, Springer Nature. d) Plot representing the AEC values of some of the LDHs. Reproduced with permission.[177] Copyright 2001, American Chemical Society. e) Illustration of the trapping mechanism of polysulfide anions by LDH in S||Li cells. Reproduced with permission.[180] Copyright 2016, Wiley-VCH. f) Scheme representing hydrotalcite LDH encapsulated in PEO host. g) Comparison of cycling stability of an LFP||Li cell with and without hydrotalcite nanofiller in a polymer electrolyte. Reproduced with permission.[181] Copyright 2020, Elsevier.

LDHs.[174] The "intra" and "inter" terms in the structural formula indicate the intralayer domains and interlayer galleries, respectively. Typically, the distinct net positive charged layers in LDHs arise due to the partial substitution of divalent cations (M^{II}) by trivalent counterparts (M^{III}).[172b,174] LDHs containing monovalent metal ions, such as Li^+ in place of M^{II} are also known, although rare.[175] Indeed, these Li^+ LDHs could be exciting candidates as active nanofillers in PCEs since recent reports suggest their capability of Li^+ diffusion.[176] The representative structure of $M(OH)_6$ octahedron, LDH structure, its exfoliation, and the AEC values of certain LDHs are shown in Figure 27a–d.[173,177]

Due to the low CEC values of LDHs, during the last two decades (the year 2000 to 2020), they have only rarely found applications in cation-conducting PCEs for lithium- and post-lithium batteries. For example, in the works of Liao and Ye from the early 2000s, anionic surfactants based on sulfonate (SLDH) and phosphonate (PLDH) were used for modifying the LDH structure.[178] Due to the AEC of LDHs, anionic surfactants/polymers are suitable for surface modification. The intercalation and exfoliation induced by the surfactant molecules improve the compatibility of LDHs with polymers, such as PEO, thereby finding application in PCEs. It is worth noting that the PLDH displays effective exfoliation, but SLDH exists as aggregated nanosheets. When used in d-PCEs, the exfoliated PLDH improves interactions with PEO and helps reduce its crystallinity, favoring ionic conduction (0.015 mS cm^{-1}, 30 °C).[178a] Similarly, incorporating PEO, phosphonate improves the t_{Li}^+ value of the d-PCE to 0.42, as reported in another work from the same group.[178b] This high t_{Li}^+ value, despite using PEO as the PCE host, could be due to the anion-trapping capability of LDHs owing to their high AEC values. Another work from Bhat and co-workers reports a PCE based on PEG (M_w = 2000 g mol^{-1}), $LiClO_4$, and hydrotalcite LDH

($[Mg_{0.67}Al_{0.33}(OH)_2]$ $[(CO_3)_{0.17}\cdot mH_2O]$).[179] Despite the low CEC value of hydrotalcite LDH, the d-PCE in this work exhibits RT ionic conductivity of 0.01 mS cm^{-1} due to the low M_w of PEG and the improved percolation effects at the LDH/polymer interfaces.

Inspired by these earlier reports, the prospect of LDHs for PCE preparation is recently gaining immense attention among battery researchers. For instance, the anion trapping capability of LDHs has been of great interest to modify polymeric separators in Li–S batteries to trap the dissolved polysulfide anions (Figure 27e), thereby improving cycling stability.[171a,180] Unlike earlier reports on PCEs based on LDHs, which primarily emphasized ion transport properties, recent reports have also demonstrated the application of LDH-based PCEs in LMB cells. For instance, Wang et al. used a combination of hydrotalcite and LiTFSI in PEO for d-PCE preparation, which resulted in an RT ionic conductivity of 0.01 mS cm^{-1} and a t_{Li^+} of 0.42 (Figure 27f).[181] This d-PCE further exhibited dendrite inhibition capability when used in LMBs employing an LFP cathode (practical specific capacity of 138 mAh g^{-1}, 0.2 C, 60 °C, 88% retention after 100 cycles), thereby inspiring subsequent works on LDHs for PCEs. Although not used for PCE preparation, another recent report suggests the compatibility of PMMA and FeAl-LDHs for polymer composite preparation.[182] The compatibility of various LDHs with polymer hosts other than PEO could be exciting for designing better PCEs based on LDH in the future. In line with this, the latest report from Xia et al. suggests the prospect of an LDH containing Li^+ in the crystal structure ($LiAl_2$-LDH) for d-PCE preparation (**Figure 28**a).[183] The exfoliated $LiAl_2$-LDH incorporated in PVDF-HFP polymer host in the presence of LiTFSI salt by a solution-blending method results in a PCE with a high RT ionic conductivity of 0.22 mS cm^{-1}. This PCE displays an excellent t_{Li^+} value of 0.78 due to the anion trapping capability of the $LiAl_2$-LDH. The high oxidation stability of the PCE (4.9 V vs $Li|_{Li^+}$) is an additional advantage, which is significantly higher than the nanofiller-free counterpart (4.10 V vs $Li|_{Li^+}$). Moreover, LMB cells based

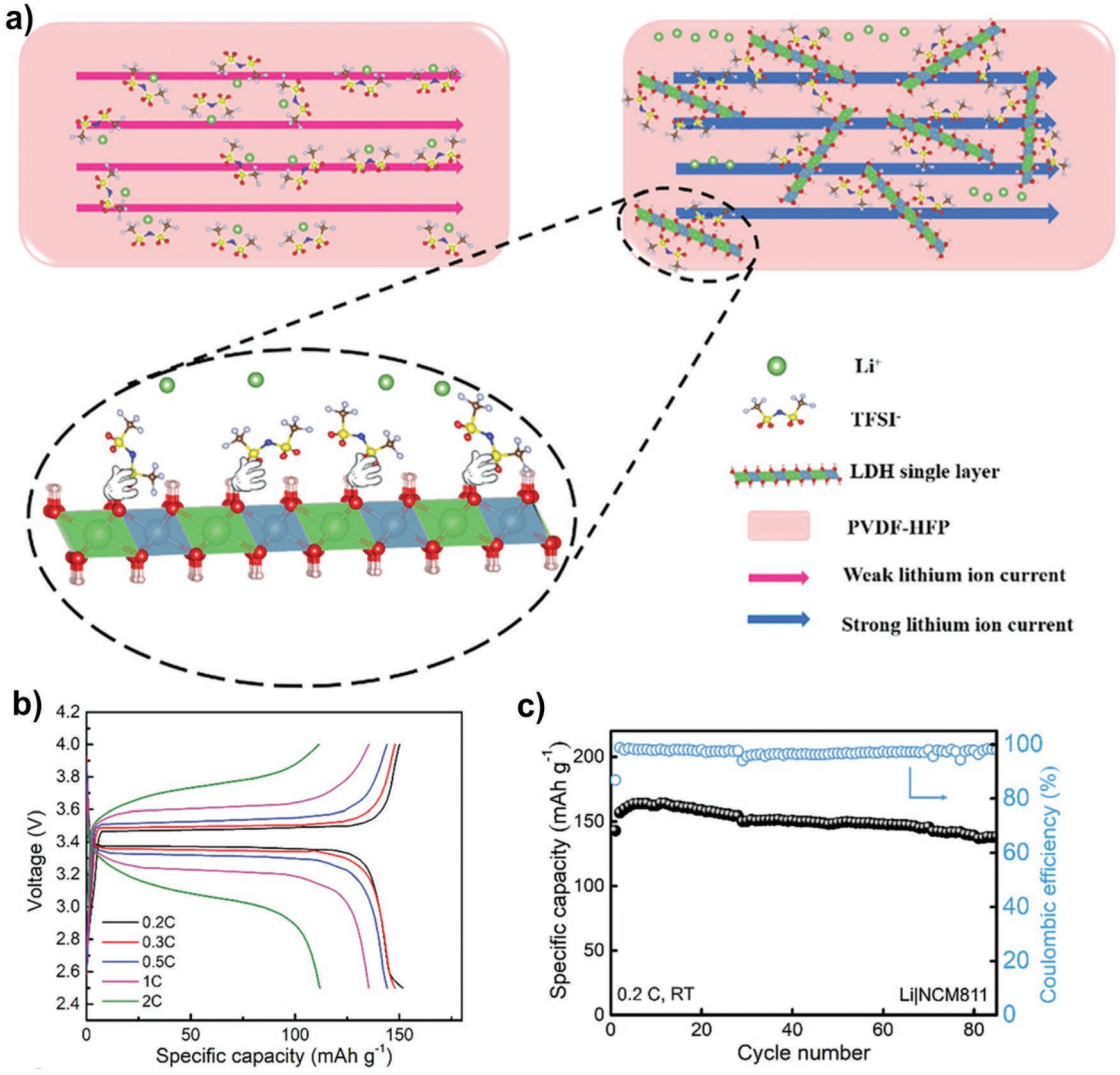

Figure 28. a) Illustration of the crystal structure of $LiAl_2$-LDH and their exfoliated layers encapsulated within the PVDF-HFP host. The anion trapping capability of $LiAl_2$-LDH assists in improved Li^+-ion transport pathways. b) GCD and c) cycling stability profiles of LFP||Li and NMC-811||Li cells, respectively. Reproduced with permission.[183] Copyright 2021, Wiley-VCH.

on LFP cathodes using this d-PCE displays excellent RT cycling stability with a retention of 98% of initial capacity (190 cycles, 157 mAh g^{-1}, 0.1 C) (Figure 28b). Besides, the d-PCE exhibits decent cycling behavior also with LCO and NMC-811 cathodes (Figure 28c).

6. MOFs: 2D Organic–Inorganic Hybrid Nanofillers for PCEs

MOFs are crystalline organic–inorganic porous materials made of ordered arrays of molecular building blocks consisting of metal centers coordinated to electron-donating multidentate organic ligands.[184] MOFs, also called "coordination polymer,"[185] are characterized by their unique open framework structure with tuneable porosity and high surface area (≈6000 m^2 g^{-1}).[186] Apart from coordination bonds, other weak interactions such as hydrogen bonding, van der Waals interactions, and π–π stacking contribute to stabilizing their framework under harsh conditions.[187] Interestingly, it is possible to localize the coordination process within the desired space to obtain MOFs with 0D, 1D, 2D, or 3D spatial dimensionalities (**Figure 29**).[188] The uniqueness of MOFs lies in their structural versatility and extended porous (nano- to macroscale pores) networks. According to the pore diameter, a wide variety of guest moieties (gas molecule, organic solvent molecule, dyes, etc.) can fit into the cavities in MOFs through host–guest interaction involving the metal cations and the functional organic linkers. Such structural and dimensional flexibilities open possibilities to tailor the properties of MOFs that are crucial for applications such as gas storage and separation, catalysis, and electrochemical energy storage.[189,190] Another emerging approach is to utilize MOFs as stand-alone electrolytes or additives in PCEs.[191,192] The organic functional groups in MOFs can facilitate homogeneous blending of MOF additives and polymers through Lewis acid–base complexation interactions. For instance, the 3D porous MOF, $Zn_4O(BDC)_3$ (MOF-5) has been proven to interact with the PEO and $TFSI^-$ to reduce the polymer crystallinity and increase the Li^+-salt dissociation when used in a d-PCE (**Figure 30**a,b).[191] Although MOF-5 with a cage-like framework structure does not fall into the 2D layered nanomaterials category, in recent years, MOFs possessing layered structure (2D MOFs/MOF nanosheets) are gaining great attention as nanofillers in PCEs.

Like other 2D layered nanomaterials discussed in the previous sections, the synthesis of 2D MOFs also proceeds through bottom-up or top-down strategies, involving mechanical exfoliation, surfactant-assisted reactions, and interfacial reactions (Figure 30c).[193] 2D MOFs are fascinating because they have high aspect ratio and contain more exposed active sites on the surface, which is beneficial for creating better functional

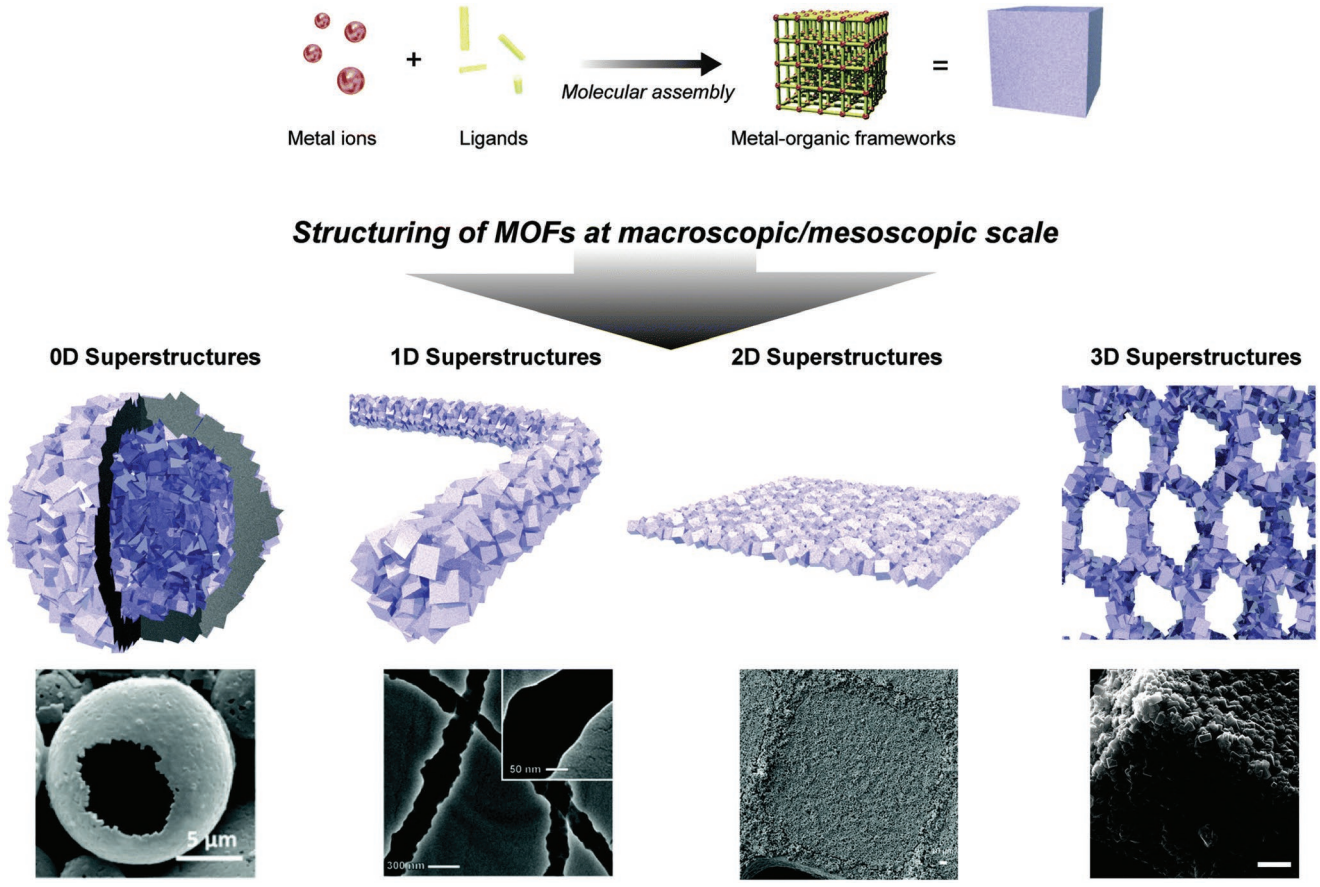

Figure 29. The illustration shows the preparation of MOFs with different dimensionalities (0D, 1D, 2D, and 3D), their structure, and electron microscopy images. Reproduced with permission.[188a] Copyright 2014, Royal Society of Chemistry.

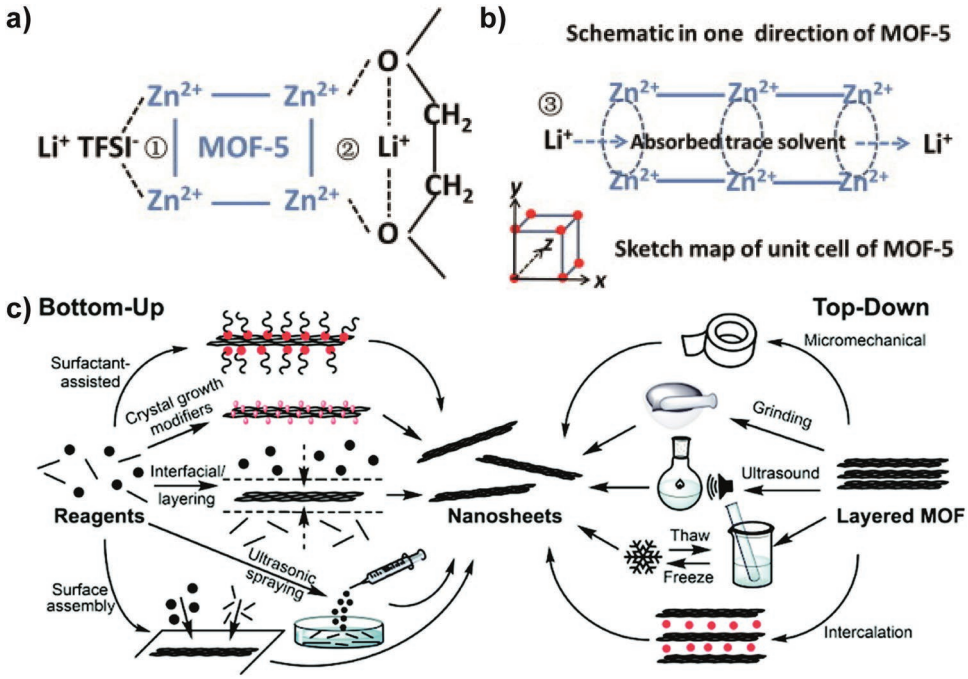

Figure 30. A plausible mechanism for improved ionic conductivity of PCE assisted by MOF-5: a) interaction of anion with the unsaturated metal sites of MOF, and Li^+-ions with the PEO chains in PCE and b) ion transport in 3D directions through the pore channels of MOF-5. Reproduced with permission.[191] Copyright 2013, Elsevier. c) Bottom-up and top-down strategies for preparing 2D MOF nanosheets. Reproduced under the terms of the CC BY 3.0 license.[193] Copyright 2018, The authors, published by Royal Society of Chemistry.

interfaces with the polymer matrix. Han et al. developed a d-PCE of Ni-based 2D MOF (constructed from Ni(II) node and 1,4-benzenedicarboxylic acid (BDC) ligand) nanosheet (NMS) mixed with PEO–LiTFSI following a solution casting strategy (**Figure 31**a).[194] The ionic conductivity of the d-PCE containing an optimum concentration (8 wt%) of NMS was 0.017 mS cm^{-1} (t_{Li}^+ = 0.38), one order magnitude higher than the Al_2O_3 counterpart. The NMS nanofiller also imparted higher anodic stability and interfacial stability to the d-PCE in contact with the Li-metal anode, as reflected in the better plating/stripping profile (Figure 31b,c), Li deposition morphology (Figure 31d,e), and specific capacity of the Li||Li and LFP||Li cells. The favorable impact of the NMS nanofiller originated from several possible factors: 1) the large lateral dimension of NMS helps reduce the extent of polymer crystallization, 2) NMS can cross-link the PEO chains and improve the mechanical strength of the PCE, and 3) the Lewis-acidic surface of NMS (due to the unsaturated Ni sites) facilitates Li^+-ion mobility by blocking the diffusion of $TFSI^-$ ions.

In contrast to the conventional approach of preparing PCEs by mixing the nanofiller with the polymer host of interest, Yu et al. developed a 3D continuous nanofiller scaffold using Cu(BDC) 2D MOF (**Figure 32**a) nanosheets and a nonwoven fabric (NWF) substrate.[45] They decorated the NWF by sequentially soaking the substrate in the ligand (BDC) and Cu(II) salt solution. Finally, the impregnation of PVDF-$LiClO_4$/DMF solution into the NWF@Cu(BDC) scaffold and subsequent evaporation of the solvent resulted in the desired d-PCE (NWF@Cu(BDC)-PVDF). Figure 32b depicts the steps involved in the NWF@Cu(BDC)-PVDF preparation process. The 3D continuous architecture of the d-PCE provides high mechanical strength and accelerates the Li^+-ion diffusion in two pathways: 1D channels (Figure 32a) inside MOF and 3D through the MOF/PVDF interface. The experimental findings, coupled with DFT studies, further elucidated the coordination of ClO_4^- anions with the uncoordinated Cu^{2+} site, which eases the $LiClO_4$ salt dissociation and makes the Li^+-ion mobility more facile (Figure 32a). As a combined effect, the ionic conductivity of the d-PCE (0.24 mS cm^{-1} at 30 °C) was higher than the MOF-free DPE and Cu(BDC)-PVDF d-PCE, prepared by the conventional cast-then-dry method. The performance of NWF@Cu(BDC)-PVDF d-PCE in an LMB cell with high-voltage NMC-811 cathode delivering 164 mAh g^{-1} capacity and good capacity retention over 80 cycles is appreciable (Figure 32c,d).

Despite the advantages mentioned above, the application of 2D MOFs for developing PCEs for LBs is still underexplored. Hence, future studies on introducing new 2D MOFs and understanding the interface of MOF nanosheet with polymer and salt constituents are essential to exploit the full advantages of 2D MOF-based nanofillers. In this direction, an exciting approach could be developing cationic 2D MOF by grafting organic cations onto the MOF surface, since such cationic nanofiller can immobilize the electrolyte anions and provide seamless passage for Li^+-ion conduction.[195]

7. COFs: Organic Nanofillers for POCEs

Similar to MOFs that are porous organic–inorganic hybrid materials, organic porous materials possessing framework

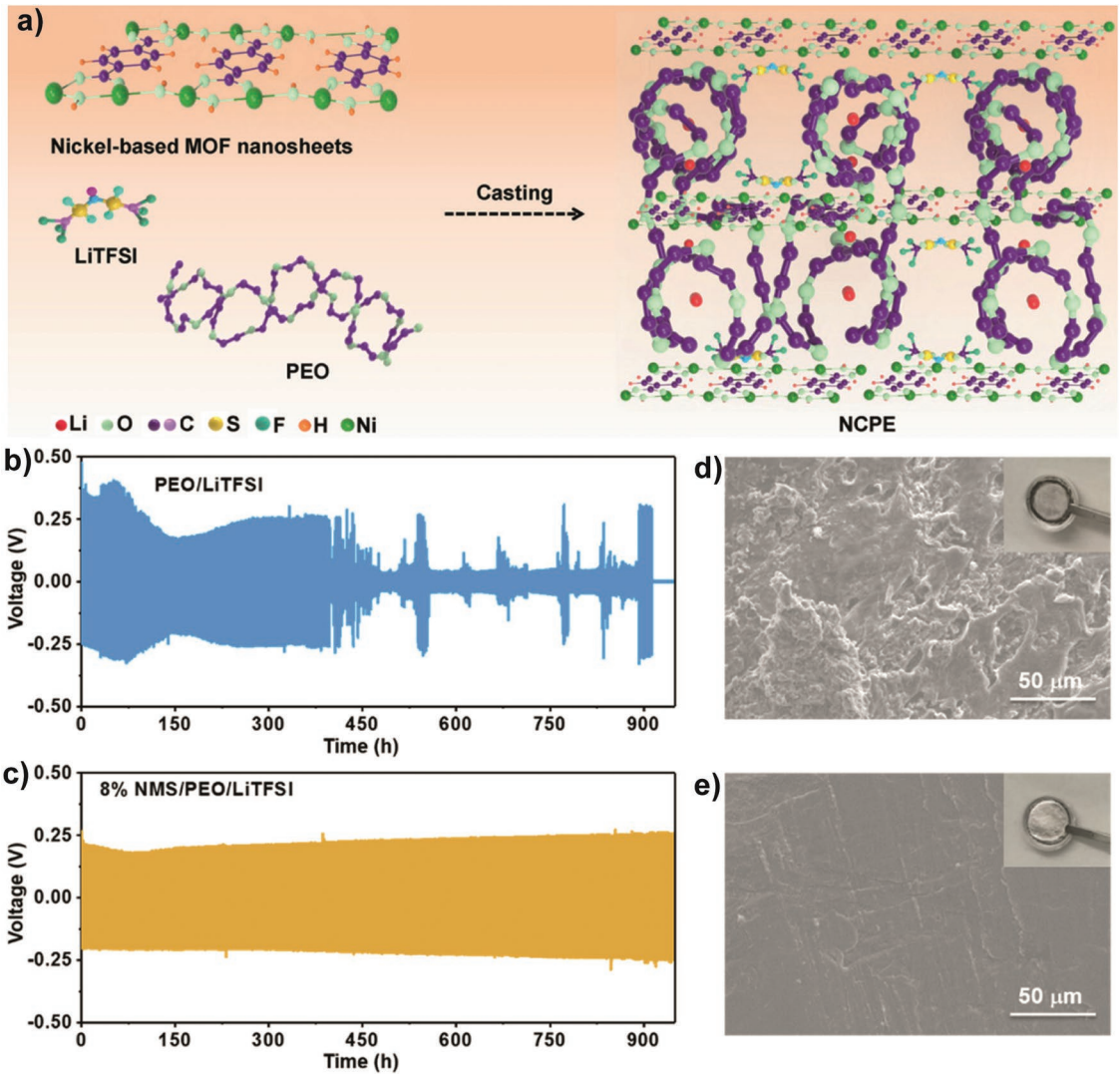

Figure 31. a) Illustration showing the preparation of d-PCE comprising Ni MOF nanosheets; cycling test of Li||Li cell with b) PE and c) MOF-based d-PCE at 0.3 mA cm^{-2} and 50 °C. d) and e) Ex situ scanning electron microscope images and digital photographs (inset) of the Li electrodes recovered from the cells mentioned in (b) and (c), respectively. Adapted with permission.[194] Copyright 2020, American Chemical Society.

structure also offer opportunities to develop solid- and quasi-solid-state electrolytes for LBs. In this regard, COFs are suitable candidates, which are organic framework materials composed of organic ligands that are covalently bonded to each other. COFs are generally classified into 2D and 3D COFs.[196] 2D COFs are the most common, which crystallize as stacked sheets with 1D porous channels, whereas 3D COFs are characterized by crystalline, extended, net-like reticular structures. One of the attractive properties of 2D COFs is that they are often prone to exfoliation into 2D nanosheets through physical or chemical processes. Envisaging the future potential of such 2D COFs as nanofillers in PCEs, this dedicated section aims to give the readers a summary of several COF-based electrolytes reported for LBs so far. Herein, one of the objectives is to enlighten the readers about the prospects of the emerging field of COFs for LB electrolyte applications. Therefore, this section also considers reports on both 2D and 3D COF electrolytes though they do not really fall into any PCE category. In any case, the term polymer organic composite electrolytes "POCEs" is used to account for the organic nature of COFs whenever a report on COF-based PCE is under discussion.

In 2015, Park et al. reported a Li^+-ion conducting crystalline covalent organic porous network based on cucurbit[6]uril (**CB[6]**), a well-known macrocyclic molecule resembling a 2D COF.[196e] The ionic conductivity of the **CB[6]** pellets soaked in a carbonate-based liquid electrolyte showed values in the range of 0.08–0.10 mS cm^{-1} at RT. The low activation energy (0.32–0.38 eV) and a high t_{Li^+} value (0.7–0.8) were attributed to the excellent Li^+-ion transport predominantly provided by the narrow 1D channels and the capability to block the bulky anions transport through these pores (**Figure 33**). This report on **CB[6]**-based electrolyte opened up new avenues toward developing 2D COF-based electrolytes with Li^+-ion conducting properties. For example, research in similar direction was reported by Vasquez-Molina et al. using electrolyte-impregnated COF pellets made of 2D COFs with different symmetries and functionalities (**COF-5** and

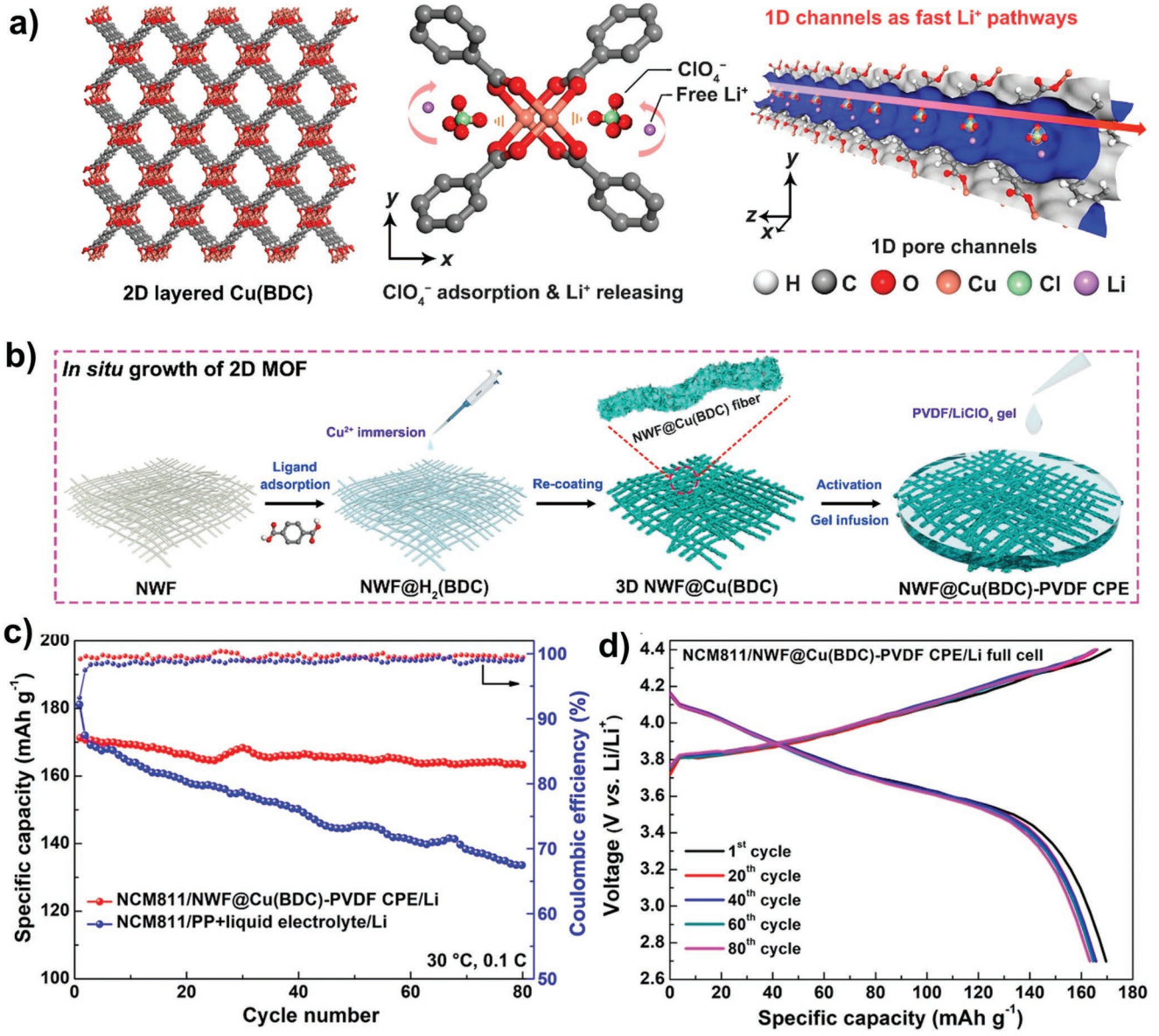

Figure 32. a) The structure of Cu(BDC), mechanism of $LiClO_4$ salt dissociation assisted by Cu(BDC), and representation of 1D porous channels in the MOF for fast Li^+-ion conduction. b) Process involved in the in situ growth of Cu(BDC) nanosheets over the nonwoven fabric and developing 3D Cu(BDC)-based PCE in the subsequent steps. c) Cycling stability data and d) voltage profile of the NMC-811||Li cell with NWF@Cu(BDC)-PVDF PCE. Reproduced with permission.[45] Copyright 2021, American Chemical Society.

TpPa-1, **Figure 34**).[196a] They observed improved electrochemical stability and fast Li^+-ion conduction, especially through crystallographically aligned 2D COF materials than the nonaligned counterparts. Later, Zhang et al. used simulation studies and found that short-range diffusion of Li^+-ions and their coordination are driven by the rotation of anions and the solvent, which facilitates the 1D liquid-like diffusion of Li^+-ions in 2D COFs.[197]

A recent report focused on developing boron-containing 2D COF as a nanofiller to prepare a gel POCE (g-POCE) for LIBs (Figure 34). For this purpose, the 2D COF named **H-COF-1@10** was encapsulated within PVDF host followed by activation in a liquid electrolyte (1 M $LiClO_4$/EC:DMC (1:1)).[198] The **H-COF-1@10**-based POCE exhibited an ionic conductivity of 0.25 mS cm^{-1} (RT). The higher ionic conductivity arises from the strong adsorption of anionic moieties to the **H-COF-1@10** fillers. The presence of polarizable ClO_4^- ion enables the formation of the complex with more B atoms in the 2D COF framework, resulting in a high t_{Li}^+ of 0.71. The incorporation of electron-withdrawing groups such as fluorinated aryl and alkyl groups in the framework structure may be a suitable strategy for further reducing the anion mobility and improving the t_{Li}^+ values for POCEs based on these 2D COFs.

A common feature of the 2D COFs discussed in the above-mentioned reports is that none of them bear a charged moiety, or put in other words, they are all neutral. However, it is possible to design COFs with positive or negatively charge bearing functional groups. Hu et al. developed a series of crystalline imidazolate 2D ionic COFs (ICOFs) with ionic linkages that

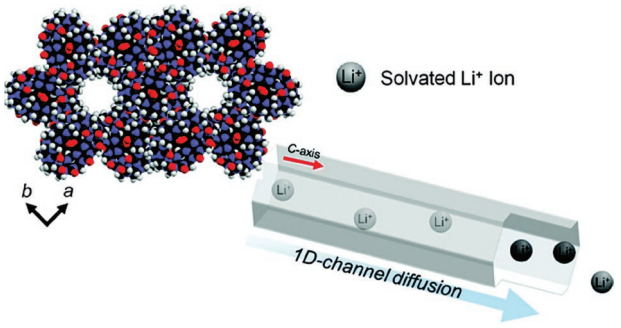

Figure 33. CB[6]-based electrolyte illustrating the Li^+-ion transport pathway in the 1D channels. Reproduced under the terms of the CC BY 3.0 license.[196e] Copyright 2015, The authors, published by Royal Society of Chemistry.

inherently possess Li^+-ions in the structural framework suitable for ion conduction. Interestingly, these ICOFs with immobile anionic moieties resembled SIC-PEs and may be called single-ion conducting COFs (SIC-COFs).[1a,200] These 2D ICOFs activated in a liquid electrolyte displayed exceptional ionic conductivity at RT and lower activation energy (**Figure 35**).[46] Herein, the imidazolate groups in the ICOFs displayed weak imidazolate-Li^+ binding interactions, and the presence of well-defined 1D porous channels facilitated the free movement of Li^+-ions. The lithiated **CF_3-Li-ImCOF** displayed the maximum RT ionic conductivity (7.2 mS cm^{-1}), low activation energy (0.10 eV), and high t_{Li}^+ value of 0.93. The weaker ion pairing and the anionic character are justified for **CF_3-ImCOF** due to the electron-withdrawing effect of $-CF_3$ than the $-CH_3$ in **CH_3-ImCOF**. Although 2D ICOFs are yet to be used for PCOEs, Du et al. used a 3D ICOF (**ICOF-2**, Figure 35) for g-POCE preparation in combination with PVDF polymer host.[196b,199,201] The g-POCE membranes (soaked in PC (24 h)), showed an ionic conductivity of 0.03 mS cm^{-1} (RT) and activation energy of 0.24 eV. The POCE displayed a high t_{Li}^+ value of 0.80 ± 0.02 due to the anionic character of the **ICOF-2**.

Most of the COF materials developed for electrolyte application use liquid electrolytes for activation in one way or another. However, the new concept of using COFs without any solvent for Li^+-ion conduction is also gathering immense attention among researchers as an alternative to ISEs. Such COFs with inherent Li^+-ion conduction feature could be called "all-solid-state COF electrolytes".[202a,203,204] For instance, an all-solid-state

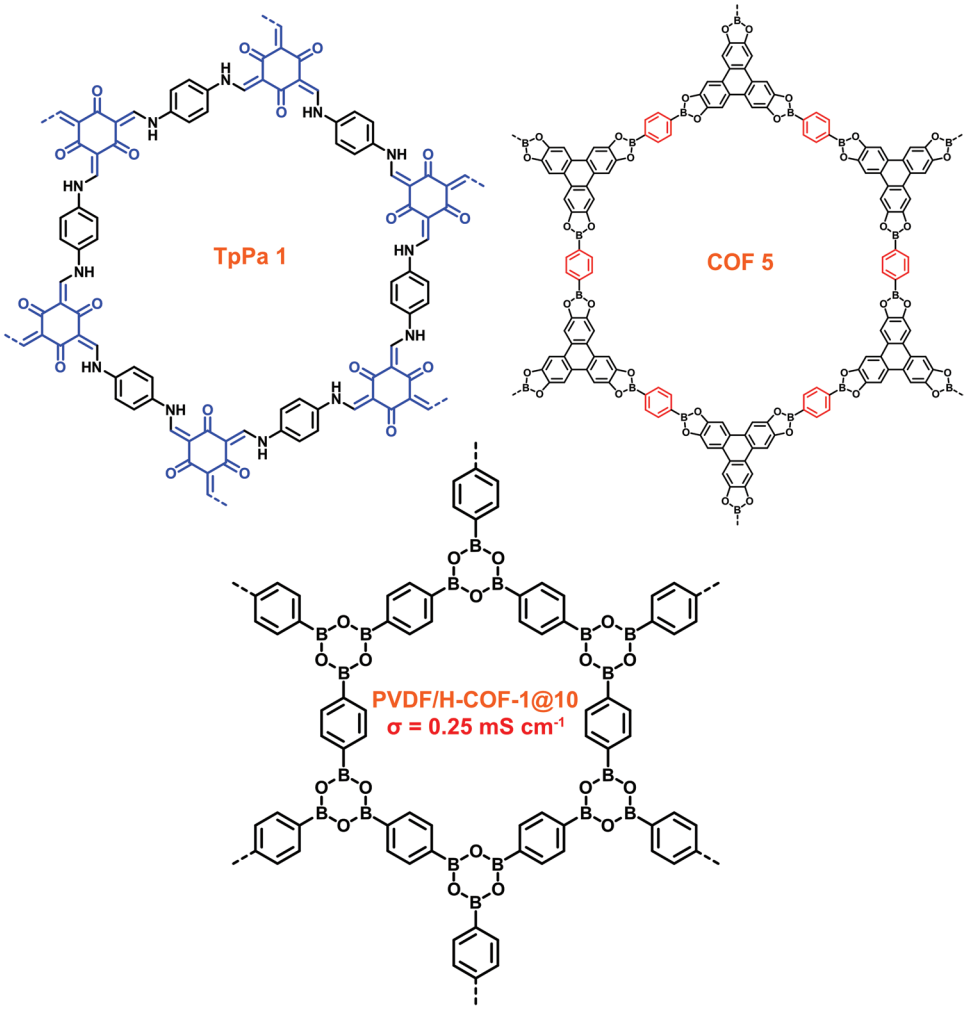

Figure 34. Chemical structures of neutral 2D COFs: COF-5, TpPa-1, and H-COF-1@10 used for various electrolyte applications.

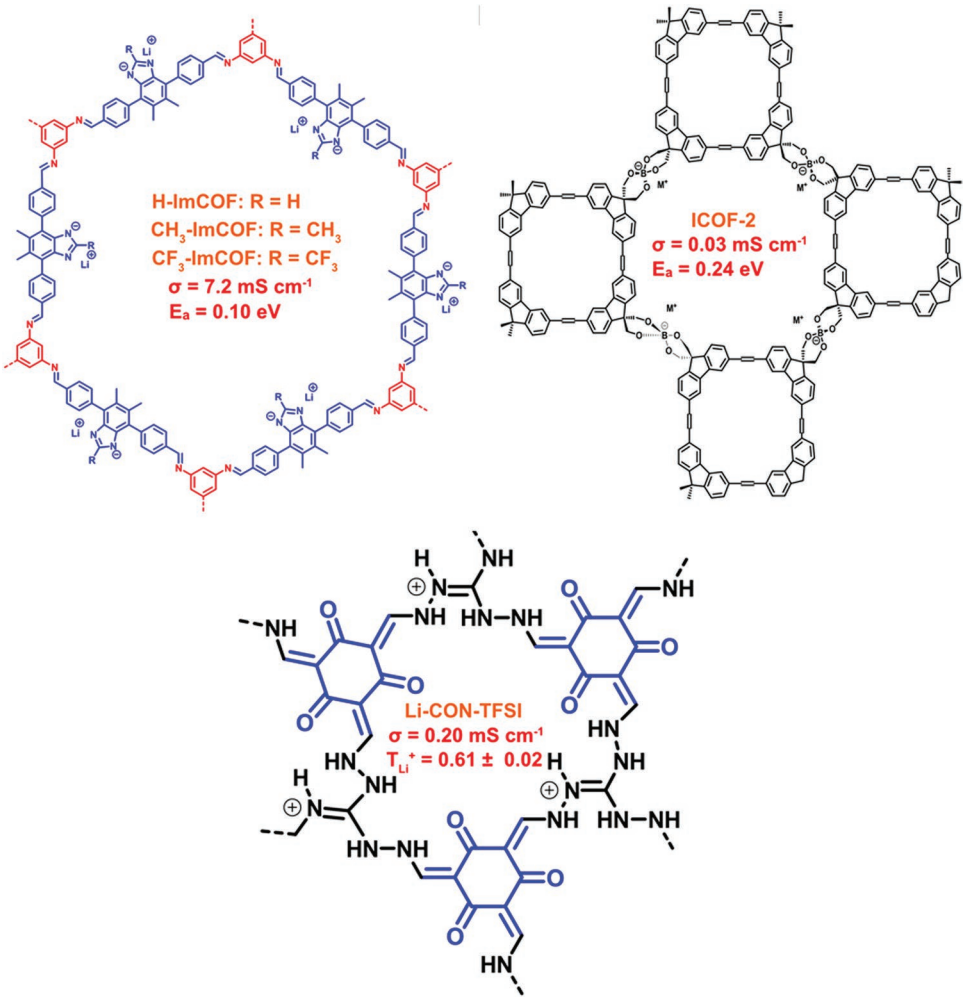

Figure 35. Chemical structures of ionic COFs: anionic spiroborate-based 3D ionic COF (ICOF-2), anionic imidazolate ICOF (ImCOF), and 2D COF nanosheets (CONs, Li-CON-TFSI).

COF electrolyte based on a 2D cationic ICOF nanosheet (CON) was reported by Chen et al.[202a] The **Li-CON-TFSI** (Figure 35) prepared by ion-exchange reaction between **CON-Cl** and LiTFSI exhibited ionic conductivities of 0.06 and 0.21 mS cm^{-1} at 30 and 70 °C, respectively. The irregular 2D nanosheets showed an activation energy of 0.34 eV $atom^{-1}$ with an average t_{Li}^{+} of 0.61 ± 0.02. In this case, faster Li^{+}-ion conduction in CONs was achieved due to the interaction of $TFSI^{-}$ ions with the 2D CON framework, which further liberated Li^{+}-ions freely. Similarly, reports on all-solid-state anionic COFs based on lithium sulfonated 2D COFs exhibiting t_{Li}^{+} value as high as 0.90 are also known.[204] Despite these advancements in the preparation and validation of ICOFs as all-solid-state electrolytes, they are yet to be used as a nanofiller in POCEs, which is highly likely to come into the limelight in the upcoming years.

Functionalized 2D COFs having PEO/PEG units directly attached to their framework structure are innovative materials, which bridge benefits of COFs and the polymer host used in conventional PEs.[205–208] These polymer units can influence the crystallinity of COFs and are often suitable for improving the thermal and mechanical properties of nonfunctionalized 2D COFs. In this regard, Zhang et al. introduced PEO into the inner space of a 2D COF by self-assembly approach to prepare glassy COF electrolytes (**Figure 36**).[206] Three PEO functionalized hydrazone-linked COFs, **COF-PEO-*x***: x = 3, 6, and 9, were synthesized using a solvothermal method. To investigate the Li^{+}-ion conductivity, **COF-PEO-*x*-Li** was prepared by immersing **COF-PEO-*x*** in LiTFSI-containing THF solution. Ionic conductivity of 1.33 mS cm^{-1} was obtained for **COF-PEO-9-Li** at 200 °C. A decline in ionic conductivity was observed at lower temperatures and in COFs with less density of PEO chain accumulation. Later, there have been attempts to introduce various branched PEO chains onto the pores of COF by condensing 1,3,5-tris(4-formyl-phenyl)-benzene with three PEG-based hydrazide monomers.[207] LiTFSI was introduced into the COF through a soaking process to obtain **COF-PEG-Bn-Li** (Figure 36, Bn represents no. of chains with n = 1,3,6). The ionic conductivity of **COF-PEG-B6- Li** showed the highest ionic conductivity values of 3.4×10^{-3} mS cm^{-1} at 60 °C, 0.16 mS cm^{-1} at 140 °C, and 1.5 mS cm^{-1} at 200 °C. However, with an increase in chain length, a higher activation energy of 0.60 eV was observed for **COF-PEG-B6-Li**.

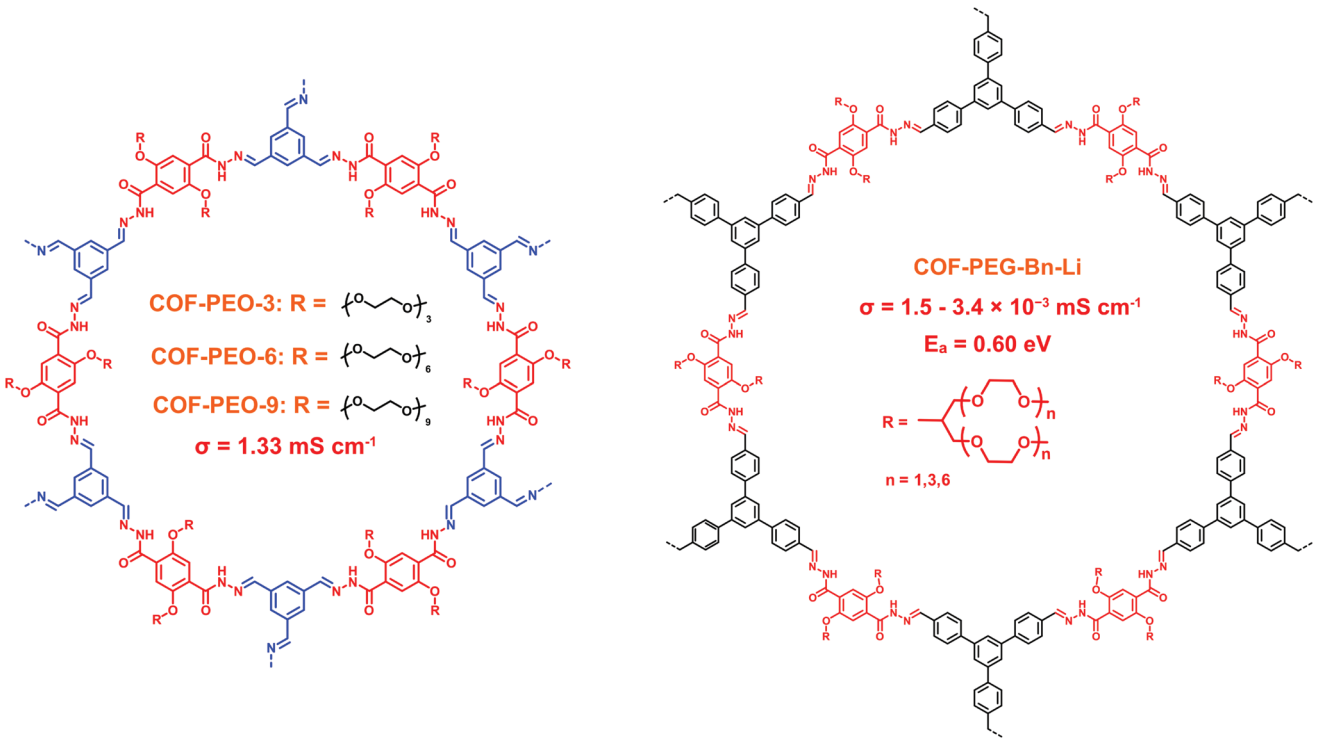

Figure 36. Chemical structures of PEO/PEG functionalized COFs (COF-PEO-*x* and COF-PEG-Bn-Li).

In conclusion, different strategies have been employed to design 2D COF materials for their use as stand-alone electrolytes and nanofillers in POCEs. **Table 3** further summarizes the characteristic features of 2D COF-based materials and POCEs evolved from these efforts. Introduction of ionic moieties, PEOs, defect engineering, and post-functionalization has improved Li^+-ion conductivity and Coulombic efficiency, and lowered activation energy. The field is relatively new, and innovative synthetic modifications and molecular engineering to achieve realistic COF systems with acceptable electrochemical performance are inevitable for their widespread application and commercial demonstration.

8. Conclusion and Future Perspectives

This review article thoroughly covered the potential uses of 2D layered nanomaterials as nanofillers in PCEs. Compared to classical PCEs using ceramic nanoparticle fillers, the 2D layered nanomaterial encompassed PCEs deliver targeted characteristics even in very low quantities. Indeed, polymer molecules and ions can intercalate into the interlayer galleries of 2D layered nanofillers, which can significantly impact the physicochemical and electrochemical properties of the resulting PCEs.

Being natural and easily available, clays (2D silicates and LDHs) dominated the early reports on 2D nanofillers-based PCEs. Synthetic 2D layered nanomaterials (MXenes, GO, phosphorene, h-BN, etc.) have also been emerged as suitable nanofillers finding a great deal of application in PCEs. The most recent entrants such as 2D MOFs and COFs into the 2D material landscape, further add to the research portfolio accessible in this field. For the same reason, identifying, designing, and engineering the most reliable candidates among the variety of 2D layered nanomaterials are important, however such a step is challenging as no performance benchmark is available to compare. In this scenario, it is important to develop standard protocols to test and report these materials for rapid screening for both academic and commercial purposes.

It is clear from this review that the electronic conductivity/semiconducting properties of several 2D layered nanomaterials, which could be detrimental to any electrolyte, do not pose a significant problem when present in PCEs in extremely low amounts, e.g., graphene. If required, the detrimental electronic conductivity can often be made minimal by straightforward methods, e.g., the oxidation of graphene to GO, which can provide a chemical functionalization pathway that is generally beneficial for the PCE. Moreover, it is clear that the 2D layered nanomaterials generally improve mechanical and thermal stability, and prevent Li dendrite formation, which can otherwise be problematic for neat DPEs or (especially) GPEs. Indeed, the high-aspect-ratio characteristic of these nanofillers was focused, which favored more polymer-nanofiller interfaces for creating fast ion-transport pathways with low activation energy, ultimately influencing the global Li^+-ion transport mechanism in PCEs. In other words, at the polymer–nanofiller interfaces, an otherwise semicrystalline polymer turns amorphous; or 2D layered nanomaterials act as solid-plasticizers, promoting the bulk ionic conductivity in the resulting PCE. Even though, the low-aspect-ratio 3D nanofillers used in the classical PCEs also contribute to bulk ionic conductivity, they generally display a weaker contribution towards global ionic conductivity through the interfacial transport processes.

Table 3. Summary of COF-based electrolytes and POCEs for LB application.

Sr. no	Material	Salt	Solvent	Conductivity [mS cm^{-1}]	t_{Li^+}	Activation energy [eV]	Refs.
1.	Cucurbit[6]uril	1 M $LiPF_6$ or $LiClO_4$	PC	0.08–0.10 (RT)	0.7–0.8	0.32–0.38	[196e]
2.	COF-5	1 M $LiClO_4$	THF	0.26 (RT)			[196a]
3.	ICOF-2		PC	0.03 (RT)	0.80 ± 02	0.24	[199]
4.	H-Li-ImCOF	Lithiation by n-BuLi in hexane	PC	5.3 (RT)			[46]
	CH_3-Li-ImCOF			0.08 (RT)			
	CF_3-Li-Im-COF			7.2 (RT)			
5.	PVDF/H-COF-1@10	$LiClO_4$	EC/DMC	0.25 (RT)	0.71		[198]
6.	Li-CON-TFSI			0.06 (30 °C) 0.21 (70 °C)	0.61 ± 0.02		[202a]
7.	dCOF-ImTFSI-60@Li	LiTFSI		7.05 (150 °C)	0.72	0.28	[202b]
8.	PEG-Li^+@EB-COF-ClO_4	$LiClO_4$		0.02 (30 °C) 1.78 (120 °C)	0.60	0.21	[203]
9.	TpPa-SO3Li	LiOAc		0.027 (RT)	0.9	0.18	[204]
10.	Li^+@TPB-DMTP-COF Li^+@TPB-BMTP-COF	$LiClO_4$		1.36×10^{-4} (40 °C) 6.74×10^{-4} (60 °C) 5.37×10^{-3} (80 °C) 6.04×10^{-3} (40 °C) 0.03 (60 °C) 0.17 (80 °C)		0.96 0.87	[205]
11	COF-PEO-*x*-Li	LiTFSI		1.33 (200 °C)			[206]
12	COF-PEG-B6- Li	LiTFSI		1.5 (200 °C)	0.30	0.60	[207]

Another benefit of 2D nanofillers is their net surface charge, which aids in improving salt dissociation and often contributes to enhancing the cation transference numbers in PCEs. For example, the high cation exchange capacity of 2D silicates is known to favor the interlayer diffusion of Li^+-ions in PCEs. Similarly, the trapping of the salt anions by LDHs due to their net positive surface charge also enhances the cation transference number of the resulting PCEs. It is worth mentioning that the net positive charge of the LDH has the capability of minimizing the diffusion of polysulfides, especially when used in Li–S batteries. The application of 2D silicates and LDHs in inherently conducting Li^+-ions is highly promising, as they can open up the field of 2D layered ISEs as potential active fillers for PCEs. However, the bulk of the scientific literature is focused more on materials performance than on elucidating the origins of ionic conduction. As can be concluded from this review, there is an apparent lack of MD simulation studies that can elucidate the global and local transport mechanisms existing in multicomponent PCEs, and hence it is difficult to scientifically and systematically tailor, identify, and optimize these materials further. Another common observation regarding natural and synthetic 2D layered nanomaterials is the selection of polymer hosts, mostly conventional polymers such as PEO, PVdF-HFP, etc. have been employed, nevertheless, other polymer hosts, poly(trimethylene carbonate), poly(caprolactone), polyketones, etc., have also emerged as promising new candidates in PCE research. In this regard, while considering the prospects of inorganic 2D layered nanomaterials and related PCEs, it is worth highlighting that new and target-specific polymer hosts that are available from the large pool of PE literature need to be considered.

With the progress in solid-state batteries, it is a good sign that the recent works on 2D layered nanomaterials based PCEs emphasize achieving enhanced electrochemical properties and performance in LMB cell batteries. It is noticed that LFP is the most studied cathode material for 2D layered nanofiller-based PCEs, and there are several early reports on LCO as well. However, it is vital to investigate their performance against other commercially crucial high-voltage cathode materials free of Co and having high Ni content (e.g., NMC 811, LNMO, etc.). More studies are needed to understand their electrochemical degradation in LMB cells, especially against Li metal anodes and high-voltage cathodes, to make them competitive with existing or futuristic solid-state and/or gel electrolytes. In this respect, going beyond sweep-voltametric techniques could be attractive in gaining a realistic picture of the electrochemical stability of these PCEs.[208]

A critical observation from this review article is the foray of organic and organic–inorganic hybrid 2D layered nanomaterials into the PCE research landscape. In this regard, several academic publications on 2D COF and 2D MOF nanofillers for PCEs are already available. Unlike inorganic layered materials, there are many additional opportunities with these organic and organic–inorganic hybrid 2D layered nanomaterials for molecular engineering because of the presence of organic building blocks. For instance, there are 2D COFs that are inherently conducting while possessing single-ion conducting properties. 2D MOFs may also imbibe similar features by tweaking the organic ligands with the targeted functional moieties. Although the field of MOFs are just two decades old, it is interesting to note that PCEs based on 2D MOFs are used against high-voltage cathodes such as NMC-811 on a lab-scale. Recent reports of MOFs with

inherent Li^+-ion conduction in the solid-state are also promising for solid-state batteries, as these MOFs may find application as active fillers in PCEs. Ultimately, 2D COFs and MOFs are interesting nanofillers for PCEs and certainly demand further attention from the battery community. However, more validation is required to understand how the organic moieties present in these materials reacts in high-oxidative and reductive environments in contact with reactive electrodes inside a battery.

In summary, the role of 2D layered nanomaterials as nanofillers in PCEs is encouraging due to the possibility of tailoring their properties according to the targeted battery chemistry. This comparatively new research field hence demands thorough investigations and explorations, which could revolutionize the field of PCEs and its application in solid-state lithium and post-lithium battery systems.

Acknowledgements

M.W. and J.R.N. gratefully acknowledge the support provided by the German Federal Ministry of Education and Research within the (BMBF) project "Benchbatt" (03XP0047B) and "FestBatt" (13XP0175A), respectively. V.V., J.M., and D.B. wish to acknowledge funding through (1) European Research Council (ERC), Grant No. 771777 FUN POLYSTORE and STandUP for Energy and (2) European Union's Horizon 2020 research and innovation programme under Grant Agreement No. 875514 (project ECO^2 LIB). The authors thank Andre Bar for his graphical support.

Open access funding enabled and organized by Projekt DEAL.

Conflict of Interest

The authors declare no conflict of interest.

Keywords

2D materials, clay minerals, covalent organic frameworks, metal–organic frameworks, MXene, polymer composite electrolyte, solid-state batteries

Received: October 1, 2022
Revised: December 20, 2022
Published online: March 11, 2023

[1] a) V. Vijayakumar, B. Anothumakkool, S. Kurungot, M. Winter, J. R. Nair, *Energy Environ. Sci.* **2021**, *14*, 2708; b) M. Winter, B. Barnett, K. Xu, *Chem. Rev.* **2018**, *118*, 11433; c) A. Yoshino, *Angew. Chem., Int. Ed.* **2012**, *51*, 5798; d) B. Scrosati, *Chem. Rec.* **2005**, *5*, 286; e) S. Dühnen, J. Betz, M. Kolek, R. Schmuch, M. Winter, T. Placke, *Small Methods* **2020**, *4*, 2000039.

[2] a) J. Mindemark, M. J. Lacey, T. Bowden, D. Brandell, *Prog. Polym. Sci.* **2018**, *81*, 114; b) J. Kalhoff, G. G. Eshetu, D. Bresser, S. Passerini, *ChemSusChem* **2015**, *8*, 2154; c) N. Nitta, F. Wu, J. T. Lee, G. Yushin, *Mater. Today* **2015**, *18*, 252.

[3] J.-L. Brédas, J. M. Buriak, F. Caruso, K.-S. Choi, B. A. Korgel, M. R. Palacín, K. Persson, E. Reichmanis, F. Schüth, R. Seshadri, M. D. Ward, *Chem. Mater.* **2019**, *31*, 8577.

[4] I. Cekic-Laskovic, N. von Aspern, L. Imholt, S. Kaymaksiz, K. Oldiges, B. R. Rad, M. Winter, *Top. Curr. Chem.* **2017**, *375*, 37.

[5] J. R. Nair, L. Imholt, G. Brunklaus, M. Winter, *Electrochem Soc Interface* **2019**, *28*, 55.

[6] a) T. Placke, R. Kloepsch, S. Dühnen, M. Winter, *J. Solid State Electrochem.* **2017**, *21*, 1939; b) J. Betz, G. Bieker, P. Meister, T. Placke, M. Winter, R. Schmuch, *Adv. Energy Mater.* **2019**, *9*, 1803170.

[7] A. Mukhopadhyay, M. K. Jangid, *Science* **2018**, *359*, 1463.

[8] a) Z. Xue, D. He, X. Xie, *J. Mater. Chem. A* **2015**, *3*, 19218; b) D. Brandell, J. Mindemark, G. Hernández, in *Polymer-Based Solid State Batteries*, De Gruyter, Berlin, Boston **2021**, p. 1.

[9] V. Vijayakumar, M. Ghosh, P. K. Samantaray, S. Kurungot, M. Winter, J. R. Nair, in *Two-Dimensional Inorganic Nanomaterials for Conductive Polymer Nanocomposites*, The Royal Society of Chemistry, London **2021**, p. 204.

[10] a) P. V. Wright, *MRS Bull.* **2002**, *27*, 597; b) D. E. Fenton, J. M. Parker, P. V. Wright, *Polymer* **1973**, *14*, 589; c) P. V. Wright, *Br. Polym. J.* **1975**, *7*, 319.

[11] a) M. Armand, *Solid State Ionics* **1983**, *9–10*, 745; b) M. Armand, J. Chabagno, M. Duclot, *Second International Meeting on Solid Electrolytes, St Andrews*, Scotland, September **1978**; c) M. Armand, J. M. Chabagno, M. Duclot, in *Fast Ion Transport in Solids*, (Ed: P. Vashishta, J. N. Mundy, G. K. Shenoy), North Holland, Amterdam **1979**, p. 131; d) A. Mauger, C. M. Julien, J. B. Goodenough, K. Zaghib, *J. Electrochem. Soc.* **2019**, *167*, 070507; e) D. Brandell, J. Mindemark, G. Hernández, in *Polymer-Based Solid State Batteries*, De Gruyter, Berlin, **2021**, p. 16.

[12] a) E. W. Stacy, C. P. Gainaru, M. Gobet, Z. Wojnarowska, V. Bocharova, S. G. Greenbaum, A. P. Sokolov, *Macromolecules* **2018**, *51*, 8637; b) M. A. Ratner, D. F. Shriver, *Chem. Rev.* **1988**, *88*, 109; c) Y. An, X. Han, Y. Liu, A. Azhar, J. Na, A. K. Nanjundan, S. Wang, J. Yu, Y. Yamauchi, *Small* **2022**, *18*, 2103617; d) W. H. Meyer, *Adv. Mater.* **1998**, *10*, 439.

[13] D. Bresser, S. Lyonnard, C. Iojoiu, L. Picard, S. Passerini, *Mol. Syst. Des. Eng.* **2019**, *4*, 779.

[14] J. Popovic, *Macromol. Chem. Phys.* 2100344.

[15] D. Zhou, D. Shanmukaraj, A. Tkacheva, M. Armand, G. Wang, *Chem* **2019**, *5*, 2326.

[16] D. R. Gallus, R. Wagner, S. Wiemers-Meyer, M. Winter, I. Cekic-Laskovic, *Electrochim. Acta* **2015**, *184*, 410.

[17] a) X. Zhao, Q.-C. Zhuang, Y.-L. Shi, X.-X. Zhang, *J. Appl. Electrochem.* **2015**, *45*, 1013; b) T. Zhang, J. Zhang, S. Yang, Y. Li, R. Dong, J. Yuan, Y. Liu, Z. Wu, Y. Song, Y. Zhong, W. Xiang, Y. Chen, B. Zhong, X. Guo, *ACS Appl. Mater. Interfaces* **2021**, *13*, 44497; c) H. Jia, H. Onishi, N. von Aspern, U. Rodehorst, K. Rudolf, B. Billmann, R. Wagner, M. Winter, I. Cekic-Laskovic, *J. Power Sources* **2018**, *397*, 343.

[18] a) V. Vijayakumar, D. Diddens, A. Heuer, S. Kurungot, M. Winter, J. R. Nair, *ACS Appl. Mater. Interfaces* **2020**, *12*, 567; b) I. Shaji, D. Diddens, N. Ehteshami, M. Winter, J. R. Nair, *Energy Storage Mater.* **2022**, *44*, 263; c) S. Li, Y.-M. Chen, W. Liang, Y. Shao, K. Liu, Z. Nikolov, Y. Zhu, *Joule* **2018**, *2*, 1838; d) B. Xu, X. Li, C. Yang, Y. Li, N. S. Grundish, P.-H. Chien, K. Dong, I. Manke, R. Fang, N. Wu, H. Xu, A. Dolocan, J. B. Goodenough, *J. Am. Chem. Soc.* **2021**, *143*, 6542; e) I. L. Johansson, C. Sångeland, T. Uemiya, F. Iwasaki, M. Yoshizawa-Fujita, D. Brandell, J. Mindemark, *ACS Appl. Energy Mater.* **2022**, *5*, 10002.

[19] a) K. Dai, Y. Zheng, W. Wei, *Adv. Funct. Mater.* **2021**, *31*, 2008632; b) K. Dai, C. Ma, Y. Feng, L. Zhou, G. Kuang, Y. Zhang, Y. Lai, X. Cui, W. Wei, *J. Mater. Chem. A* **2019**, *7*, 18547.

[20] a) L. Han, C. Liao, X. Mu, N. Wu, Z. Xu, J. Wang, L. Song, Y. Kan, Y. Hu, *Nano Lett.* **2021**, *21*, 4447; b) R. V. Morford, E. C. Kellam, M. A. Hofmann, R. Baldwin, H. R. Allcock, *Solid State Ionics* **2000**, *133*, 171.

[21] a) N. Meng, X. Zhu, F. Lian, *Particuology* **2022**, *60*, 14; b) Z. Shen, Y. Cheng, S. Sun, X. Ke, L. Liu, Z. Shi, *Carbon Energy* **2021**, *3*, 482; c) J. Popovic, D. Brandell, S. Ohno, K. B. Hatzell, J. Zheng, Y.-Y. Hu, *J. Mater. Chem. A* **2021**, *9*, 6050.

[22] a) J. Guo, J. Zheng, W. Zhang, Y. Lu, *Energy Fuels* **2021**, *35*, 11118; b) F. Croce, G. B. Appetecchi, L. Persi, B. Scrosati, *Nature* **1998**, *394*, 456; c) W. Liao, C. Liu, *ChemNanoMat* **2021**, *7*, 1177.

[23] J. Weston, B. Steele, *Solid State Ionics* **1982**, *7*, 75.

[24] a) J. Przyluski, M. Siekierski, W. Wieczorek, *Electrochim. Acta* **1995**, *40*, 2101; b) F. Capuano, F. Croce, B. Scrosati, *J. Electrochem. Soc.* **1991**, *138*, 1918.
[25] a) B. Scrosati, F. Croce, L. Persi, *J. Electrochem. Soc.* **2000**, *147*, 1718; b) F. Croce, R. Curini, A. Martinelli, L. Persi, F. Ronci, B. Scrosati, R. Caminiti, *J. Phys. Chem. B* **1999**, *103*, 10632.
[26] D. Lin, W. Liu, Y. Liu, H. R. Lee, P.-C. Hsu, K. Liu, Y. Cui, *Nano Lett.* **2016**, *16*, 459.
[27] R. J. Sengwa, S. Choudhary, *J. Phys. Chem. Solids* **2014**, *75*, 765.
[28] W. Liu, D. Lin, J. Sun, G. Zhou, Y. Cui, *ACS Nano* **2016**, *10*, 11407.
[29] S. Jung, D.-W. Kim, S.-D. Lee, M. C. Cheong, D. Q. Nguyen, B.-W. Cho, H.-S. Kim, *Bull. Korean Chem. Soc.* **2009**, *30*, 2355.
[30] J. R. Nair, F. Bella, N. Angulakshmi, A. M. Stephan, C. Gerbaldi, *Energy Storage Mater.* **2016**, *3*, 69.
[31] J. Feng, L. Wang, Y. Chen, P. Wang, H. Zhang, X. He, *Nano Converg* **2021**, *8*, 2.
[32] A. Manthiram, X. Yu, S. Wang, *Nat. Rev. Mater.* **2017**, *2*, 16103.
[33] a) P. Johansson, P. Jacobsson, *Solid State Ionics* **2004**, *170*, 73; b) M. A. Sattar, *ChemistrySelect* **2021**, *6*, 5068; c) Q. Zhou, J. Ma, S. Dong, X. Li, G. Cui, *Adv. Mater.* **2019**, *31*, 1902029.
[34] a) K. He, S. H. S. Cheng, J. Hu, Y. Zhang, H. Yang, Y. Liu, W. Liao, D. Chen, C. Liao, X. Cheng, *Angew. Chem.* **2021**, *133*, 12223; b) X. Zhang, J. Xie, F. Shi, D. Lin, Y. Liu, W. Liu, A. Pei, Y. Gong, H. Wang, K. Liu, *Nano Lett.* **2018**, *18*, 3829.
[35] a) J. Bae, Y. Li, J. Zhang, X. Zhou, F. Zhao, Y. Shi, J. B. Goodenough, G. Yu, *Angew. Chem., Int. Ed.* **2018**, *57*, 2096; b) T. K. Lee, R. Andersson, N. A. Dzulkurnain, G. Hernández, J. Mindemark, D. Brandell, *Batteries Supercaps* **2021**, *4*, 653.
[36] a) E. P. Nguyen, C. de Carvalho Castro Silva, A. Merkoçi, *Nanoscale* **2020**, *12*, 19043; b) N. R. Glavin, R. Rao, V. Varshney, E. Bianco, A. Apte, A. Roy, E. Ringe, P. M. Ajayan, *Adv. Mater.* **2020**, *32*, 1904302; c) Z.-W. Li, Y.-H. Hu, Y. Li, Z.-Y. Fang, *Chin. Phys. B* **2017**, *26*, 036802.
[37] a) C. Tan, X. Cao, X.-J. Wu, Q. He, J. Yang, X. Zhang, J. Chen, W. Zhao, S. Han, G.-H. Nam, M. Sindoro, H. Zhang, *Chem. Rev.* **2017**, *117*, 6225; b) N. Baig, I. Kammakakam, W. Falath, *Mater. Adv.* **2021**, *2*, 1821.
[38] S. Pei, Q. Wei, K. Huang, H.-M. Cheng, W. Ren, *Nat. Commun.* **2018**, *9*, 145.
[39] N. Alem, R. Erni, C. Kisielowski, M. D. Rossell, W. Gannett, A. Zettl, *Phys. Rev. B* **2009**, *80*, 155425.
[40] B. Radisavljevic, A. Radenovic, J. Brivio, V. Giacometti, A. Kis, *Nat. Nanotechnol.* **2011**, *6*, 147.
[41] K. R. G. Lim, A. D. Handoko, S. K. Nemani, B. Wyatt, H.-Y. Jiang, J. Tang, B. Anasori, Z. W. Seh, *ACS Nano* **2020**, *14*, 10834.
[42] M. Ezawa, *New J. Phys.* **2014**, *16*, 115004.
[43] J. Wimpenny, in *Encyclopedia of Geochemistry: A Comprehensive Reference Source on the Chemistry of the Earth*, (Ed: W. M. White), Springer International Publishing, Cham **2018**, p. 265.
[44] H. Liang, F. Meng, M. Cabán-Acevedo, L. Li, A. Forticaux, L. Xiu, Z. Wang, S. Jin, *Nano Lett.* **2015**, *15*, 1421.
[45] J. Yu, T. Guo, C. Wang, Z. Shen, X. Dong, S. Li, H. Zhang, Z. Lu, *Nano Lett.* **2021**, *21*, 5805.
[46] Y. Hu, N. Dunlap, S. Wan, S. Lu, S. Huang, I. Sellinger, M. Ortiz, Y. Jin, S.-h. Lee, W. Zhang, *J. Am. Chem. Soc.* **2019**, *141*, 7518.
[47] W. Work, K. Horie, M. Hess, R. Stepto, *Pure Appl. Chem.* **2004**, *76*, 1985.
[48] a) N. Verdier, G. Foran, D. Lepage, A. Prébé, D. Aymé-Perrot, M. Dollé, *Polymers* **2021**, *13*, 323; b) S. Chua, R. Fang, Z. Sun, M. Wu, Z. Gu, Y. Wang, J. N. Hart, N. Sharma, F. Li, D.-W. Wang, *Chemistry* **2018**, *24*, 18180.
[49] a) C. Huo, Z. Yan, X. Song, H. Zeng, *Sci. Bull.* **2015**, *60*, 1994; b) M. Rajapakse, B. Karki, U. O. Abu, S. Pishgar, M. R. K. Musa, S. S. Riyadh, M. Yu, G. Sumanasekera, J. B. Jasinski, *npj 2D Mater. Appl.* **2021**, *5*, 30; c) V. Nicolosi, M. Chhowalla, M. G. Kanatzidis, M. S. Strano, J. N. Coleman, *Science* **2013**, *340*, 1226419; d) S. Mukherjee, Z. Ren, G. Singh, *Nano-Micro Lett.* **2018**, *10*, 70.
[50] S. Z. Butler, S. M. Hollen, L. Cao, Y. Cui, J. A. Gupta, H. R. Gutiérrez, T. F. Heinz, S. S. Hong, J. Huang, A. F. Ismach, E. Johnston-Halperin, M. Kuno, V. V. Plashnitsa, R. D. Robinson, R. S. Ruoff, S. Salahuddin, J. Shan, L. Shi, M. G. Spencer, M. Terrones, W. Windl, J. E. Goldberger, *ACS Nano* **2013**, *7*, 2898.
[51] a) J. Cai, X. Han, X. Wang, X. Meng, *Matter* **2020**, *2*, 587; b) L. Tang, J. Tan, H. Nong, B. Liu, H.-M. Cheng, *Acc Mater. Res.* **2021**, *2*, 36; c) S. Zhao, B. Dong, H. Wang, H. Wang, Y. Zhang, Z. V. Han, H. Zhang, *Nanoscale Adv* **2020**, *2*, 109; d) E. Cha, M. D. Patel, J. Park, J. Hwang, V. Prasad, K. Cho, W. Choi, *Nat. Nanotechnol.* **2018**, *13*, 337; e) S. B. Mujib, Z. Ren, S. Mukherjee, D. M. Soares, G. Singh, *Mater. Adv.* **2020**, *1*, 2562; f) H. Zhang, *ACS Nano* **2015**, *9*, 9451; g) J. Xu, J. Zhang, W. Zhang, C.-S. Lee, *Adv. Energy Mater.* **2017**, *7*, 1700571.
[52] a) C. Xu, L. Chen, Z. Liu, H.-M. Cheng, W. Ren, in *2D Metal Carbides and Nitrides (MXenes): Structure, Properties and Applications*, (Eds: B. Anasori, Y. Gogotsi), Springer International Publishing, Cham **2019**, p. 89; b) Z. Liu, S. Fu, X. Liu, A. Narita, P. Samorì, M. Bonn, H. I. Wang, *Adv. Sci.* **2022**, *9*, 2106055; c) S. H. Choi, S. J. Yun, Y. S. Won, C. S. Oh, S. M. Kim, K. K. Kim, Y. H. Lee, *Nat. Commun.* **2022**, *13*, 1484; d) V. Shanmugam, R. A. Mensah, K. Babu, S. Gawusu, A. Chanda, Y. Tu, R. E. Neisiany, M. Försth, G. Sas, O. Das, *Part. Part. Syst. Charact.* **2022**, *39*, 2200031.
[53] F. Moghadam, H. B. Park, *Curr. Opin. Chem. Eng.* **2018**, *20*, 28.
[54] a) P. Sun, S. Kuga, M. Wu, Y. Huang, *Cellulose* **2014**, *21*, 2469; b) W. Zhao, M. Fang, F. Wu, H. Wu, L. Wang, G. Chen, *J. Mater. Chem.* **2010**, *20*, 5817; c) Y. Yao, Z. Lin, Z. Li, X. Song, K.-S. Moon, C.-p. Wong, *J. Mater. Chem.* **2012**, *22*, 13494; d) C. Li, J. Lin, L. Shen, N. Bao, *Chem. Eng. Sci.* **2020**, *213*, 115414; e) J. Stafford, A. Patapas, N. Uzo, O. K. Matar, C. Petit, *AIChE J.* **2018**, *64*, 3246.
[55] K. S. Novoselov, A. K. Geim, S. V. Morozov, D.-e. Jiang, Y. Zhang, S. V. Dubonos, I. V. Grigorieva, A. A. Firsov, *Science* **2004**, *306*, 666.
[56] a) D. Pacilé, J. C. Meyer, Ç. Ö. Girit, A. Zettl, *Appl. Phys. Lett.* **2008**, *92*, 133107; b) M. F. da Costa, H. Ribeiro, F. Kessler, E. de Souza, G. Fechine, *Mater. Res. Express* **2016**, *3*, 025303.
[57] H. Yu, B. Zhang, C. Bulin, R. Li, R. Xing, *Sci. Rep.* **2016**, *6*, 36143.
[58] W. Hong, B. C. Wyatt, S. K. Nemani, B. Anasori, *MRS Bull.* **2020**, *45*, 850.
[59] a) J. Zhou, Z. Lin, H. Ren, X. Duan, I. Shakir, Y. Huang, X. Duan, *Adv. Mater.* **2021**, *33*, 2004557; b) Y. Jung, Y. Zhou, J. J. Cha, *Inorg. Chem. Front.* **2016**, *3*, 452.
[60] a) F. I. Alzakia, W. Jonhson, J. Ding, S. C. Tan, *ACS Appl. Mater. Interfaces* **2020**, *12*, 28840; b) W. Cao, J. Wang, M. Ma, *J. Phys. Chem. Lett.* **2019**, *10*, 981; c) A. Ciesielski, P. Samorì, *Chem. Soc. Rev.* **2014**, *43*, 381.
[61] a) Y. Zhang, L. Wen, X. Bai, N. Song, X. Huang, Y. Li, *Chem. Lett.* **2019**, *48*, 1148; b) N. Mao, C. H. Zhou, D. S. Tong, W. H. Yu, C. X. Cynthia Lin, *Appl. Clay Sci.* **2017**, *144*, 60; c) J. Ma, L. Liu, S. Li, Y. Chen, M. Zhuo, F. Shao, J. Gong, Z. Tong, *Dalton Trans.* **2014**, *43*, 9909.
[62] Z. Zeng, Z. Yin, X. Huang, H. Li, Q. He, G. Lu, F. Boey, H. Zhang, *Angew. Chem., Int. Ed.* **2011**, *50*, 11093.
[63] a) T. H. Le, Y. Oh, H. Kim, H. Yoon, *Chemistry* **2020**, *26*, 6360; b) A. Yoshida, Y. Hishiyama, M. Inagaki, *Carbon* **1991**, *29*, 1227; c) Q. Zhang, L. Mei, X. Cao, Y. Tang, Z. Zeng, *J. Mater. Chem. A* **2020**, *8*, 15417; d) J. Zheng, H. Zhang, S. Dong, Y. Liu, C. Tai Nai, H. Suk Shin, H. Young Jeong, B. Liu, K. Ping Loh, *Nat. Commun.* **2014**, *5*, 2995.
[64] R. Muzyka, M. Kwoka, Ł. Smędowski, N. Díez, G. Gryglewicz, *New Carbon Mater.* **2017**, *32*, 15.
[65] a) M. Naguib, M. Kurtoglu, V. Presser, J. Lu, J. Niu, M. Heon, L. Hultman, Y. Gogotsi, M. W. Barsoum, *Adv. Mater.* **2011**, *23*, 4248; b) M. Naguib, O. Mashtalir, J. Carle, V. Presser, J. Lu,

L. Hultman, Y. Gogotsi, M. W. Barsoum, *ACS Nano* **2012**, *6*, 1322; c) J. Xu, T. Peng, X. Qin, Q. Zhang, T. Liu, W. Dai, B. Chen, H. Yu, S. Shi, *J. Mater. Chem. A* **2021**, *9*, 14147.

[66] a) K. C. Knirsch, N. C. Berner, H. C. Nerl, C. S. Cucinotta, Z. Gholamvand, N. McEvoy, Z. Wang, I. Abramovic, P. Vecera, M. Halik, S. Sanvito, G. S. Duesberg, V. Nicolosi, F. Hauke, A. Hirsch, J. N. Coleman, C. Backes, *ACS Nano* **2015**, *9*, 6018; b) X. Fan, P. Xu, D. Zhou, Y. Sun, Y. C. Li, M. A. T. Nguyen, M. Terrones, T. E. Mallouk, *Nano Lett.* **2015**, *15*, 5956; c) G. Eda, H. Yamaguchi, D. Voiry, T. Fujita, M. Chen, M. Chhowalla, *Nano Lett.* **2011**, *11*, 5111; d) P. Joensen, R. F. Frindt, S. R. Morrison, *Mater. Res. Bull.* **1986**, *21*, 457.

[67] a) F. I. Alzakia, S. C. Tan, *Adv. Sci.* **2021**, *8*, 2003864; b) Y. Yang, H. Hou, G. Zou, W. Shi, H. Shuai, J. Li, X. Ji, *Nanoscale* **2019**, *11*, 16; c) Y. Huang, Y.-H. Pan, R. Yang, L.-H. Bao, L. Meng, H.-L. Luo, Y.-Q. Cai, G.-D. Liu, W.-J. Zhao, Z. Zhou, L.-M. Wu, Z.-L. Zhu, M. Huang, L.-W. Liu, L. Liu, P. Cheng, K.-H. Wu, S.-B. Tian, C.-Z. Gu, Y.-G. Shi, Y.-F. Guo, Z. G. Cheng, J.-P. Hu, L. Zhao, G.-H. Yang, E. Sutter, P. Sutter, Y.-L. Wang, W. Ji, X.-J. Zhou, et al., *Nat. Commun.* **2020**, *11*, 2453.

[68] a) E. Lago, P. S. Toth, G. Pugliese, V. Pellegrini, F. Bonaccorso, *RSC Adv.* **2016**, *6*, 97931; b) L.-C. Tang, L. Zhao, F. Qiang, Q. Wu, L.-X. Gong, J.-P. Peng, in *Carbon-Based Nanofillers and Their Rubber Nanocomposites*, (Eds: S. Yaragalla, R. K. Mishra, S. Thomas, N. Kalarikkal, H. J. Maria), Elsevier, Amsterdam **2019**, p. 367.

[69] A. Vasudeo Rane, K. Kanny, V. K. Abitha, S. S. Patil, S. Thomas, in *Clay–Polymer Nanocomposites*, (Eds: K. Jlassi, M. M. Chehimi, S. Thomas), Elsevier, Amsterdam **2017**, p. 113.

[70] F. P. Nkosi, M. Valvo, J. Mindemark, N. A. Dzulkurnain, G. Hernández, A. Mahun, S. Abbrent, J. Brus, L. Kobera, K. Edström, *ACS Appl. Energy Mater.* **2021**, *4*, 2531.

[71] M. Sikka, L. N. Cerini, S. S. Ghosh, K. I. Winey, *J. Polym. Sci., Part B: Polym. Phys.* **1996**, *34*, 1443.

[72] R. A. Vaia, S. Vasudevan, W. Krawiec, L. G. Scanlon, E. P. Giannelis, *Adv. Mater.* **1995**, *7*, 154.

[73] M. Falco, L. Castro, J. R. Nair, F. Bella, F. Bardé, G. Meligrana, C. Gerbaldi, *ACS Appl. Energy Mater.* **2019**, *2*, 1600.

[74] R. Raccichini, A. Varzi, S. Passerini, B. Scrosati, *Nat. Mater.* **2015**, *14*, 271.

[75] a) V. B. Mbayachi, E. Ndayiragije, T. Sammani, S. Taj, E. R. Mbuta, A. u. khan, *Results Chem.* **2021**, *3*, 100163; b) M. S. A. Bhuyan, M. N. Uddin, M. M. Islam, F. A. Bipasha, S. S. Hossain, *Int. Nano Lett.* **2016**, *6*, 65.

[76] F.-Y. Su, C. You, Y.-B. He, W. Lv, W. Cui, F. Jin, B. Li, Q.-H. Yang, F. Kang, *J. Mater. Chem.* **2010**, *20*, 9644.

[77] W. S. Hummers, R. E. Offeman, *J. Am. Chem. Soc.* **1958**, *80*, 1339.

[78] a) M. Yuan, J. Erdman, C. Tang, H. Ardebili, *RSC Adv.* **2014**, *4*, 59637; b) W. Jia, Z. Li, Z. Wu, L. Wang, B. Wu, Y. Wang, Y. Cao, J. Li, *Solid State Ionics* **2018**, *315*, 7.

[79] X. Zhao, Z. Wu, Z. Zhang, N. Wang, C.-A. Tao, J. Wang, H. Gong, *Mater. Res. Express* **2021**, *8*, 105305.

[80] J. Shim, D.-G. Kim, H. J. Kim, J. H. Lee, J.-H. Baik, J.-C. Lee, *J. Mater. Chem. A* **2014**, *2*, 13873.

[81] a) Z. Hu, X. Zhang, J. Liu, Y. Zhu, *Front Chem* **2020**, *8*, 232; b) W. Bao, Z. Hu, Y. Wang, J. Jiang, S. Huo, W. Fan, W. Chen, X. Jing, X. Long, Y. Zhang, *Chem. Eng. J.* **2022**, *437*, 135420.

[82] I. Nicotera, C. Simari, M. Agostini, A. Enotiadis, S. Brutti, *J. Phys. Chem. C* **2019**, *123*, 27406.

[83] M. Fouladvand, L. Naji, M. Javanbakht, A. Rahmanian, *J. Membr. Sci.* **2021**, *636*, 119563.

[84] J. Liu, X. Wu, J. He, J. Li, Y. Lai, *Electrochim. Acta* **2017**, *235*, 500.

[85] a) H. Zeng, C. Zhi, Z. Zhang, X. Wei, X. Wang, W. Guo, Y. Bando, D. Golberg, *Nano Lett.* **2010**, *10*, 5049; b) C. Zheng, *Batteries* **2022**, *8*, 187.

[86] a) M. Jansen, B. Jäschke, T. Jäschke, in *High Performance Non-Oxide Ceramics I*, (Ed: M. Jansen), Springer, Berlin **2002**, p. 137; b) R. R. Wills, *Int. J. High Technol. Ceram.* **1985**, *1*, 139; c) N. Izyumskaya, D. O. Demchenko, S. Das, Ü. Özgür, V. Avrutin, H. Morkoç, *Adv. Electron. Mater.* **2017**, *3*, 1600485.

[87] a) K. Zhang, Y. Feng, F. Wang, Z. Yang, J. Wang, *J. Mater. Chem. C* **2017**, *5*, 11992; b) A. Ranjan, N. Raghavan, M. Holwill, K. Watanabe, T. Taniguchi, K. S. Novoselov, K. L. Pey, S. J. O'Shea, *ACS Appl. Electron. Mater.* **2021**, *3*, 3547; c) N. Kostoglou, K. Polychronopoulou, C. Rebholz, *Vacuum* **2015**, *112*, 42; d) C. Steinborn, M. Herrmann, U. Keitel, A. Schönecker, J. Räthel, D. Rafaja, J. Eichler, *J. Eur. Ceram. Soc.* **2013**, *33*, 1225; e) A. M. Patki, A. A. Maharanwar, S. K. Harde, R. K. Goyal, *SN Appl. Sci.* **2019**, *1*, 775.

[88] S. Li, X. Lu, Y. Lou, K. Liu, B. Zou, *ACS Omega* **2021**, *6*, 27814.

[89] J. Wang, F. Ma, M. Sun, *RSC Adv.* **2017**, *7*, 16801.

[90] a) P. L. de Andres, R. Ramírez, J. A. Vergés, *Phys. Rev. B* **2008**, *77*, 045403; b) Z. Zhang, J. Su, A. S. Matias, M. Gordon, Y.-S. Liu, J. Guo, C. Song, C. Dun, D. Prendergast, G. A. Somorjai, J. J. Urban, *Proc. Natl. Acad. Sci. USA* **2020**, *117*, 29442.

[91] H. Li, R. Y. Tay, S. H. Tsang, W. Liu, E. H. T. Teo, *Electrochim. Acta* **2015**, *166*, 197.

[92] Y. Li, L. Zhang, Z. Sun, G. Gao, S. Lu, M. Zhu, Y. Zhang, Z. Jia, C. Xiao, H. Bu, K. Xi, S. Ding, *J. Mater. Chem. A* **2020**, *8*, 9579.

[93] a) J. Shim, H. J. Kim, B. G. Kim, Y. S. Kim, D.-G. Kim, J.-C. Lee, *Energy Environ. Sci.* **2017**, *10*, 1911; b) X. Zhang, W. Guo, L. Zhou, Q. Xu, Y. Min, *J. Mater. Chem. A* **2021**, *9*, 20530

[94] H. Aydın, S. Ü. Çelik, A. Bozkurt, *Solid State Ionics* **2017**, *309*, 71.

[95] Z. Zhang, R. G. Antonio, K. L. Choy, *J. Power Sources* **2019**, *435*, 226736.

[96] T. Eriksson, J. Mindemark, M. Yue, D. Brandell, *Electrochim. Acta* **2019**, *300*, 489.

[97] a) F. Haque, T. Daeneke, K. Kalantar-zadeh, J. Z. Ou, *Nano-Micro Lett.* **2017**, *10*, 23; b) Y. Kim, W. J. Woo, D. Kim, S. Lee, S.-m. Chung, J. Park, H. Kim, *Adv. Mater.* **2021**, *33*, 2005907; c) S. Manzeli, D. Ovchinnikov, D. Pasquier, O. V. Yazyev, A. Kis, *Nat. Rev. Mater.* **2017**, *2*, 17033.

[98] D. W. Murphy, G. W. HullJr., *J. Chem. Phys.* **1975**, *62*, 973.

[99] C. Liu, O. Singh, P. Joensen, A. E. Curzon, R. F. Frindt, *Thin Solid Films* **1984**, *113*, 165.

[100] a) M. A. Py, R. R. Haering, *Can. J. Phys.* **1983**, *61*, 76; b) N. Imanishi, K. Kanamura, Z. i. Takehara, *J. Electrochem. Soc.* **1992**, *139*, 2082.

[101] J. Wu, H. Zeng, Q. Shi, X. Li, Q. Xia, Z. Xue, Y. Ye, X. Xie, *J. Power Sources* **2018**, *405*, 7.

[102] a) X. Wang, W. Xing, X. Feng, L. Song, Y. Hu, *Polym. Rev.* **2017**, *57*, 440; b) M. Ahmadi, O. Zabihi, S. Jeon, M. Yoonessi, A. Dasari, S. Ramakrishna, M. Naebe, *J. Mater. Chem. A* **2020**, *8*, 845.

[103] D. Yang, P. Westreich, R. F. Frindt, *Nanostruct. Mater.* **1999**, *12*, 467.

[104] M. A. Santa Ana, E. Benavente, P. Gómez-Romero, G. González, *J. Mater. Chem.* **2006**, *16*, 3107.

[105] Y. Li, Z. Sun, D. Liu, Y. Gao, Y. Wang, H. Bu, M. Li, Y. Zhang, G. Gao, S. Ding, *J. Mater. Chem. A* **2020**, *8*, 2021.

[106] a) M. Azhagurajan, T. Kajita, T. Itoh, Y.-G. Kim, K. Itaya, *J. Am. Chem. Soc.* **2016**, *138*, 3355; b) N. Imanishi, M. Toyoda, Y. Takeda, O. Yamamoto, *Solid State Ionics* **1992**, *58*, 333.

[107] a) G. Zhuang, J. Yan, Y. Wen, Z. Zhuang, Y. Yu, *Sol. RRL* **2021**, *5*, 2000403; b) Z. Lei, J. M. Lee, G. Singh, C. I. Sathish, X. Chu, A. a. H. Al-Muhtaseb, A. Vinu, J. Yi, *Energy Storage Mater.* **2021**, *36*, 514; c) M. A. Timmerman, R. Xia, P. T. P. Le, Y. Wang, J. E. ten Elshof, *Chemistry* **2020**, *26*, 9084.

[108] K. West, B. Zachau-Christiansen, T. Jacobsen, S. Skaarup, *Electrochim. Acta* **1993**, *38*, 1215.

[109] L. F. Nazar, H. Wu, W. P. Power, *J. Mater. Chem.* **1995**, *5*, 1985.

[110] a) Y. Gogotsi, B. Anasori, *ACS Nano* **2019**, *13*, 8491; b) B. Anasori, M. R. Lukatskaya, Y. Gogotsi, *Nat. Rev. Mater.* **2017**, *2*, 16098.

[111] a) M. Naguib, V. N. Mochalin, M. W. Barsoum, Y. Gogotsi, *Adv. Mater.* **2014**, *26*, 992; b) M. Ghosh, S. Szunerits, N. Cao, S. Kurungot, R. Boukherroub, *ChemistrySelect* **2022**, *7*, 202201166.
[112] a) R. Syamsai, J. R. Rodriguez, V. G. Pol, Q. Van Le, K. M. Batoo, S. F. Adil, S. Pandiaraj, M. Muthumareeswaran, E. H. Raslan, A. N. Grace, *Sci. Rep.* **2021**, *11*, 688; b) B. Anasori, Y. Xie, M. Beidaghi, J. Lu, B. C. Hosler, L. Hultman, P. R. Kent, Y. Gogotsi, M. W. Barsoum, *ACS Nano* **2015**, *9*, 9507.
[113] a) A. Bhat, S. Anwer, K. S. Bhat, M. I. H. Mohideen, K. Liao, A. Qurashi, *npj 2D Mater. Appl.* **2021**, *5*, 61; b) V. Natu, M. Sokol, L. Verger, M. W. Barsoum, *J. Phys. Chem. C* **2018**, *122*, 27745.
[114] a) M. Ghidiu, M. R. Lukatskaya, M.-Q. Zhao, Y. Gogotsi, M. W. Barsoum, *Nature* **2014**, *516*, 78; b) M. Ghidiu, J. Halim, S. Kota, D. Bish, Y. Gogotsi, M. W. Barsoum, *Chem. Mater.* **2016**, *28*, 3507.
[115] X. Sheng, Y. Zhao, L. Zhang, X. Lu, *Compos. Sci. Technol.* **2019**, *181*, 107710.
[116] a) Z. Huang, S. Wang, S. Kota, Q. Pan, M. W. Barsoum, C. Y. Li, *Polymer* **2016**, *102*, 119; b) C. Chen, M. Boota, X. Xie, M. Zhao, B. Anasori, C. E. Ren, L. Miao, J. Jiang, Y. Gogotsi, *J. Mater. Chem. A* **2017**, *5*, 5260.
[117] Q. Pan, Y. Zheng, S. Kota, W. Huang, S. Wang, H. Qi, S. Kim, Y. Tu, M. W. Barsoum, C. Y. Li, *Nanoscale Adv.* **2019**, *1*, 395.
[118] a) W. Peng, R. Hu, W. Jiang, J. Kang, J. Li, Y. Cao, M. Xiang, *ACS Omega* **2021**, *6*, 19973; b) W. Ma, K. Yang, H. Wang, H. Li, *ACS Appl. Nano Mater.* **2020**, *3*, 7992.
[119] S. Ha, D. Kim, H. K. Lim, C. M. Koo, S. J. Kim, Y. S. Yun, *Adv. Funct. Mater.* **2021**, *31*, 2101261.
[120] T. Yang, C. Shu, R. Zheng, A. Hu, Z. Hou, M. Li, Z. Ran, P. Hei, J. Long, *J. Membr. Sci.* **2020**, *604*, 118051.
[121] a) Z. Huang, T. Huang, X. Ye, X. Feng, X. Yang, J. Liang, S. Ye, Y. Li, X. Ren, W. Xiong, X. Ouyang, Q. Zhang, J. Liu, *Appl. Surf. Sci.* **2022**, *605*, 154586; b) W. Yao, S. He, Y. Xue, Q. Zhang, J. Wang, M. He, J. Xu, C. Chen, X. Xiao, *ACS Sustainable Chem. Eng.* **2021**, *9*, 9961.
[122] Y. Hou, Z. Huang, Z. Chen, X. Li, A. Chen, P. Li, Y. Wang, C. Zhi, *Nano Energy* **2022**, *97*, 107204.
[123] X. Zhao, M. Zhu, C. Tang, K. Quan, Q. Tong, H. Cao, J. Jiang, H. Yang, J. Zhang, *J. Colloid Interface Sci.* **2022**, *620*, 478.
[124] Y. Shi, B. Li, Q. Zhu, K. Shen, W. Tang, Q. Xiang, W. Chen, C. Liu, J. Luo, S. Yang, *Adv. Energy Mater.* **2020**, *10*, 1903534.
[125] R. Rojaee, S. Cavallo, S. Mogurampelly, B. K. Wheatle, V. Yurkiv, R. Deivanayagam, T. Foroozan, M. G. Rasul, S. Sharifi-Asl, A. H. Phakatkar, M. Cheng, S.-B. Son, Y. Pan, F. Mashayek, V. Ganesan, R. Shahbazian-Yassar, *Adv. Funct. Mater.* **2020**, *30*, 1910749.
[126] A. Carvalho, M. Wang, X. Zhu, A. S. Rodin, H. Su, A. H. Castro Neto, *Nat. Rev. Mater.* **2016**, *1*, 16061.
[127] X. Ling, H. Wang, S. Huang, F. Xia, M. S. Dresselhaus, *Proc. Natl. Acad. Sci. USA* **2015**, *112*, 4523.
[128] L. Li, Y. Yu, G. J. Ye, Q. Ge, X. Ou, H. Wu, D. Feng, X. H. Chen, Y. Zhang, *Nat. Nanotechnol.* **2014**, *9*, 372.
[129] a) W. Zhang, J. Zhao, W. He, L. Luan, C. He, *Chem. Phys. Lett.* **2017**, *675*, 20; b) T. Zhao, C. He, S. Ma, K. Zhang, X. Peng, G. Xie, J. Zhong, *J. Phys.: Condens. Matter* **2015**, *27*, 265301.
[130] Q. Peng, Z. Wang, B. Sa, B. Wu, Z. Sun, *ACS Appl. Mater. Interfaces* **2016**, *8*, 13449.
[131] a) Y. Kim, D. Koo, S. Ha, S. C. Jung, T. Yim, H. Kim, S. K. Oh, D.-M. Kim, A. Choi, Y. Kang, *ACS Nano* **2018**, *12*, 4419; b) G. Nazri, *Solid State Ionics* **1989**, *34*, 97; c) N. Wu, Y. Li, A. Dolocan, W. Li, H. Xu, B. Xu, N. S. Grundish, Z. Cui, H. Jin, J. B. Goodenough, *Adv. Funct. Mater.* **2020**, *30*, 2000831; d) W. Yu, J. Yang, J. Li, K. Zhang, H. Xu, X. Zhou, W. Chen, K. P. Loh, *Adv. Mater.* **2021**, *33*, 2102083.
[132] X. Fu, D. Yu, J. Zhou, S. Li, X. Gao, Y. Han, P. Qi, X. Feng, B. Wang, *CrystEngComm* **2016**, *18*, 4236.
[133] a) G. L. GainesJr., *J. Phys. Chem.* **1957**, *61*, 1408; b) H. Tang, M. Sun, C. Wang, *Chem Asian J* **2021**, *16*, 2842.
[134] a) F. Guo, S. Aryana, Y. Han, Y. Jiao, *Appl. Sci.* **2018**, *8*, 1696; b) M. Alamgir, in *Environmental Remediation Technologies for Metal-Contaminated Soils*, Springer, Tokyo **2016**, p. 1; c) J. I. Dawson, R. O. C. Oreffo, *Adv. Mater.* **2013**, *25*, 4069.
[135] a) C. Weber, M. Heuser, H. Stanjek, *Clay Miner.* **2014**, *49*, 495; b) J. Karger-Kocsis, D. Felhős, in *Tribology of Polymeric Nanocomposites*, 2nd ed., (Eds: K. Friedrich, A. K. Schlarb), Butterworth-Heinemann, Oxford **2013**, p. 437.
[136] a) C. Yang, R. Gao, H. Yang, *EnergyChem* **2021**, *3*, 100062; b) S. C. Aboudi Mana, M. M. Hanafiah, A. J. K. Chowdhury, *Geol Ecol Landscapes* **2017**, *1*, 155; c) J.-L. Robert, J.-M. Beny, G. D Ventura, *Eur. J. Mineral.* **1993**, 7.
[137] a) M. F. Brigatti, E. Galan, B. Theng, in *Developments in Clay Science*, Vol. *5*, Elsevier, New York **2013**, p. 21; b) T. Preocanin, A. Abdelmonem, G. Montavon, J. Luetzenkirchen, *Clays, Clay Miner. Ceram. Mater. Clay Miner.* **2016**, 51.
[138] a) G. E. Christidis, in *Developments in Clay Science*, Vol. *5* (Eds: F. Bergaya, G. Lagaly), Elsevier, Amsterdam **2013**, p. 425; b) G. E. Christidis, in *Advances in the Characterization of Industrial Minerals*, Vol. *9* (Ed: G. E. Christidis), European Mineralogical Union and the Mineralogical Society of Great Britain & Ireland, London **2011**, p. 341; c) A. R. Mermut, G. Lagaly, *Clays Clay Miner.* **2001**, *49*, 393; d) S. Ismadji, F. E. Soetaredjo, A. Ayucitra, in *Clay Materials for Environmental Remediation* (Eds: S. Ismadji, F. E. Soetaredjo, A. Ayucitra), Springer International Publishing, Cham **2015**, p. 5; e) F. Bergaya, G. Lagaly, M. Vayer, in *Developments in Clay Science*, Vol. *1* (Eds: F. Bergaya, B. K. G. Theng, G. Lagaly), Elsevier, Amsterdam **2006**, p. 979.
[139] a) D. G. Strawn, *Soil Syst.* **2021**, *5*, 13; b) A. Doi, M. Khosravi, M. Ejtemaei, T. A. H. Nguyen, A. V. Nguyen, *Appl. Clay Sci.* **2020**, *190*, 105557; c) M. J. Angove, B. B. Johnson, J. D. Wells, *Colloids Surf. A* **1997**, *126*, 137.
[140] W. R. Schell, J. V. Jordan, *Plant Soil* **1959**, *10*, 303.
[141] C. Manoratne, R. Rajapakse, M. Dissanayake, *Int J Electrochem Sci* **2006**, *1*, 32.
[142] B. Wang, M. Tang, Y. Wu, Y. Chen, C. Jiang, S. Zhuo, S. Zhu, C. Wang, *ACS Appl. Energy Mater.* **2019**, *2*, 5909.
[143] Y. Zhao, Y. Wang, *Nanoscale Res. Lett.* **2019**, *14*, 366.
[144] W. Chen, T. Lei, W. Lv, Y. Hu, Y. Yan, Y. Jiao, W. He, Z. Li, C. Yan, J. Xiong, *Adv. Mater.* **2018**, *30*, 1804084.
[145] a) S. Kim, S.-J. Park, *Solid State Ionics* **2007**, *178*, 973; b) E. R. Dyartanti, A. Purwanto, I. N. Widiasa, H. Susanto, *Membranes* **2018**, *8*, 36; c) Y. Zhang, Y. Zhao, Z. Bakenov, D. Gosselink, P. Chen, *J. Solid State Electrochem.* **2014**, *18*, 1111.
[146] a) S. i. Ishimaru, R. Ikeda, *Z Naturforsch C Biosci* **1997**, *52*, 863; b) M. W. Riley, P. S. Fedkiw, S. A. Khan, B. Davies, *U.S. Patent No. 6544689*, **2003**.
[147] M.-S. Chen, W. Fu, Y. Hu, M.-Y. Chen, Y.-J. Chiou, H.-M. Lin, M. Zhang, Z. Shen, *Nanoscale* **2020**, *12*, 16262.
[148] W. Chen, T. Lei, T. Qian, W. Lv, W. He, C. Wu, X. Liu, J. Liu, B. Chen, C. Yan, J. Xiong, *Adv. Energy Mater.* **2018**, *8*, 1702889.
[149] M. Moreno, R. Quijada, M. A. Santa Ana, E. Benavente, P. Gomez-Romero, G. González, *Electrochim. Acta* **2011**, *58*, 112.
[150] M. Moreno, M. A. S. Ana, G. Gonzalez, E. Benavente, *Electrochim. Acta* **2010**, *55*, 1323.
[151] S. R. Mohapatra, A. K. Thakur, R. N. P. Choudhary, *J. Power Sources* **2009**, *191*, 601.
[152] S. Choudhary, R. Sengwa, *Ionics* **2012**, *18*, 379.
[153] S. Kitajima, M. Matsuda, M. Yamato, Y. Tominaga, *Polym. J.* **2013**, *45*, 738.

[154] N. Shubha, R. Prasanth, H. H. Hoon, M. Srinivasan, *Mater. Res. Bull.* **2013**, *48*, 526.
[155] a) R. J. Sengwa, S. Choudhary, *J. Appl. Polym. Sci.* **2014**, 131; b) S. Choudhary, R. J. Sengwa, *J. Appl. Polym. Sci.* **2015**, 132; c) P. Dhatarwal, R. Sengwa, S. Choudhary, *SN Appl. Sci.* **2019**, *1*, 112.
[156] R. Prasanth, N. Shubha, H. H. Hng, M. Srinivasan, *Eur. Polym. J.* **2013**, *49*, 307.
[157] L. Chen, W. Li, L.-Z. Fan, C.-W. Nan, Q. Zhang, *Adv. Funct. Mater.* **2019**, *29*, 1901047.
[158] a) A. Mentbayeva, S. Sukhishvili, M. Naizakarayev, N. Batyrgali, Z. Seitzhan, Z. Bakenov, *Electrochim. Acta* **2021**, *366*, 137454; b) M. Yang, N. Jue, Y. Chen, Y. Wang, *Nanoscale Res. Lett.* **2021**, *16*, 52; c) J. Li, J. Yu, Y. Wang, J. Zhu, Z. Hu, *Ind. Eng. Chem. Res.* **2020**, *59*, 12879; d) M. Yang, J. Nan, W. Chen, A. Hu, H. Sun, Y. Chen, C. Wu, *Electrochem. Commun.* **2021**, *125*, 106971; e) H. Zhao, W. Kang, N. Deng, M. Liu, B. Cheng, *Chem. Eng. J.* **2020**, *384*, 123312; f) J. Zhao, D. Chen, B. Boateng, G. Zeng, Y. Han, C. Zhen, J. B. Goodenough, W. He, *J. Power Sources* **2020**, *451*, 227773.
[159] G. Walker, W. Garrett, *Science* **1967**, *156*, 385.
[160] a) J. Feng, M. Liu, L. Fu, K. Zhang, Z. Xie, D. Shi, X. Ma, *RSC Adv.* **2020**, *10*, 7635; b) S. Hillier, E. Marwa, C. Rice, *Clay Miner.* **2013**, *48*, 563; c) S. Williams-Daryn, R. Thomas, *J. Colloid Interface Sci.* **2002**, *255*, 303.
[161] a) W. Tang, S. Tang, C. Zhang, Q. Ma, Q. Xiang, Y. W. Yang, J. Luo, *Adv. Energy Mater.* **2018**, *8*, 1800866; b) W. Tang, S. Tang, X. Guan, X. Zhang, Q. Xiang, J. Luo, *Adv. Funct. Mater.* **2019**, *29*, 1900648.
[162] P. Zhai, N. Peng, Z. Sun, W. Wu, W. Kou, G. Cui, K. Zhao, J. Wang, *J. Mater. Chem. A* **2020**, *8*, 23344.
[163] L. J. Michot, I. Bihannic, M. Pelletier, E. Rinnert, J.-L. Robert, *Am. Mineral.* **2005**, *90*, 166.
[164] Z. Wen, Z. Gu, T. Itoh, Z. Lin, O. Yamamoto, *J. Power Sources* **2003**, *119–121*, 427.
[165] K. Tamura, S. Yokoyama, C. S. Pascua, H. Yamada, *Chem. Mater.* **2008**, *20*, 2242.
[166] M. A. Osman, U. W. Suter, *J. Colloid Interface Sci.* **2000**, *224*, 112.
[167] a) M. F. Brigatti, D. E. Kile, M. Poppi, *Can. Mineral.* **2001**, *39*, 1171; b) K. L. Marchal, W. B. Simmons, A. U. Falster, K. L. Webber, E. Roda-Robles, *Can. Mineral.* **2014**, *52*, 221.
[168] B. Wang, Y. Wu, S. Zhuo, S. Zhu, Y. Chen, C. Jiang, C. Wang, *J. Mater. Chem. A* **2020**, *8*, 5968.
[169] G. Zeng, Y. Liu, D. Chen, C. Zhen, Y. Han, W. He, *Adv. Energy Mater.* **2021**, *11*, 2102058.
[170] a) W. Liu, N. Liang, P. Peng, R. Qu, D. Chen, H. Zhang, *J. Solid State Chem.* **2017**, *246*, 324; b) J. Ni, J. Wang, S. Zhao, F. Zhong, T. Qu, F. Hu, H. Liu, C. Gong, S. Wen, *Appl. Clay Sci.* **2022**, *217*, 106391.
[171] a) W. Yu, N. Deng, K. Cheng, J. Yan, B. Cheng, W. Kang, *J. Energy Chem.* **2021**, *58*, 472; b) Z. Cai, X. Bu, P. Wang, J. C. Ho, J. Yang, X. Wang, *J. Mater. Chem. A* **2019**, *7*, 5069; c) X. Li, D. Du, Y. Zhang, W. Xing, Q. Xue, Z. Yan, *J. Mater. Chem. A* **2017**, *5*, 15460.
[172] a) C. Taviot-Guého, Y. Feng, A. Faour, F. Leroux, *Dalton Trans.* **2010**, *39*, 5994; b) T.-H. Kim, W.-J. Lee, J.-Y. Lee, S.-M. Paek, J.-M. Oh, *Dalton Trans.* **2014**, *43*, 10430; c) S. Weiß, M. Ertl, S. D. Varhade, A. V. Radha, W. Schuhmann, J. Breu, C. Andronescu, *Electrochim. Acta* **2020**, *350*, 136256.
[173] F. Song, X. Hu, *Nat. Commun.* **2014**, *5*, 4477.
[174] A. Vaccari, *Catal. Today* **1998**, *41*, 53.
[175] L. Huang, J. Wang, Y. Gao, Y. Qiao, Q. Zheng, Z. Guo, Y. Zhao, D. O'Hare, Q. Wang, *J. Mater. Chem. A* **2014**, *2*, 18454.
[176] Y. Zhang, X. Cheng, C. Wu, J. Köhler, S. Deng, *Molecules* **2019**, *24*, 2667.
[177] F. Leroux, J.-P. Besse, *Chem. Mater.* **2001**, *13*, 3507.
[178] a) C.-S. Liao, W.-B. Ye, *J. Polym. Res.* **2003**, *10*, 241; b) C.-S. Liao, W.-B. Ye, *Mater. Chem. Phys.* **2004**, *88*, 84.
[179] M. M. Borgohain, T. Joykumar, S. V. Bhat, *Solid State Ionics* **2010**, *181*, 964.
[180] H.-J. Peng, Z.-W. Zhang, J.-Q. Huang, G. Zhang, J. Xie, W.-T. Xu, J.-L. Shi, X. Chen, X.-B. Cheng, Q. Zhang, *Adv. Mater.* **2016**, *28*, 9551.
[181] Q. Wang, J.-F. Wu, Z.-Y. Yu, X. Guo, *Solid State Ionics* **2020**, *347*, 115275.
[182] M. M. Vuksanović, A. Egelja, T. Barudžija, N. Tomić, M. Petrović, A. Marinković, V. Radojević, R. J. Heinemann, *R. Soc. Open Sci.* **2021**, *8*, 210835.
[183] S. Xia, B. Yang, H. Zhang, J. Yang, W. Liu, S. Zheng, *Adv. Funct. Mater.* **2021**, *31*, 2101168.
[184] O. M. Yaghi, H. Li, *J. Am. Chem. Soc.* **1995**, *117*, 10401.
[185] R. Robson, *Dalton Trans.* **2008**, 5113.
[186] W. Xuan, C. Zhu, Y. Liu, Y. Cui, *Chem. Soc. Rev.* **2012**, *41*, 1677.
[187] O. M. Yaghi, R. Jernigan, H. Li, C. E. Davis, T. L. Groy, *J. Chem. Soc., Dalton Trans.* **1997**, 2383.
[188] a) S. Furukawa, J. Reboul, S. Diring, K. Sumida, S. Kitagawa, *Chem. Soc. Rev.* **2014**, *43*, 5700; b) M. Pang, A. J. Cairns, Y. Liu, Y. Belmabkhout, H. C. Zeng, M. Eddaoudi, *J. Am. Chem. Soc.* **2013**, *135*, 10234; c) R. Ostermann, J. Cravillon, C. Weidmann, M. Wiebcke, B. M. Smarsly, *Chem. Commun.* **2011**, *47*, 442; d) M. Tsotsalas, A. Umemura, F. Kim, Y. Sakata, J. Reboul, S. Kitagawa, S. Furukawa, *J. Mater. Chem.* **2012**, *22*, 10159; e) J. Reboul, S. Furukawa, N. Horike, M. Tsotsalas, K. Hirai, H. Uehara, M. Kondo, N. Louvain, O. Sakata, S. Kitagawa, *Nat. Mater.* **2012**, *11*, 717.
[189] a) A. Dhakshinamoorthy, M. Alvaro, H. Garcia, *Chem. Commun.* **2012**, *48*, 11275; b) R. S. Kumar, S. S. Kumar, M. A. Kulandainathan, *Electrochem. Commun.* **2012**, *25*, 70; c) C. Chen, J. Kim, D.-A. Yang, W.-S. Ahn, *Chem. Eng. J.* **2011**, *168*, 1134; d) A. Morozan, F. Jaouen, *Energy Environ. Sci.* **2012**, *5*, 9269.
[190] a) G. Férey, F. Millange, M. Morcrette, C. Serre, M. L. Doublet, J. M. Grenèche, J. M. Tarascon, *Angew. Chem., Int. Ed.* **2007**, *46*, 3259; b) X. Li, F. Cheng, S. Zhang, J. Chen, *J. Power Sources* **2006**, *160*, 542; c) X. Xu, R. Cao, S. Jeong, J. Cho, *Nano Lett.* **2012**, *12*, 4988.
[191] C. Yuan, J. Li, P. Han, Y. Lai, Z. Zhang, J. Liu, *J. Power Sources* **2013**, *240*, 653.
[192] a) C. Gerbaldi, J. R. Nair, M. A. Kulandainathan, R. S. Kumar, C. Ferrara, P. Mustarelli, A. M. Stephan, *J. Mater. Chem. A* **2014**, *2*, 9948; b) N. Angulakshmi, R. S. Kumar, M. A. Kulandainathan, A. M. Stephan, *J. Phys. Chem. C* **2014**, *118*, 24240.
[193] D. J. Ashworth, J. A. Foster, *J. Mater. Chem. A* **2018**, *6*, 16292.
[194] Q. Han, S. Wang, Z. Jiang, X. Hu, H. Wang, *ACS Appl. Mater. Interfaces* **2020**, *12*, 20514.
[195] H. Huo, B. Wu, T. Zhang, X. Zheng, L. Ge, T. Xu, X. Guo, X. Sun, *Energy Storage Mater.* **2019**, *18*, 59.
[196] a) D. A. Vazquez-Molina, G. S. Mohammad-Pour, C. Lee, M. W. Logan, X. Duan, J. K. Harper, F. J. Uribe-Romo, *J. Am. Chem. Soc.* **2016**, *138*, 9767; b) W. H. Huang, X. M. Li, X. F. Yang, X. X. Zhang, H. H. Wang, H. Wang, *Mater. Chem. Front.* **2021**,*5*, 3593; c) Q. Zhu, X. Wang, R. Clowes, P. Cui, L. Chen, M. A. Little, A. I. Cooper, *J. Am. Chem. Soc.* **2020**, *142*, 16842; d) D. Saikat, S. Taishu, M. Haruna, I. Tsukasa, S. Jin, Z. Yu, F. Qianrong, N. Yuichi, *ACS Appl. Mater. Interfaces* **2022**, *14*, 48045; e) J. H. Park, K. Suh, M. R. Rohman, W. Hwang, M. Yoon, K. Kim, *Chem. Commun.* **2015**, *51*, 9313.
[197] K. Zhang, B. Zhang, M. Weng, J. Zheng, S. Li, F. Pan, *Phys. Chem. Chem. Phys.* **2019**, *21*, 9883.
[198] D. Dong, H. Zhang, B. Zhou, Y. Sun, H. Zhang, M. Cao, J. Li, H. Zhou, H. Qian, Z. Lin, H. Chen, *Chem. Commun.* **2019**, *55*, 1458.
[199] Y. Du, H. Yang, J. M. Whiteley, S. Wan, Y. Jin, S.-H. Lee, W. Zhang, *Angew. Chem., Int. Ed.* **2016**, *55*, 1737.
[200] J. Gao, C. Wang, D.-W. Han, D.-M. Shin, *Chem. Sci.* **2021**, *12*, 13248.

[201] P. Zhang, Z. Wang, P. Cheng, Y. Chen, Z. Zhang, *Coord. Chem. Rev.* **2021**, *438*, 213873.
[202] a) H. Chen, H. Tu, C. Hu, Y. Liu, D. Dong, Y. Sun, Y. Dai, S. Wang, H. Qian, Z. Lin, L. Chen, *J. Am. Chem. Soc.* **2018**, *140*, 896; b) Z. Li, Z.-W. Liu, Z. Li, T.-X. Wang, F. Zhao, X. Ding, W. Feng, B.-H. Han, *Adv. Funct. Mater.* **2020**, *30*, 1909267.
[203] Z. Guo, Y. Zhang, Y. Dong, J. Li, S. Li, P. Shao, X. Feng, B. Wang, *J. Am. Chem. Soc.* **2019**, *141*, 1923.
[204] K. Jeong, S. Park, G. Y. Jung, S. H. Kim, Y.-H. Lee, S. K. Kwak, S.-Y. Lee, *J. Am. Chem. Soc.* **2019**, *141*, 5880.
[205] Q. Xu, S. Tao, Q. Jiang, D. Jiang, *J. Am. Chem. Soc.* **2018**, *140*, 7429.
[206] G. Zhang, Y.-l. Hong, Y. Nishiyama, S. Bai, S. Kitagawa, S. Horike, *J. Am. Chem. Soc.* **2019**, *141*, 1227.
[207] Y. Wang, K. Zhang, X. Jiang, Z. Liu, S. Bian, Y. Pan, Z. Shan, M. Wu, B. Xu, G. Zhang, *ACS Appl. Energy Mater.* **2021**, *4*, 11720.
[208] a) A. Mathew, M. J. Lacey, D. Brandell, *J Power Sources* **2021**, *11*, 100071; b) G. Hernández, I. L. Johansson, A. Mathew, C. Sångeland, D. Brandell, J. Mindemark, *J. Electrochem. Soc.* **2021**, *168*, 100523.

Vidyanand Vijayakumar received his Ph.D. in Chemical Sciences (2021) from CSIR-National Chemical Laboratory, Pune, India. With a background in electrochemistry and material science, his research interest shifted to next-generation polymer and liquid electrolytes for lithium and post-lithium batteries during his one-year research associate stint at the Helmholtz Institute Muenster, Germany. Later, he spent another year as a postdoctoral researcher at the Ångströmlaboratoriet, Uppsala University, Sweden, and stepped into the industry as a battery scientist. He currently works on electrolytes and technologies for commercial production of high-energy-dense lithium-ion batteries based on Si anodes.

Meena Ghosh completed her Ph.D. in Chemical Sciences (2021) from CSIR-National Chemical Laboratory, India. As a Raman-Charpak Fellow, she was a visiting scholar at the Universite de Lille, France. Later, she spent one year as a postdoctoral researcher at the Universitat Ulm and the POLiS Cluster of Excellence, Germany. Recently, she joined the Humboldt-Universitat zu Berlin as an Alexander von Humboldt Postdoctoral Fellow. Her current research interests are focused on understanding electrochemical reactions and structural evolution in sodium battery electrodes using advanced characterization tools.

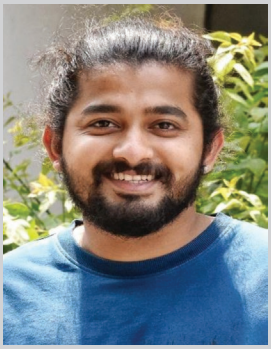

Kiran Asokan obtained his masters in Chemistry from Mahatma Gandhi University, Kerala, India. Later joined as a Project Associate with Dr. Santhosh Babu Sukumaran in the Organic Chemistry Division of CSIR-National Chemical Laboratory, Pune, India. Currently, he is pursuing doctoral studies in the area of organic 2D materials for catalytic applications. Research interests include the synthesis and applications of 2D polymers in gas storage, photocatalysis, energy storage, etc.

Santhosh Babu Sukumaran obtained his Ph.D. on Oligo(p-phenylenevinylene) self-assembly from National Institute for Interdisciplinary Science and Technology (CSIR-NIIST), Trivandrum, India. After several years of postdoctoral studies in Max Planck Institute of Colloids and Interfaces, Germany, National Institute for Materials Science (NIMS), Japan, and the University of Namur, Belgium, he joined National Chemical Laboratory (CSIR-NCL) in 2014 as a senior scientist. His research interests include solvent-free organic liquids, luminescent organic materials, and 2D-polymers for catalytic and energy applications.

Sreekumar Kurungot is working as Senior Principal Scientist at CSIR-National Chemical Laboratory (CSIR-NCL), India. He received his Ph.D. in Chemistry from Cochin University of Science & Technology (CUSAT), India, in 2000. His research interest includes material and system designing for energy applications including fuel cells, batteries, electrolyzers, and supercapacitors. He has more than 230 publications and 20 patent applications to his credit. Dr. Sreekumar is serving as an Associate Editor for RSC Advances from 2015 onward and also as an Editorial Advisory Board Member of ACS Applied Materials & Interfaces from 2020 onward.

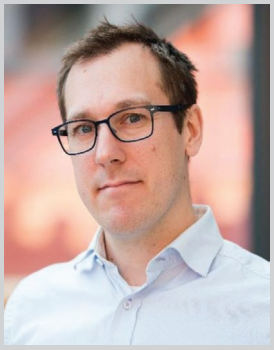

Jonas Mindemark received his Ph.D. in polymer chemistry from Uppsala University, Sweden, in 2012. With a background in polymers for biomaterials applications, his research focus shifted to polymer electrolytes during postdoctoral research at Uppsala University and Umeå University, Sweden. He is currently an associate professor at Uppsala University, with a focus on development and fundamental understanding of next-generation solid and liquid electrolytes.

Daniel Brandell received his Ph.D. at Uppsala University, Sweden, in 2005. After postdoctoral studies in Estonia and the USA, he returned to Uppsala in 2008. There, he has built a research environment focused on soft matter—primarily polymer electrolytes—in electrochemical storage and conversion systems, using both experimental and computational methodology. Since 2016, he is Professor of Materials Chemistry at Uppsala University.

Martin Winter has been researching in the field of electrochemical energy storage and conversion for more than 30 years. His focus is on the development of new materials, components, and cell designs for lithium-ion, lithium-metal, and alternative battery systems. Martin Winter currently holds a professorship for "Materials Science, Energy and Electrochemistry" at the Institute of Physical Chemistry at the University of Münster, Germany. He is founder and scientific director of MEET Battery Research Centre at the University of Münster and of Helmholtz Institute Münster (HI MS) "Ionics in Energy Storage", a division of Forschungszentrum Jülich.

Jijeesh Ravi Nair received his Ph.D., a European Doctorate (2010), in Materials Science and Technology from Politecnico di Torino, Italy. Currently, he is a research associate/group leader at IEK 12, Forschungszentrum Jülich GmbH. His group focuses on the development of cross-linked polymer electrolytes for lithium metal batteries. He won several awards including the Oronzio and Niccolo De Nora Foundation Prize (2010) of the Italian Chemical Society (SCI) for the best Ph.D. thesis and the researcher under 30 years of age category (Italy, 2012), "ENI AWARD 2012 – debut in research".